Cohesive Transitions in Decentralized Networks with Delays

Anuj Kumar Tiwari

A dissertation
submitted in partial fulfillment of the
requirements for the degree of

Doctor of Philosophy

University of Washington

2022

Reading Committee:

Santosh Devasia, Chair

Ashis Banerjee

Xu Chen

Program Authorized to Offer Degree:
Department of Mechanical Engineering

University of Washington

Abstract

Cohesive Transitions in Decentralized Networks with Delays

Anuj Kumar Tiwari

Chair of the Supervisory Committee:
Santosh Devasia
Department of Mechanical Engineering

This dissertation involves development of controls for cohesive transitions in non-ideal networks with delays. Most existing network control strategies focus on improving the convergence rate of networks to consensus, say from one operating value to another. However, maintaining consensus during the transitions, (i.e. achieving cohesive transitions), can be as important as achieving the final consensus value, for instance, in spacing control of connected vehicles, and flexible-object transport using decentralized robot networks. It is shown that increasing the convergence rate to consensus does not necessarily lead to cohesive networks. Recent work on delayed self reinforcement (DSR) has shown to improve the cohesion during transitions in decentralized networks using delayed versions of already available local neighbor information. However the DSR-based approach assumes ideal networks with no agent or network delays. Agent delays represent potential delays due to time taken during actuation or due to local agent dynamics, and network delays can occur due to the time lost during sensing or communication between neighboring agents. The presence of such delays can cause instability, and further, can lead to loss of cohesion with the DSR-based approach. The thesis develops stability conditions, as sufficient delay margins on the network and agent delays in the DSR-based approach, and methods to maintain for cohesive transitions in networks with delays.

TABLE OF CONTENTS

LIST OF FIGURES

LIST OF TABLES

ACKNOWLEDGMENTS

I would like to express my deep gratitude towards Prof. Santosh Devasia for his support and encouragement throughout my graduate studies. His patience and thoughtful guidance has allowed me to develop the skills necessary to become a better researcher.

I would also like to thank my colleagues in the Precision Controls lab who contributed immensely in the completion of the research work presented in this thesis.

Finally, I would not have been able to focus on my research work completely without the support of my family, for which I am deeply indebted.

DEDICATION

to my mother, father and my late grandparents, who laid an initial foundation in me, strong enough to complete my goals.

Chapter 1

INTRODUCTION

The study of interconnected systems as networks is important for gaining understanding of natural systems, and modeling and control of engineered systems. How networks respond to external inputs is essential in several such systems, for instance, to avoid predators and maintain formation in natural systems such as bird flocks and fish schools, and to control engineered multiagent systems such as decentralized robots and autonomous vehicle fleets. Consensus, where agents in a network come to agreement over a joint state value [7], is a fundamental problem in networks, with relation to several multiagent system applications, such as flocking, swarming, distributed sensing, and formation control. The thesis develops methods for achieving cohesive transitions in networks, in the presence of network delays, which can arise during sensing or communication between neighboring agents, as well as computation of control actions of each agent. Furthermore, the method for cohesive transitions is shown to be a potential explanation of the superfluid-type information transfer observed in natural swarming behavior [8], which is not predicted by existing standard network models.

A brief discussion on the goal and main contributions of the thesis is presented below. Detailed introductions are included at the beginning of the subsequent chapters.

1.1 Research Goal

The main goal of the research is presented, which then leads to the development of the research questions and contributions of the dissertation, described in subsequent sections.

Definition of Cohesive Networks

Cohesion in networks during transitions from one consensus value to another refers to the ability of agents to respond in a similar manner during the transition, which can be as important as achieving the new consensus value. For instance, heavy-duty trucks arranged in a platoon formation lead to reduced wind resistance for fuel savings, provided the following vehicles can safely maintain close spacing in the platoon [9], or, in transportation of flexible object using a team of robots without potentially damaging by maintaining formation during the transportation task [10]. A standard approach for network control is through consensus algorithms, for instance, a standard consensus-based algorithm for a network of N agents with information state vector $I(t) \in \mathbb{R}^N$ can be written as,

$$\dot{I}(t) = -\gamma K I(t) + \gamma B I_s(t). \tag{1.1}$$

Standard consensus approaches, as in Eq. (1.1), which use neighbor-based laws to align the state of each agent leads to a non-cohesive network response, as illustrated through an example network in the following.

1.1.1 Consensus-based algorithms can lead to non-cohesive network response.

The cohesion performance of with standard consensus-based algorithm (Eq. (1.1)) is illustrated for an example network from [1], and is compared with a cohesive network response. The example network considered consists of six networked agents with a virtual source, as shown in Figure 1.1. The leader agent has access to a virtual source which prescribes the desired transition from the initial to final position. Simulated network responses for a unit step source input x_s, from an initial position (Figure 1.2-(ii)-a) to a final position (Figure 1.2-(ii)-c), are shown in Figure 1.2-(i) using the consensus-based approach (from Eq. (1.1)),

$$\dot{X}(t) = -\gamma K X(t) + \gamma B x_s(t), \tag{1.2}$$

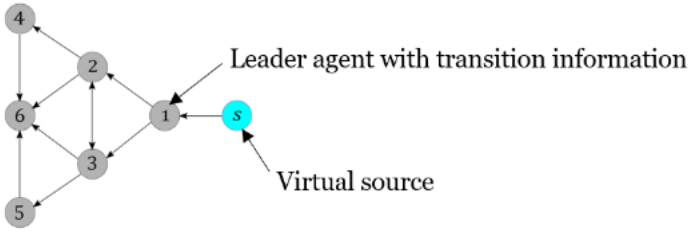

Figure 1.1: Example network with 6 non-source agents with a source agent prescribing the desired transition information to the leader agent 1.

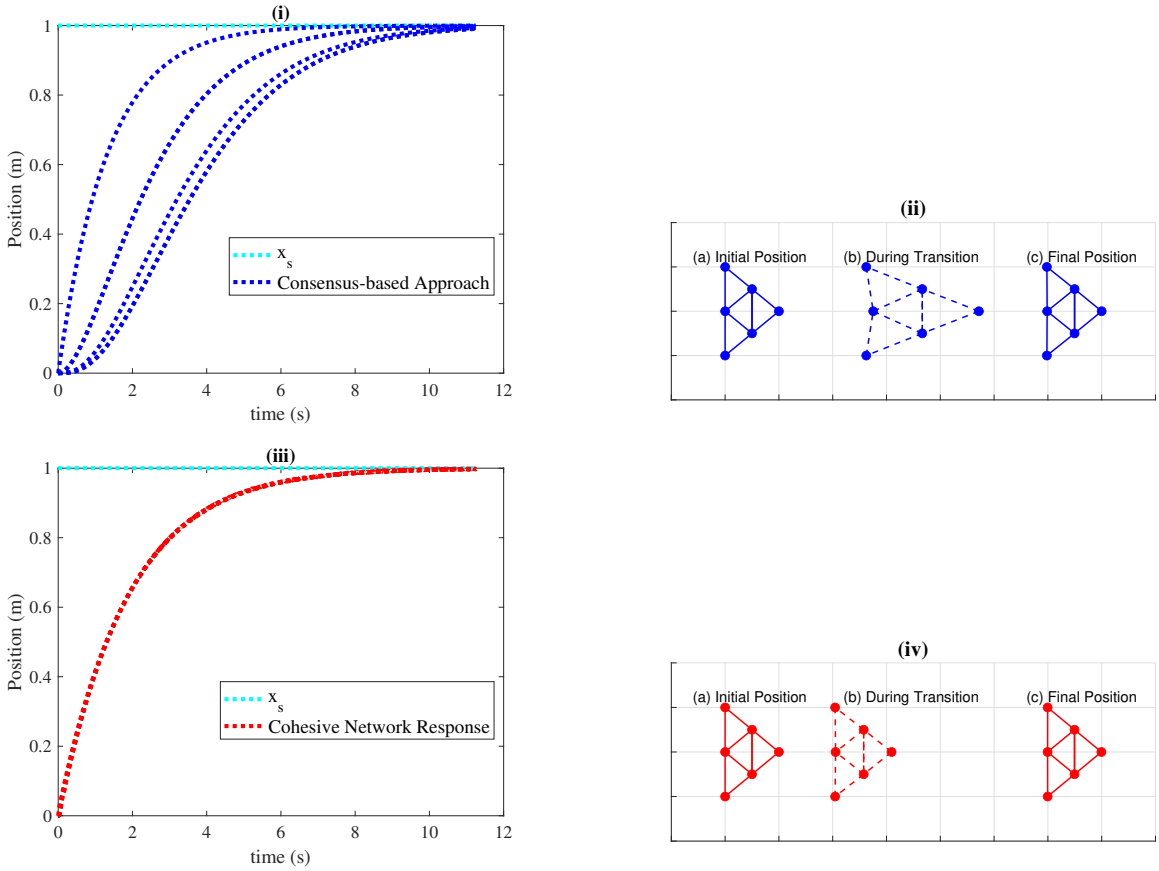

Figure 1.2: **(i)** Simulated network response to a step source input x_s using the consensus-based approach (Eq. (1.2)), which leads to **(ii)** loss of formation during the transition. **(iii)** Cohesive network response using delayed self reinforcement (DSR) approach (introduced in Section 1.4) **(iv)** leads to maintaining the network formation during the transition.

where $X(t) \in \mathbb{R}^6$ is the position state vector, K is the graph Laplacian of the underlying non-source agents in Figure 1.1. Figure 1.2-(i) shows dissimilar response among the agents which leads to loss of formation during transition as shown in Figure 1.2-(ii)-b. A cohesive network response should lead to similar responses to the step input among the agents, as shown in Figure 1.2-(iii) (obtained using delayed self reinforcement (DSR) approach introduced in Section 1.4 [1]), which helps maintain formation during transition as seen in Figure 1.2-(iv)-b.

1.1.2 Centralized network control.

Cohesion in networks, with cohesive network responses as shown in the example Figure 1.2-(iii), can be achieved through a centralized controller to ensure each agent performs similar actions, for instance using wireless communication [11] to broadcast the source information I_s to each agent in the network in Eq. (1.1), which results in,

$$\dot{I}(t) = -\gamma I(t) + \gamma \mathbf{1}_N I_s(t). \tag{1.3}$$

where $\mathbf{1}_N \in \mathbb{R}^N$ is a vector of all ones.

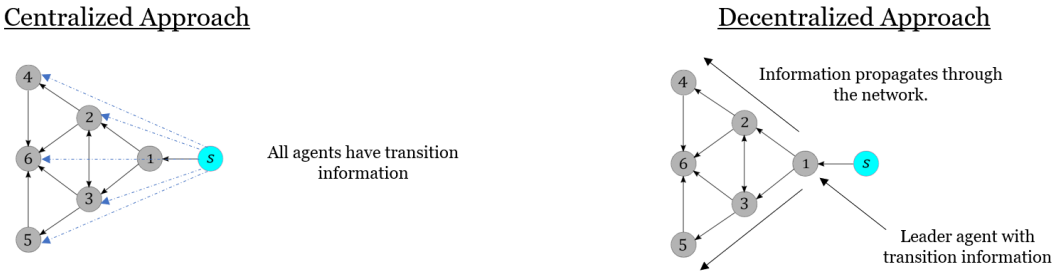

Figure 1.3: Centralized approach for the example network, which involves broadcast of the desired information to each agent, is one method to achieve cohesive network response as shown in Figure 1.2-(iii), unlike in the decentralized consensus approach, where only the leader has the desired information, and then it propagates to rest of the network, which leads to loss of cohesion.

However, such centralized approaches require explicit inter-agent communication, which

incurs additional infrastructure cost, and can be susceptible to cybersecurity threats where intruder agents obtain access to the network information [12]. Furthermore, centralized control based networks face issues as the number of agents to be controlled increases, which is not the case with the decentralized where only local neighbor-based information is used for control which scales well with network size.

Centralized	Decentralized
Cohesive network response during transitions.	Non-cohesive network response during transitions.
Requires explicit inter-agent communication : added cost.	Local sensing-based control : less cost.
Does not scale well with network size.	Scales well with network size
Security vulnerabilities, such as access to network transition information.	Neighbor-only sensing keeps network transition information secure.

Figure 1.4: Comparison of the centralized and decentralized approaches for network control, in terms of cohesiveness of response, communication cost, network size, and cyber security issues.

1.1.3 Goal: A cohesive and decentralized approach for network control.

The goal of the research is to present a decentralized approach, which has the desirable properties of less costly, scalable and secure network control (as shown in Figure 1.4), while also maintaining cohesiveness during transitions, which is not shown by current consensus-based approaches.

Based on the above research goal, the research questions (**RQ**s) of the dissertation, and the main contributions (**MC**s) and proposed research (**PR**) to address the questions are given below.

1.2 RQ1: Can increasing convergence rate of consensus improve cohesion in decentralized networks?

A potential approach towards improving cohesion in networks during transition could be by increasing the response speed of the network to external inputs, for faster convergence to consensus. Increasing the convergence rate of consensus leads to faster response of each agent to any neighbor information, which leads to faster propagation of the desired information from the leader agent to rest of the network in the decentralized framework (Figure 1.3).

1.3 MC1: Rapid transitions in networks using accelerated self-reinforcement.

This section introduces the first main contribution of the dissertation which has been published in [2]. Increasing the response speed of networks helps achieve this transition in a shorter amount of time, which can potentially improve cohesion in the sense that each agent responds faster to changes in neighbor information. The convergence rate to consensus can be improved by reinforcing the standard approach in Eq. (1.1) using accelerated approach from [2], given in a general form as,

$$I[k+1] = I[k] - \gamma\delta_t K I[k] + \gamma\delta_t B I_s[k] + (\beta_2 \mathbf{I}_N - \beta_1 K)(I[k] - I[k-1]), \tag{1.4}$$

where the added terms $\beta_1 K((I[k] - I[k-1])$ and $\beta_2(I[k] - I[k-1])$ are referred to as the outdated-feedback and momentum terms respectively. For example, the addition of only the momentum term in (1.4) (i.e., $\beta_1 = 0$) leads to the momentum-method used in [13, 14]. Adding only the outdated-feedback term (i.e., $\beta_2 = 0$) leads to the outdated-feedback approach pursued to speed up network convergence rates in [15]. The Nesterov-method uses both the outdated-feedback and the momentum terms in a specific ratio, i.e., $\frac{\beta_1}{\gamma\delta_t} = \beta_2 = \beta$ [16]. The main contribution

Self-reinforcement based on the accelerated approach in Eq. (1.4), with generalized parameters β_1 and β_2, is used for achieving rapid transitions in networks with directed topology. Rapid transitions are important for quick response of consensus-based, multi-agent networks

to external stimuli. While high-gain can increase response speed, potential instability tends to limit the maximum possible gain, and therefore, limits the maximum convergence rate to consensus during transitions. Since the update law for multi-agent networks with symmetric graphs can be considered as the gradient of its Laplacian-potential function, Nesterov-type accelerated-gradient approaches from optimization theory, can further improve the convergence rate of such networks. An advantage of the accelerated-gradient approach is that it can be implemented using accelerated self-reinforcement, which does not require new information from the network nor modifications in the network connectivity. However, the accelerated-gradient approach is not directly applicable to general directed graphs, since the update law is not the gradient of the Laplacian-potential function. The main contribution of the work in [2] is to extend the accelerated-gradient approach to general directed graph networks, without requiring the graph to be strongly connected. Additionally, while both the momentum term and outdated-feedback term in the accelerated-gradient approach are important in general, it is shown that the momentum term alone is sufficient to achieve balanced robustness and rapid transitions without oscillations in the dominant mode, for networks whose graph Laplacians have real spectrum.

While a faster convergence rate improves cohesion in the sense of speeding up agent responses to changes in neighbor information, for certain applications maximum network deformation needs to be reduced, for instance in flexible-object transport task in [10], which can remain unaffected with faster convergence rates, as shown through an example network simulation in the following.

1.3.1 Faster network response doesn't necessarily improve cohesion.

The maximum deformation during transition in an example network (Figure 1.1), is presented for increased convergence rates of network response using Eq. (1.4), and compared with the maximum deformation obtained using the standard consensus approach in Eq. (1.1).

Simulated response of the network in Figure 1.1 to a unit step input as the source input Figure 1.5 shows that using the accelerated approach in Eq. (1.4) provides significant im-

provement in the convergence rate compared to the standard consensus approach in Eq. (1.1). The settling time of the network response, defined as the time taken for all agents to achieve and stay within 2% of the final desired position, is reduced to 0.055 s using the accelerated approach in Eq. (1.4), from 10 s in the consensus-based approach, as shown in Figure 1.5-(iii) and Figure 1.5-(i) respectively. However, even with the increased convergence rate, the maximum deformation is similar with the accelerated approach when compared to the consensus-based approach, as shown through the network deformation observed during transition in Figure 1.5-(iv) and Figure 1.5-(ii) respectively. Therefore, these example simulations establish that increasing convergence rate does not necessarily lead to decrease in maximum network deformation during transitions.

A cohesive and decentralized approach of network control for cohesive transitions has been introduced in [1], which has been derived in the following section.

1.4 Background: Cohesive networks using delayed self reinforcement (DSR).

Delayed self reinforcement (DSR), proposed in [1], provides a method to achieve cohesive transitions in networks of higher-order agents. The DSR approach, given as following for first order agents,

$$\dot{I}(t) = -\gamma K I(t) + \gamma B I_s(t) + (\mathbf{I}_N - \beta K)\frac{(I(t) - I(t-\tau))}{\tau}, \tag{1.5}$$

with identity matrix $\mathbf{I}_N \in \mathbb{R}^{N\times N}$ and DSR gain $\beta \in \mathbb{R}$, approximates the centralized approach in Eq. (1.3) for relatively slow varying source trajectories I_s. Such use of derivative information has previously been shown to improve cohesion in consensus algorithms [17], however, such methods require each agent to have the derivative of neighbor agent states which in turn depend on the derivative of their neighbor agents. Therefore, each agent cannot update its own state using only local neighbor information. The advantage of the DSR

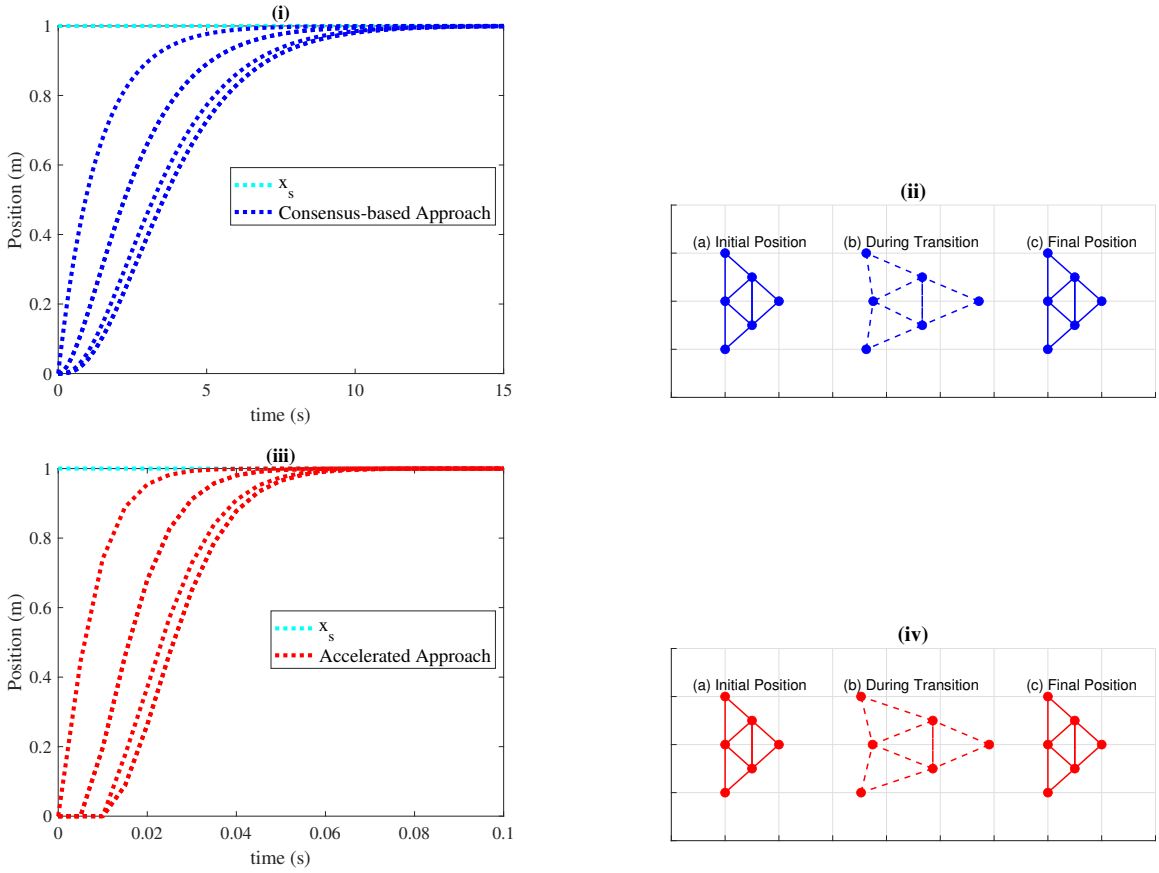

Figure 1.5: **(i)** Simulated network response to a step source input x_s using the consensus-based approach (Eq. (1.2)), which leads to **(ii)** loss of formation during the transition. **(iii)** Accelerated self-reinforcement approach from Eq. (1.4), although providing significant improvement in convergence rate by reducing the 2% settling time of the network response to 0.055 s compared to the 10 s achieved with consensus-based approach, **(iv)** shows similar maximum deformation during transition from initial position to final position.

approach in Eq. (1.5) is that it approximates the derivative of the neighbor information,

$$\dot{I}(t) \approx \frac{I(t) - I(t-\tau)}{\tau}, \tag{1.6}$$

using delayed versions of the neighbor information already available in the decentralized framework, which approximated the centralized control in Eq. (1.3), for slowly varying tra-

jectories, such that $X(t) - X(t-\tau) >> \tau$. Taking the delay as $\tau = \delta_t$, where δ_t is the update time period, and keeping the update same between updates, the DSR approach in Eq. (1.5) can be discretized as,

$$I[k+1] = I[k] - \gamma\delta_t K I[k] + \gamma\delta_t B I_s[k] + (\mathbf{I}_N - \beta K)(I[k] - I[k-1]). \tag{1.7}$$

1.4.1 DSR improves cohesion during transition in decentralized networks.

Simulated response to unit step source input, shown in Figure 1.2-(iii), using the DSR approach in Eq. (1.7) for the example network in Figure 1.1, shows that DSR leads to similar response among the agents which in turn results in nearly zero loss of formation during the transition, as shown in Figure 1.2-(iv).

1.4.2 Connections to the accelerated approach.

The discrete update equation for the first order DSR approach in Eq. (1.7) can be obtained as a special case of the accelerated approach in Eq. (1.4) with $\beta_2 = 1$. However, as seen using the example simulations, using the accelerated approach in Eq. (1.4) doesn't necessarily lead to cohesive network transitions, as seen in Figure 1.5 where accelerated approach was used to achieve faster consensus.

This leads to the second main research question addressed in the dissertation.

1.5 RQ2: Why DSR improves cohesion in networks during transitions?

The DSR approach in Eq. (1.7), although being structurally similar to and a special case of the accelerated approach in Eq. (1.4), leads to improved cohesion. The second main question addressed in this dissertation is to explain the cohesive transitions achieved using the DSR approach.

1.6 MC2.1: DSR improves network's transition cohesion by approximating strongly damped waves.

The second main contribution to explain the cohesion achieved with DSR, accepted to be presented at a conference as [4], is briefly described below.

The main contribution of the work in [4] is to show that DSR leads to a strongly-damped, wave-like propagation [18] of information at low frequencies, which improves cohesion during transitions. Furthermore, the wave-like-propagation formulation of DSR is used to show that the DSR approach implements consensus of agents in the network not only for the state information but also its time-derivative which provides a rationale for the low-dissipation propagation of information through networks that in turn leads to improved cohesion.

1.7 MC2.2: DSR leads to low distortion information propagation with noise suppression in swarm networks.

The main contribution of this work, submitted for publication in [5], is to show that delayed self-reinforcement (DSR) by the agents using prior information (e.g., using short-term memory) can lead to the wave-like information propagation at low-frequencies as seen in nature without the need for additional information sharing between the agents. Moreover, it is shown that the DSR can be designed to enable suppression of high-frequency noise transmission while limiting the dissipation and dispersion of (lower-frequency) information content leading to similar (cohesive) behavior of agents. In addition to explaining noise-suppressed wavelike information transfer in natural systems, the result impacts the design of noise-suppressing cohesive algorithms for engineered networks.

1.8 RQ3: Can cohesion be achieved using DSR for networks with delays?

The current DSR-based approach, proposed in [1], assumes ideal network conditions with agents having instant access to neighbor information without i) network delays arising during sensing or communication between neighbors, ii) as well as delays due to local agent dynamics or computation of control actions of each agent, namely agent delays, which can cause

instability and loss of cohesion during transitions. The third main question addressed in this dissertation is to enable cohesion in networks with network and agent delays.

The proposed research for the contributions to address **RQ3** are described below.

1.9 MC3: Cohesive transitions in presence of network delays.

The main contribution of this work, published in [6], is the development of a method based on Rouchè's theorem [19] to predict the delay margin (DM) for the DSR approach, which can be applied with general higher-order agents in networks. Rouchè's theorem has been previously used to determine the stability of lumped-distributed networks with nonrational system functions, which leads to characteristic equation with infinite power series [20] and Rouchè's theorem can be used to predict stability by comparing the magnitudes of the truncated sum with that of the remainder. Similar use of Rouchè's theorem for truncation of an infinite characteristic function of a time delayed system for subsequent use of Routh's stability criterion on the truncated finite characteristic function is studied in [21]. More direct applications to single-delay systems have been studied in [22, 23], which considers the addition of the delay in the characteristic function as a perturbation of a system without delays. However, the nominal DSR case without the network delay is not delay free, DSR without network delay still has an intentional delay due to the use of delayed reinforcement using past network information [1], which is accounted for in the current chapter when establishing DM for DSR. Additionally, the current work identifies a finite bounded section of the imaginary axis on the complex plane for evaluating conditions to satisfy Rouchè's theorem for the DSR case, which aids in the development of computational algorithms for estimating the DSR DM.

1.10 Networks with agent delays.

The proposed method for handling agent delays in networks, which can occur due to local agent dynamics or computation of control commands, is considered. Agent delays in networks, in the form of delayed input to the local agent dynamics, can not only lead to

unstable network dynamics, but also reduce cohesion in networks during transitions when using DSR. Therefore, a method for handling agent delays to enable cohesive transitions in such non-ideal networks is provided in Chapter 7.

1.11 Structure of the thesis

The subsequent chapters begin with a background in Chapter 2 which provides a brief review for the accelerated self-reinforcement approaches, the DSR approach proposed in [1], and available methods in literature for determining stability of systems in presence of delays. Chapter 3 deals with **MC1**, improving convergence rates in networks using accelerated self-reinforcement approaches, with generalized gains for the outdated-feedback and momentum term additions. Next, Chapter 4 and Chapter 5 address **MC2**, providing a rationale for the improved cohesion compared with the accelerated approaches with the DSR approach, which is a specific case of the more general accelerated approach with the momentum term gain $\beta_2 = 1$. Chapter 6 deals with **MC3** and develops the stability conditions for the DSR approach with network delays. Chapter 7 extends to handling of agent delays in networks by providing a method for maintaining cohesion during transitions in networks with agent delays. The main contributions (**MC1**, **MC2** and **MC3**) are briefly summarized with some concluding remarks in Chapter 8.

Each of the chapters is self-contained with individual introductions and conclusion. A bibliography is presented at the end of the thesis.

Chapter 2

BACKGROUND

This chapter provides a background and short reviews of the available literature concerning each of the three main research questions (**RQ1, RQ2** and **RQ3**) addressed in this dissertation, taken from the published versions of the main contributions (**MC1**, **MC2.1**, **MC2.2** and **MC3**) [2–4, 6].

2.1 Accelerated self-reinforcement approaches (MC1).

The performance of consensus-based, multi-agent networks, such as the response to external stimuli, depends on rapidly transitioning from one operating point (consensus value) to another, e.g., in flocking of natural systems, [24, 25], as well as engineered systems such as autonomous vehicles, swarms of robots, e.g., [26–28] and other networked systems such as aerospace control [29] microgrids [30, 31], flexible structures [32]. Rapid cohesive transitions, e.g., in the orientation of the agents from one consensus value to another, is seen in flocking behaviour during predator attacks and migration [33, 34]. Thus, there is interest to increase the convergence rate to consensus for such networked multi-agent systems.

There is a fundamental limit to the achievable rate of convergence using existing neighbor-based update laws for a given network, e.g., of the form

$$\hat{X}[k+1] = \hat{X}[k] + u[k] = \hat{X}[k] - \alpha L\hat{X}[k], \tag{2.1}$$

where the current state is $\hat{X}[k]$, the updated state is $\hat{X}[k+1]$, α is the update gain, L is the graph Laplacian, and k represents the time instants $t_k = k\delta_t$ with δ_t as the sampling time-period. The convergence rate depends on the eigenvalues of the matrix $P = (\mathbf{I} - \alpha L)$

[35], which in turn depends on the eigenvalues of the graph Laplacian L. For example, if the underlying graph is undirected and connected, it is well known that convergence to consensus can be achieved provided the update gain α is sufficiently small, e.g., [36]. The update gain can be selected to maximize the convergence rate, and typically, a larger gain α tends to increase the convergence rate. Nevertheless, for a given graph (i.e., a given graph Laplacian L), the range of the acceptable update gain α is limited, which in turn, limits the achievable rate of convergence [37]. Typically, the convergence rate tends to be slow if the number of agent inter-connections is small compared to the number of agents, e.g., [38]. Faster convergence can be achieved using randomized time-varying connections, as shown in, e.g., [38]. The update sequence of the agents can also be arranged to improve convergence, e.g., [39]. The problem is that the graph connectivity might be fixed and therefore the Laplacian L cannot be varied over time. In such cases, with a fixed Laplacian L, the need to maintain stability limits the range of acceptable update gain α, and therefore, limits the rate of convergence. This convergence-rate limitation motivates ongoing efforts to develop new approaches to improve the network performance, e.g., [40]. Furthermore, in addition to convergence-rate, an important consideration is robustness of the approach, e.g., as studied in [41, 42].

Since the neighbor-based update (u in Eq. (2.1)) can be obtained from the gradient of the Laplacian potential $\Phi_{\mathcal{G}} = \hat{X}^T L \hat{X}$ for undirected graphs, i.e., $u = -(\alpha/2)\nabla\Phi_{\mathcal{G}}$, Nestertov-type accelerated approaches, used to speed up gradient-based optimization [43–47], can be used to improve the convergence rate. Previous works have considered the use of some parts of the accelerated gradients (from optimization theory) for graph-based multi-agent networks. For example, the addition of a momentum term (of the form $\hat{X}[k] - \hat{X}[k-1]$, as in, e.g., [43]) in the update law has been shown to improve the response speed under update-bandwidth limits [37, 48]. These works have also shown that the use of such reinforcement can lead to non-diffusive, wave-like response propagation seen in natural systems such as bird flocks [8]. Similarly, the addition of a Nesterov term without the momentum term, also

referred to as an outdated-feedback (of the form $L(\hat{X}[k]-\hat{X}[k-1])$, as in e.g., [45]), has been shown to result in faster convergence in [49, 50], and to enable a linear rate of convergence using a time-varying gain in [51]. Time-varying gains, however, require a global resetting of each agent's gain at start of each transition, which might not be always feasible because the start of a transition might not be known to all agents. The combination of both, the momentum term and the outdated-feedback term, can further improve the convergence rate of consensus-based networks when compared to the use of either term alone [3, 52, 53]. Note that an advantage of such accelerated-gradient-based approach is that the update can be implemented by using an accelerated delayed-self-reinforcement (A-DSR), where each agent only uses current and past information from the network. This use of already existing information is advantageous since the convergence improvement is achieved without the need to change the network connectivity and without the need for additional information from the network. Nevertheless, the update law for more general graphs with non-symmetric Laplacian (e.g., general directed graphs) cannot be obtained from the gradient of the graph potential [54,55]. Gradients along local agent-wise potential have been considered along with weight-balancing to improve the performance for directed graphs, e.g., [56, 57]. However, these approaches rely on the graph being strongly connected, which excludes applications such as platoons where overall information flow between two agents is not bi-directional over the graph. Therefore, the current Nesterov-based approach and its stability analysis cannot be directly applied for general directed graphs (which are not strongly connected), which are addressed in the current thesis in Chapter 3.

2.2 Cohesion in networks using DSR (MC2.1).

Cohesive networks, where each agent in the network responds in a similar manner during transition from one consensus value to another (and not just at the steady state), are essential for applications where non-uniform responses among the agents lead to loss of safety, performance and efficiency, e.g., cohesive decentralized transport of flexible-object using robot networks to reduce deformations in the object [10], maintaining smaller inter-vehicle spacing

for efficiency in intelligent traffic networks [58, 59]. Standard network approaches mainly focus on the speed of convergence to consensus at the steady state and do not address cohesiveness during transitions. The loss of cohesion arises from the time taken for the transition information to propagate through the network: from the source agent where the transition initiates to agents that are farther away. Moreover, since standard consensus-based networks are diffusive, e.g., [14], the information about transition dissipates as it travels through the network, leading to slower response of the agents far from the source than those close to it. Faster transition information propagation, achieved by increasing the alignment strength of each agent with its neighbors, does not necessarily improve cohesion during the transition. Moreover, the alignment strength increase is limited by potential instability and input bounds [14], and tends to require increased update bandwidth for stability.

A centralized approach can improve cohesion by broadcasting the transition information simultaneously to all the agents, for instance through wireless communication [11]. However, such central broadcasting systems can be prone to cyber security threats where the network information can be inferred by intruder agents [12]. Furthermore, the use of wireless communication does not scale well with network size, when the distance between agents is large as well. Finally, there is additional infrastructure cost to implement such centralized methods. Recent work in [1] proposed a delayed self reinforcement (DSR) approach to maintain cohesion during transitions for decentralized networks. An advantage of using DSR is that it can be implemented using the local information already available in the decentralized framework, without requiring changes in the network connectivity. DSR has also shown improvement in flexible-object transport tasks using a robot network [10] by reducing deformation in the object through enhanced cohesion in the response of the robots. DSR can be implemented locally by each agent using delayed versions of its own state and neighbor information from the network, which is similar to the addition of momentum and outdated-feedback terms in gradient-based optimization approaches [60]. Furthermore, DSR leads to superfluid-type information transfer in networks as observed in nature [61]. The second main question addressed in this dissertation is to explain the cohesive transitions achieved using the DSR

approach in Chapter 4.

2.3 Low distortion information propagation with noise suppression in swarm networks (MC2.2)

Collective state transitions in biological and engineered networks require robust propagation of the transition information, from their spatially localized origin in the networks to other agents farther away from that origin. For instance, consider a flock of starlings changing their direction of motion while under predatory attack [8,62], where any uncertainty in the turning maneuver can lead to loss of cohesion, and some birds breaking formation. Such decoherence among the birds can lead to loss of safety. Similar collective state transitions for decision-making are seen in other animal groups [63–66], such as fish schools [67–71], honeybee social networks [72], rapid waves of escape response in marine skaters [73], and have applications in network based engineered systems [74–76], such as coordination of robot swarms [77] for precision agriculture [78], and for infrastructure inspection and monitoring operations [79].

Standard neighbor-based alignment models of swarms do not predict the superfluid-type information transfer observed in natural flocks [8]. The interactions between agents, for both natural and robotic systems, are usually local due to limitations on the bandwidth and sensing or communication range available to each agent [80]. Furthermore, observations of turning maneuvers in starlings flocks [8] show localized origins of the turning maneuver decisions, which then propagate through the rest of the network. The flocking behavior seen in natural flocks is strongly polarized, i.e., all the individual birds move in almost the same direction. The collective motion in the flocks can be explained through a social force, where each individual aligns its direction of motion with the local neighbors. Local alignment based models are able to explain the correlated directional behavior in natural flocks, among which a well studied representative model is the Viscek model proposed in [81]. The Viscek model considers collective turning behavior in a group of self-propelled particles, where each particle updates its orientation using the average neighbor information. In other words, each particle updates its orientation according to a social force. However, such local

alignment based models predict diffusive information transfer, contradicting the empirical observation of wave-like propagation of orientation information without dissipation, during turning maneuvers, in bird flocks [8].

The new model proposed in this article, which adds delayed self-reinforcement (DSR) terms to current alignment based models [8], not only predicts the low-distortion information propagation through networks, including turning information in bird flocks, but also shows noise suppression behavior during the information propagation that is not seen in the earlier models [14,62]. Such DSR-based models suppresses unwanted motions, such as higher frequency movements of neighbors (say, due to flapping of wings), and prevents such noise from spreading across the network leading to loss of coherence. In contrast, prior works do not allow such suppression of noise. For example, prior works in [8, 62] have introduced a behavioral inertia, in addition to the neighbor-based social force, in a new microscopic model to explain the propagation of turning information through bird flocks. The parameters of the model can be tuned to achieve undamped propagation of information without dissipation. Similar results are obtained in [14], where self-reinforcement of the alignment based algorithms with additional momentum term [13] leads to a wave-like information propagation in networks. However, these models also lead to undamped propagation of noise without dissipation. Adapting the network structure which leads to maximal robustness to external disturbances can be another approach, such as in [82] which shows certain structures are more robust to perturbations than others. However, changing the network structure for noise suppression might not always be feasible. The next main question addressed in this dissertation is to show low distortion information propagation with noise suppression without changing the network structure using the DSR approach in Chapter 5.

2.4 Stability of systems with delays (MC3).

Stability under delays has been studied for strongly-connected graphs, where each agent is (directly or indirectly) connected via a graph path to all other agents in the network. For example, under the strongly-connected assumption, stability conditions are developed in [83]

using Lyapunov-Krasovskii functional techniques for agents with first-order dynamics, and in [84] for second-order agents using a frequency-domain method. For undirected graphs (also a special case of strongly-connected graphs), where the eigenvalues of the Laplacian are real-valued, bounds on the delay margin (DM) can be found using the Nyquist stability criterion, e.g., [85]. A method to compute the exact DM in undirected networks has also been developed in [86] where the undirected-graph assumption results in a unimodal optimization problem to solve the otherwise challenging non-smooth max-min controller optimization problem. The DSR approach to improve consensus is applicable to networks that are not strongly connected, and therefore, the above approaches are not directly generalizable to the current issue of estimating the DM for DSR-based cohesive networks.

Another class of methods for determination of the delay margin (DM) is to assess the imaginary axis crossing, e.g., [87–91]. Such methods seek to identify critical delay values τ such that the characteristic polynomial $\mathcal{C}$, defined as a function of the Laplace variable s and delay exponential $e^{-s\tau}$ i.e. $\mathcal{C}(s, e^{-s\tau})$ [90], has purely imaginary roots, i.e.,

$$\mathcal{C}(j\omega, e^{-j\omega\tau}) = 0, \quad \omega \in \mathbb{R}. \tag{2.2}$$

Then, using the continuity of the roots with the delay τ (in case of retarded time delay systems) and assuming stability at no delay $\tau = 0$, the smallest critical value can be found to determine the delay margin [90,91]. However, these class of methods handle characteristic polynomials with delay τ appearing only in the exponential form $e^{-s\tau}$ in the characteristic equation, and cannot be used to investigate the impact of network delays in the DSR-based approach as it includes delays that appear in a non-exponential form such as $\frac{e^{-s\tau}}{\tau}$ [1]. For instance, approaches in [87, 88] use the Rekasius substitution, $e^{-s\tau} = (1 - Ts)/(1 + Ts)$, $T \in \mathbb{R}, s = j\omega$, and multiply by $(1+Ts)$ to result in a standard polynomial root finding problem that can be analyzed using the Routh-Hurwitz approach. However, the methods in [87, 88] require the delay to be in a purely exponential form and cannot be used when

it appears as $\frac{e^{-s\tau}}{\tau}$ as in the DSR case [1]. An alternative procedure, based on extended Kronecker summation properties in [89, 90], requires a substitution $z = e^{-s\tau}$, which is again not applicable to more general forms of delay in the characteristic polynomial, such as $\frac{e^{-s\tau}}{\tau}$ in the DSR approach.

The current DSR approach [1] assumes instantaneous access to neighbor information and could become unstable in the presence of network delays. Such unavoidable delays can arise due to the time needed for sensing and/or communication between the agents [85], as well as computation of control actions. As the third main contribution (**MC3**), Chapter 6 develops stability conditions for the DSR-based approach in the presence of network delays, and provides a computational method to estimate a lower bound $\overline{\tau}_{n,est} \leq \overline{\tau}_n$ on the delay margin (DM) $\overline{\tau}_n$, such that the DSR-based approach is stable when the network delay τ_n is less than the DM, i.e., $0 \leq \tau_n < \overline{\tau}_n$.

Chapter 3

MC1: RAPID TRANSITIONS IN NETWORKS USING ACCELERATED SELF-REINFORCEMENT

This chapter forms the contribution **MC1** of this dissertation, and is published as an article in [2]. The main contribution of this chapter is to design a Nesterov-type accelerated update for general graph networks using a local potential function for each agent. However, the resulting update law does not necessarily reduce the overall Laplacian potential [55] because each agent's update is in the negative gradient direction of its own local potential. Therefore, the convergence studies from optimization methods cannot be used to establish stability [46, 47] of accelerated update derived using local potential functions. Moreover, while Lyapunov functions can be found to study stability for general directed graphs [55], the gradient of these Lyapunov functions does not lead to the control update law, and hence accelerated methods cannot be directly applied using these Lyapunov functions. Prior methods that use either the momentum term alone or the outdated-feedback term alone also do not address the stability when both terms are used for general directed graphs. In this context, a contribution of this chapter is to develop stability conditions for the proposed generalized accelerated approach, with both the momentum and outdated-feedback terms. The current chapter expands on our prior work in [52], which used a fixed ratio between the momentum and outdated-feedback terms, by (i) proposing the general case with varying ratios between the momentum and outdated-feedback terms; (ii) developing a stability condition for the generalized approach, (iii) designing the A-DSR to achieve fast response while maximizing structural robustness, (iv) illustrating the importance of momentum term over the outdated-feedback term for graph networks with real spectrum and (v) presenting experimental results to comparatively evaluate the performance, with

and without A-DSR.

The chapter begins by presenting the structurally-robust, convergence-rate improvement problem, along with the limits of standard consensus-based update in Section 3.1. The proposed A-DSR based approach is introduced in Section 3.2.1, and the stability conditions of the A-DSR approach are developed in Section 3.2.2, followed by the derivation of analytical Robust A-DSR approach for maximizing robustness in Section 3.2.3. Section 3.3.1 comparatively evaluates the performance with and without A-DSR through simulations, and Section 3.3.2 presents experimental results. Lastly, conclusions from the chapter are reported in Section 3.4.

3.1 Problem formulation

This section introduces graph-based consensus dynamics used to model networked systems, and describes the convergence limits with structural robustness achievable due to stability bounds on the update gain in standard neighbor-based consensus dynamics. Finally, the problem statement of the chapter is stated.

3.1.1 Background: graph-based control

Let the multi-agent network be modeled using a graph representation, where the connectivity of the agents is represented by a directed graph (digraph) $\mathcal{G} = (\mathcal{V}, \mathcal{E})$, e.g., as defined in [36]. Here, the agents are represented by nodes $\mathcal{V} = \{1, 2, \ldots, n{+}1\}$, $n > 1$ and their connectivity by edges $\mathcal{E} \subseteq \mathcal{V} \times \mathcal{V}$, where each agent j belonging to the set of neighbors $N_i \subseteq \mathcal{V}$ of the agent i satisfies $j \neq i$ and $(j, i) \in \mathcal{E}$.

The evolution of the multi-agent network is defined using the graph $\mathcal{G}$, as in Eq. (2.1).

The elements $l_{i,j}$ of the $(n+1) \times (n+1)$ Laplacian L of the graph $\mathcal{G}$ are real and given by

$$l_{i,j} = \begin{cases} -a_{i,j} < 0, & \text{if } j \in N_i \\ \sum_{m=1}^{n+1} a_{i,m}, & \text{if } j = i, \\ 0 & \text{otherwise,} \end{cases} \tag{3.1}$$

where the weight $a_{i,j}$ is nonzero (and positive) if and only if j is in the set of neighbors $N_i \subseteq \mathcal{V}$ of the agent i, each row of the Laplacian L adds to zero, i.e., from Eq. (3.1), the $(n+1) \times 1$ vector of ones $\mathbf{1}_{n+1} = [1, \ldots, 1]^T$ is a right eigenvector of the Laplacian L with eigenvalue 0,

$$L\mathbf{1}_{n+1} = 0\mathbf{1}_{n+1}. \tag{3.2}$$

Network dynamics

One of the agents is assumed to be a virtual source agent [92], which can be used to specify a desired consensus value X_s. Without loss of generality, the state $\hat{X}_{n+1}$ of last $n+1$ node is assumed to be a virtual source agent X_s, where $s = n+1$. Moreover, each agent in the network should have access to the virtual source agent X_s through the network, as formalized below. Note that this is a less stringent requirement than the graph without the virtual source being strongly connected.

Assumption 1 (Rooted graph) *The digraph $\mathcal{G}$ is assumed to have a directed path from the source node $n+1$ to any other node i in the graph, i.e., $i \in \mathcal{V} \setminus (n+1)$.* □

Some properties of the graph $\mathcal{G}$ without the source node $s = n+1$, i.e., $\mathcal{G} \setminus s$, are listed below. In particular, consider the $n \times n$ pinned Laplacian matrix K associated with $\mathcal{G} \setminus s$ obtained by removing the row and column associated with the source node $n+1$ through

the partitioning of the Laplacian L, i.e.,

$$L = \left[\begin{array}{c|c} K & -B \\ \hline & L_b \end{array}\right] \tag{3.3}$$

where L_b is the $1 \times (n+1)$ size row vector of Laplacian L corresponding the source node $s = n+1$ and B is an $n \times 1$ vector

$$\begin{aligned} B &= [a_{1,s}, a_{2,s}, \ldots, a_{n,s}]^T \\ &= [B_1, B_2, \ldots, B_n]^T, \end{aligned} \tag{3.4}$$

and non-zero value of B_j implies that the agent j is directly connected to the source X_s. The properties of the pinned Laplacian K follow from Assumption 1, e.g., see [36].

1. The pinned Laplacian matrix K is invertible, i.e.,

$$\det\{(K)\} \neq 0. \tag{3.5}$$

2. The eigenvalues of the pinned Laplacian K have strictly-positive, real parts.

3. The product of the inverse of the pinned Laplacian K with B leads to an $n \times 1$ vector of ones, $\mathbf{1}_n$, i.e.,

$$K^{-1}B = \mathbf{1}_n. \tag{3.6}$$

The dynamics of the n non-source agents with state vector, X represented by the remaining graph $\mathcal{G}\backslash s$, can be given by

$$\begin{aligned} X[k+1] &= X[k] - \alpha K X[k] + \alpha B X_s[k] \\ &= (\mathbf{I_n} - \alpha K)\, X[k] + \alpha B X_s[k] \\ &= P X[k] + \alpha B X_s[k]. \end{aligned} \tag{3.7}$$

where the matrix $P = \mathbf{I}_n - \alpha K$, $\mathbf{I}_n$ is the $n \times n$ identity matrix, and α is the update gain.

Stability conditions

Bounds can be established on the update gain α to ensure stability. For any eigenvalue $\lambda_{K,m} = a_m + jb_m$ of graph Laplacian K, with real part $a_m > 0$ (from Assumption 1) and imaginary part b_m, the corresponding eigenvalue of the matrix P is given by

$$\lambda_{P,m} = 1 - \alpha(a_m + jb_m). \tag{3.8}$$

For stability of the non-source dynamics in Eq. (3.7), the magnitude of $\lambda_{P,m}$ needs to be less than one, i.e.,

$$|1 - \alpha(a_m + jb_m)| < 1, \forall\ m \in \{1, 2, \ldots, n\}. \tag{3.9}$$

This condition for stability is met if the update gain α satisfies [37]

$$0 < \alpha < \min_{1 \leq m \leq n} \frac{2a_m}{a_m^2 + b_m^2} = \overline{\alpha}. \tag{3.10}$$

Convergence to consensus

With a stabilizing update gain α as in Eq. (3.10), the state X of the network (of all non-source agents) converges to a fixed source value X_s, e.g., for a step change in the source value X_s from x_i to x_f, i.e., $X_s[k] = x_i$, $\forall\ k < 0$ (initial desired state) and $X_s[k] = x_f$, $\forall\ k \geq 0$. Since the eigenvalues $\lambda_{P,m}$ of the matrix P are inside the unit circle, the solution to Eq. (3.7) for the step input converges,

$$\begin{aligned} X[k+1] - X[k] &= P\left(X[k] - X[k-1]\right) \\ &= P^k\left(X[1] - X[0]\right) \to 0, \end{aligned} \tag{3.11}$$

as $k \to \infty$ because $P^k \to 0$. Thus, $\lim_{k\to\infty} X[k+1] = \lim_{k\to\infty} X[k]$, and from the first line of Eq. (3.7),

$$\lim_{k\to\infty} KX[k] = Bx_f. \tag{3.12}$$

As a result, from the invertibility of K in Eq. (3.5), and $K^{-1}B = \mathbf{1}_n$ from Eq. (3.6), the limit for the state $X[k]$ is found to be

$$X[k] \to K^{-1}Bx_f =\to \mathbf{1}_n x_f \quad \text{as} \quad k \to \infty. \tag{3.13}$$

Thus, the control law in Eq. (3.7) achieves consensus.

Spectral radius and rate of convergence

The rate of convergence to consensus depends on the spectral radius $\sigma(P)$ of the matrix P given by

$$\sigma(P) = \max_m |\lambda_{P,m}| = \max_m |1 - \alpha\lambda_{K,m}| < 1. \tag{3.14}$$

Note that for any $\epsilon > 0$, say

$$\epsilon = \frac{1 - \sigma(P)}{2} > 0 \tag{3.15}$$

there exists a nonsingular matrix Q such that the modified vector norm $\|X\| = \|QX\|_\infty$ with the corresponding induced matrix norm $\|\cdot\|$ satisfies, see [93] (Section 5.3.5),

$$\|P\| \ \leq \ \sigma(P) + \epsilon \ = \frac{1 + \sigma(P)}{2} \ < 1. \tag{3.16}$$

Hence, from Eq. (3.11),

$$\begin{aligned} \|X[k+1] - X[k]\| &\leq \|P\|^{k+1} \|\mathbf{1}_n(x_f - x_i)\| \\ &\leq \left[\sigma(P) + \epsilon\right]^{k+1} \|\mathbf{1}_n(x_f - x_i)\|. \end{aligned} \tag{3.17}$$

Since ϵ can be chosen to be arbitrarily small, minimizing the spectral radius $\sigma(P)$ of the matrix P results in faster convergence.

3.1.2 Convergence with structural robustness

The structural robustness of the network's stability depends on the spectral radius $\sigma(P)$ of the matrix P [35]. For the network to be stable, the eigenvalues of the matrix P need to be inside the unit circle. Hence, the smallest distance d of its eigenvalues $\lambda_{P,m}$ from the unit circle is a measure of the network's structural stability, i.e., robustness to perturbations, where

$$d = 1 - \sigma(P). \tag{3.18}$$

Minimizing the spectral radius $\sigma(P)$ results in increased structural robustness. Therefore, rapid structurally-robust convergence is achieved during transitions if the spectral radius $\sigma(P)$ is minimized. The optimal update gain α^* for minimum spectral radius σ^*, with the standard consensus dynamics (in Eq. (3.7)) referred to as no-DSR approach hereon, can be found through a search based method, as

$$\sigma^* = \min_{\alpha} \sigma(P) = \min_{0<\alpha<\overline{\alpha}} \left[\max_{m} |1 - \alpha\lambda_{K,m}| \right]. \tag{3.19}$$

Remark 1 *[Optimal no-DSR for real spectrum] For the special case when the graph has real spectrum, i.e., eigenvalues of the pinned Laplacian K are real and satisfy*

$$0 < \underline{\lambda} = \lambda_{K,1} \leq \lambda_{K,2} \leq \ldots \leq \lambda_{K,n} = \overline{\lambda} = \sigma(K), \tag{3.20}$$

the stability condition in Eq. (3.10)*, becomes*

$$0 < \alpha < \frac{2}{(\overline{\lambda})} = \overline{\alpha}. \tag{3.21}$$

If the extremal eigenvalues are distinct, i.e., $\underline{\lambda} \neq \overline{\lambda}$, then the update gain α^* that minimizes the spectral radius $\sigma(P)$ is given by [94]

$$\alpha^* = \frac{2}{\overline{\lambda} + \underline{\lambda}} < \frac{2}{(\overline{\lambda})}, \tag{3.22}$$

and the associated minimum spectral radius is

$$\sigma^* = \sigma(P^*) = \frac{\overline{\lambda} - \underline{\lambda}}{\overline{\lambda} + \underline{\lambda}}. \tag{3.23}$$

If the extremal eigenvalues are the same, $\underline{\lambda} = \overline{\lambda}$ (e.g., in first-order platoon networks), then the spectral radius of the matrix ($\sigma(P)$) can be made the ideal value of zero, $\sigma^* = 0$, resulting in maximally fast convergence.

3.1.3 The robust convergence optimization problem

The range of acceptable update gain α in Eq. (3.10), limits the convergence rate. The research problem addressed is to further reduce the spectral radius of the matrix P, i.e. to improve the structural robustness and convergence rate, when each agent can modify its update law

1. using only existing information from the network neighbors, and

2. without changing the network structure (network connectivity K).

3.2 Proposed Solution

This section introduces the proposed Accelerated Delayed Self Reinforcement (A-DSR) approach to achieve structurally-robust convergence and establishes stability conditions.

3.2.1 The A-DSR approach

Graph's Laplacian potential

For undirected graphs, the control law u in Eq. (2.1) can be considered as a gradient-based search on the graph's Laplacian potential $\Phi_{\mathcal{G}}$ [54, 95]

$$\Phi_{\mathcal{G}}(\hat{X}) = \frac{1}{2}\sum_{i,j=1}^{n} a_{i,j}\left(\hat{X}_j - \hat{X}_i\right)^2 = \hat{X}^T L \hat{X}, \tag{3.24}$$

which results in the standard graph-based update law as in Eq. (2.1),

$$\begin{aligned}\hat{X}[k+1] &= \hat{X}[k] - \frac{\alpha}{2}\nabla\Phi_{\mathcal{G}}(\hat{X}[k]) \\ &= \hat{X}[k] - \alpha L\hat{X}[k].\end{aligned} \tag{3.25}$$

Nesterov's accelerated-gradient-based update

In general, the convergence of the gradient-based approach as in Eq. (3.25) can be improved using accelerated methods. In particular, applying the Nesterov modification [43, 44] of the traditional gradient-based method to Eq. (3.25) results in the accelerated-gradient-based modification of the system in Eq. (2.1) to

$$\begin{aligned}\hat{X}[k+1] &= \hat{X}[k+1] + \beta\left(\hat{X}[k] - \hat{X}[k-1]\right) \\ &\quad - \frac{\alpha}{2}\nabla\Phi_{\mathcal{G}}\left\{\hat{X}[k] + \beta\left(\hat{X}[k] - \hat{X}[k-1]\right)\right\} \\ &= \hat{X}[k] + \beta\left(\hat{X}[k] - \hat{X}[k-1]\right) \\ &\quad - \hat{\alpha}L\left\{\hat{X}[k] + \beta\left(\hat{X}[k] - \hat{X}[k-1]\right)\right\},\end{aligned} \tag{3.26}$$

where β is a scalar gain on the Nesterov-based terms and

$$\hat{\alpha} = \alpha(1+\beta). \tag{3.27}$$

Consequently, the dynamics of the non-source agents X represented by the remaining graph $\mathcal{G}\backslash s$, i.e., Eq. (3.7), becomes

$$\begin{aligned} X[k+1] \;\; &= X[k] - \hat{\alpha}K\left\{X[k] + \beta\left(X[k] - X[k-1]\right)\right\} \\ &\quad +\beta\left(X[k] - X[k-1]\right) \\ &\quad +\hat{\alpha}B\{X_s[k] + \beta\left(X_s[k] - X_s[k-1]\right)\} \end{aligned} \tag{3.28}$$

The additional third term $\beta\left(X[k] - X[k-1]\right)$ on the right hand side of Eq. (3.28) is referred to as the momentum term (this term alone forms the Heavy ball method in [96]) and the similar terms inside the curly brackets of the second and fourth terms are referred to as the outdated-feedback addition.

Directed graphs

For general directed graphs, the potential function $\Phi_{\mathcal{G}}$ in Eq. (3.24) does not lead to the standard update equations [54,55]. Nevertheless, motivated by the gradient-based approach, for each non-source agent, $1 \leq i \leq n$, a modified potential can be considered as

$$\Phi_{\mathcal{G},i}(\hat{X}) = \sum_{j=1}^{n+1} a_{i,j}\left(\hat{X}_i - \hat{X}_j\right)^2. \tag{3.29}$$

Here $\Phi_{\mathcal{G},i}$ is a localized version of the graph's Laplacian potential [54, 55], whose gradient with respect to $\hat{X}_i = X_i$

$$u_i(\hat{X}) = -\frac{\alpha}{2}\frac{\partial \Phi_{\mathcal{G},i}}{\partial \hat{X}_i} = -\alpha K_i X + \alpha B_i X_s \tag{3.30}$$

with K_i as the i^{th} row of K, B_i the i^{th} row of the source connectivity vector B, will lead to the standard update equations for each agent's state X_i in the state vector X of non-source agents, as

$$X_i[k+1] = X_i[k] - \alpha K_i X[k] + \alpha B_i X_s[k]. \tag{3.31}$$

The application of the accelerated-gradient approach for local potential $\Phi_{\mathcal{G},i}(\hat{X})$ in Eq. (3.29) (which does not necessarily decrease the graph potential ($\Phi_{\mathcal{G}}(\hat{X})$) in Eq. (3.24), [43,44]) leads to the same Eq. (3.28).

A-DSR update

The Nesterov-update law in Eq. (3.28) uses the same gain β for the momentum and the outdated-feedback terms (Nesterov's accelerated method in [97]). A generalization of this is to use different gains β_1, β_2 for the outdated-feedback and momentum terms (respectively), as used before in optimization theory [98],

$$\begin{aligned} X[k+1] \quad &= X[k] - \hat{\alpha} K \{X[k] + \beta_1 (X[k] - X[k-1])\} \\ &\quad + \beta_2 (X[k] - X[k-1]) \\ &\quad + \hat{\alpha} B \{X_s[k] + \beta_1 (X_s[k] - X_s[k-1])\}. \end{aligned} \tag{3.32}$$

where, from Eq. (3.27), $\hat{\alpha} = \alpha(1+\beta_1)$. The above accelerated approach, is referred to as the accelerated delayed self reinforcement (A-DSR) in the following, since it does not require additional information from the network, or having to change the network connectivity. Rather, each agent uses delayed versions of known information to reinforce its own update. To illustrate, for each non-source agent i, let x_i be the information obtained from the network, i.e.,

$$x_i[k] \quad = \hat{\alpha} K_i X[k], \tag{3.33}$$

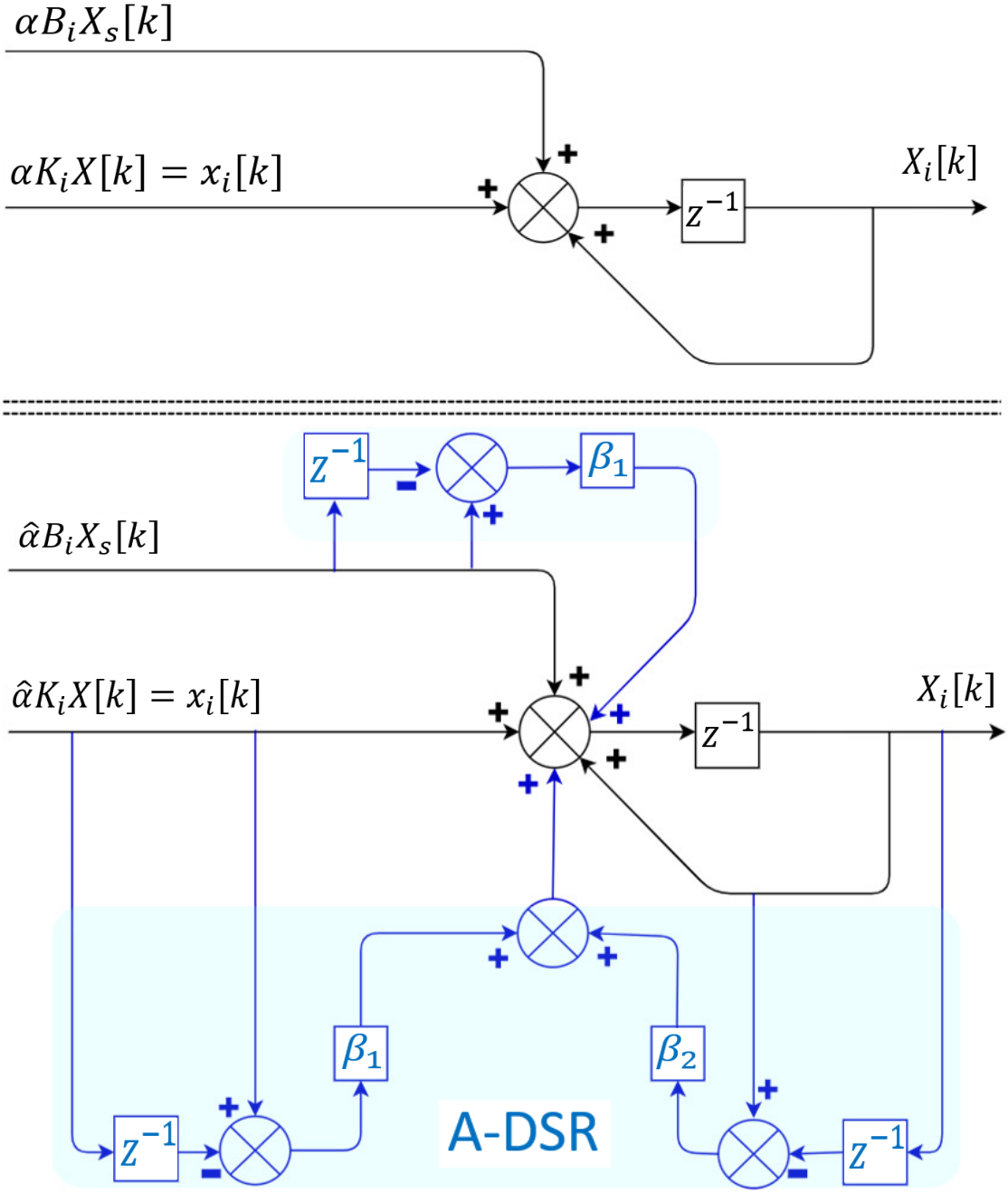

Figure 3.1: (Top) Implementation of standard consensus-based approach to multi-agent networks for the i^{th} agent as in Eq. (3.7). (Bottom) Accelerated delayed self reinforcement (A-DSR) approach for the i^{th} agent in Eq. (3.32) without using additional network information.

where K_i is the i^{th} row of the pinned Laplacian K. Then, the update of agent X_i is, from Eq. (3.32),

$$\begin{aligned} X_i[k+1] \;\; &= X_i[k] - \{x_i[k] + \beta_1(x_i[k] - x_i[k-1])\} \\ &\quad +\beta_2\left(X_i[k] - X_i[k-1]\right) \\ &\quad +\hat{\alpha}B_i\{X_s[k] + \beta_1\left(X_s[k] - X_s[k-1]\right)\}, \end{aligned} \tag{3.34}$$

where B_i is the i^{th} row of the source connectivity vector B. The delayed self-reinforcement (DSR) approach, however, requires each agent to store delayed versions $X_i[k-1]$ and $x_i[k-1]$ of its current state $X_i[k]$ and information $x_i[k]$ from the network, as illustrated in Fig. 3.1. □

Remark 2 *The A-DSR method in Eq.* (3.32) *without the momentum term (i.e., $\beta_2 = 0$) is referred to as the Outdated-feedback method, without the outdated-feedback term (i.e., $\beta_1 = 0$) is referred to as the Momentum method, and with equal parameters (i.e., $\beta_1 = \beta_2 = \beta$) is referred to as the Nesterov-update method.*

Remark 3 (Stability for directed graphs) *The local Laplacian potential in Eq.* (3.29) *whose gradient is used for deriving each agent's standard update (in Eq.* (3.31)*) and A-DSR approach (in Eq.* (3.34)*), doesn't reduce the overall Laplacian potential [55] of the directed graph. Thus the convergence studies from optimization theory (which require the graphs to be strongly connected, e.g., [56, 57]) cannot be used to establish stability for general directed graphs.*

3.2.2 Stability of A-DSR

The stability conditions for the general A-DSR approach in Eq. (3.32) are presented below.

Diagonalizing the pinned Laplacian

The network with A-DSR in Eq. (3.32) can be decomposed into subsystems using an invertible transformation matrix P_K as

$$X[k] = P_K X_J[k], \tag{3.35}$$

where the transformation matrix P_K is selected to diagonalize the pinned Laplacian K as

$$K_J = P_K^{-1} K P_K \tag{3.36}$$

where the diagonal terms of matrix K_J are the eigenvalues $\lambda_{K,m}$ for $m = 1, 2, ..., n$, which can be complex and with multiplicity greater than 1. Since input doesn't affect stability, setting $X_s[k] = 0$, $\forall\, k$, and pre-multiplying the Eq. (3.32) with P_k^{-1} results in

$$\begin{aligned} &X_J[k+1] - X_J[k] + \hat{\alpha} K_J (X_J[k] \\ &+ \beta_1 (X_J[k] - X_J[k-1])) \\ &- \beta_2 (X_J[k] - X_J[k-1]) = 0. \end{aligned} \tag{3.37}$$

The stability of network with A-DSR in Eq. (3.32) is equivalent to the stability of Eq. (3.37) in the transformed coordinate.

Characteristic equations

Taking the z-transform of Eq. (3.37) results in

$$\begin{aligned} &(z^2 \mathbf{I}_n - z\left[(1+\beta_2)\mathbf{I}_n - \hat{\alpha}(1+\beta_1) K_J\right] \\ &- (\hat{\alpha}\beta_1 K_J - \beta_2 \mathbf{I}_n)) X_J(z) = 0. \end{aligned} \tag{3.38}$$

Therefore, the network with A-DSR update in Eq. (3.32) is stable if and only if, for each eigenvalue $\lambda_{K,m}$ of the pinned Laplacian K, the roots of the following characteristic equation

$$\begin{aligned} D(z) = z^2 + z\left[\hat{\alpha}(1+\beta_1)\lambda_{K,m} - (1+\beta_2)\right] \\ + (\beta_2 - \hat{\alpha}\beta_1\lambda_{K,m}) \quad = 0 \end{aligned} \tag{3.39}$$

have magnitude less than one. For the case of complex eigenvalue $\lambda_{K,m} = a_m + jb_m$, the real Jordan form of the z-transform of the diagonalized general A-DSR update equation in Eq. (3.37), for the block associated with the Laplacian eigenvalue pair $a_m \pm jb_m$ is

$$\begin{aligned} z^2\mathbf{I}_2 - z\left((1+\beta_2)\mathbf{I}_2 - \hat{\alpha}(1+\beta_1)\begin{bmatrix} a_m & b_m \\ -b_m & a_m \end{bmatrix}\right) \\ - \left(\hat{\alpha}\beta_1\begin{bmatrix} a_m & b_m \\ -b_m & a_m \end{bmatrix} - \beta_2\mathbf{I}_2\right), \end{aligned} \tag{3.40}$$

where $\mathbf{I}_2$ denotes an identity matrix of size 2×2, a_m and b_m are the real and imaginary parts of $\lambda_{K,m}$. The determinant of Eq. (3.40) yields a fourth order equation of the form

$$D(z) = z^4 + a_3 z^3 + a_2 z^2 + a_1 z + a_0 = 0, \tag{3.41}$$

where

$$\begin{aligned} a_0 &= (a_m\hat{\alpha}\beta_1 - \beta_2)^2 + \hat{\alpha}^2 b_m^2\beta_1^2, \\ a_1 &= -2\{(a_m\hat{\alpha}\beta_1 - \beta_2)^2 + a_m\hat{\alpha}\beta_1(a_m\hat{\alpha} - 1) \\ &\quad + \hat{\alpha}(\hat{\alpha}b_m^2\beta_1 - a_m\beta_2) + \hat{\alpha}^2 b_m^2\beta_1^2 + \beta_2\}, \\ a_2 &= (a_m\hat{\alpha}\beta_1 - \beta_2)^2 + (a_m\hat{\alpha} - 1)^2 + 2\hat{\alpha}^2\beta_1(a_m^2 + b_m^2), \\ &\quad + 4\beta_2 - 2a_m\hat{\alpha}(2\beta_1 + \beta_2) + \hat{\alpha}^2 b_m^2(\beta_1^2 + 1), \\ a_3 &= 2a_m\hat{\alpha}(\beta_1 + 1) - 2(\beta_2 + 1). \end{aligned} \tag{3.42}$$

Hence, for the complex eigenvalue case, the stability of the A-DSR (in Eq. (3.32)) can be determined by obtaining conditions for the roots of Eq. (3.41) to be within unit circle on the

complex plane.

Stability conditions

Stability conditions follow from the Jury test.

Lemma 1 *[Jury test based stability] The generalized A-DSR in Eq.* (3.32) *is stable if and only if the A-DSR gains* $\hat{\alpha}$, β_1 *and* β_2 *satisfy the following conditions, for each eigenvalue* $\lambda_{K,m}$ *of the pinned Laplacian* K.

1. *If the eigenvalue* $\lambda_{K,m} = a_m$ *is real valued, then*

$$\begin{aligned} &(i)\ 0 < \hat{\alpha} \\ &(ii)\ \left[\hat{\alpha} a_m(\beta_1 + \frac{1}{2}) - 1\right] < \beta_2 < (\hat{\alpha}\beta_1 a_m + 1) \end{aligned} \tag{3.43}$$

2. *If the eigenvalue* $\lambda_{K,m} = a_m + jb_m$ *is complex valued (i.e.,* $b_m \neq 0$*), then*

$$\begin{aligned} &(i)\ 0 < \hat{\alpha}^2, \\ &(ii)\ 0 < (2(\beta_2+1) - \hat{\alpha}(2\beta_1+1)a_m)^2 \\ &\qquad\qquad + \hat{\alpha}^2(2\beta_1+1)^2 b_m^2, \\ &(iii)\ -1 < (a_m\hat{\alpha}\beta_1 - \beta_2)^2 + \hat{\alpha}^2 b_m^2 \beta_1^2 < 1, \\ &(iv)\ |a_0 a_3 - a_1| < |a_0^2 - 1|, \\ &(v)\ |a_2(a_0^2-1)(a_0-1) - (a_0a_1 - a_3)(a_0a_3 - a_1)| \\ &\qquad < |(a_0^2-1)^2 - (a_0a_3 - a_1)^2|. \end{aligned} \tag{3.44}$$

Proof If the eigenvalue $\lambda_{K,m}$ is real valued, then, the Jury test leads to the following three necessary and sufficient conditions for the roots of the characteristic equation in Eq. (3.39) to have magnitude less than one.

1. $D(z=1)>0$

$$\begin{aligned} &1+[\hat{\alpha}(1+\beta_1)\lambda_{K,m}-(1+\beta_2)]+(\beta_2-\hat{\alpha}\beta_1\lambda_{K,m})>0 \\ &=>\hat{\alpha}>0, \end{aligned} \tag{3.45}$$

which is satisfied due to the first condition in Eq. (3.43).

2. $(-1)^2 D(z=-1)>0$

$$\begin{aligned} &1-[\hat{\alpha}(1+\beta_1)\lambda_{K,m}-(1+\beta_2)]+(\beta_2-\hat{\alpha}\beta_1\lambda_{K,m})>0 \\ &=>\beta_2>\hat{\alpha}\lambda_{K,m}\left(\beta_1+\frac{1}{2}\right)-1 \end{aligned} \tag{3.46}$$

or

$$(\hat{\alpha}\beta_1\lambda_{K,m}-1)+\frac{\hat{\alpha}\lambda_{K,m}}{2}<\beta_2. \tag{3.47}$$

3. $|D(z=0)|<1$

$$|\beta_2-\hat{\alpha}\beta_1\lambda_{K,m}|<1$$

or

$$(\hat{\alpha}\beta_1\lambda_{K,m}-1)<\beta_2<(1+\hat{\alpha}\beta_1\lambda_{K,m}). \tag{3.48}$$

As $\hat{\alpha}\lambda_{K,m}>0$ (since $\hat{\alpha}>0$ from Eq. (3.45) and $\lambda_{K,m}>0$ from Assumption 1), the condition in Eq. (3.47) is more stringent than the lower bound on β_2 in Eq. (3.48), resulting in condition (ii) of Eq. (3.43).

If the eigenvalue $\lambda_{K,m}=a_m+jb_m$ is complex valued ($b_m\neq 0$), then, the Jury test leads to the following necessary and sufficient conditions for stable roots of the characteristic equation in Eq. (3.41).

1. $D(z=1)>0$

$$\begin{aligned} &1+a_3+a_2+a_1+a_0>0, \\ &=>\hat{\alpha}^2(a_m^2+b_m^2)>0, \end{aligned} \tag{3.49}$$

which can be simplified further (since $a_m>0$ from Assumption 1) as condition (i) in Eq. (3.44).

2. $(-1)^4 D(z=-1)>0$ resulting in condition (ii) of Eq. (3.44) since

$$\begin{aligned} 0 &< 1-a_3+a_2-a_1+a_0 \\ &= (2(\beta_2+1)-\hat{\alpha}(2\beta_1+1)a_m)^2 \\ &\quad +\hat{\alpha}^2(2\beta_1+1)^2 b_m^2. \end{aligned} \tag{3.50}$$

3. $|D(z=0)|<1$

$$\begin{aligned} &|(a_m\hat{\alpha}\beta_1-\beta_2)^2+\hat{\alpha}^2 b_m^2\beta_1^2|<1. \\ &=> -1<(a_m\hat{\alpha}\beta_1-\beta_2)^2+\hat{\alpha}^2 b_m^2\beta_1^2<1. \end{aligned} \tag{3.51}$$

In addition to the above three conditions (which are similar to the real eigenvalue case), the complex case has two additional stability conditions (iv) and (v) in Eq. (3.44) from the Jury test. □

Robust stability with general A-DSR

Independently varying the gains of momentum and outdated-feedback terms gives additional flexibility, which can be used to further improve the robust convergence when compared to the case without A-DSR. More formally, the general A-DSR approach can be used to minimize the maximum magnitude $\bar{z}_m$ of the roots $(z_{\lambda_{K,m},1}, z_{\lambda_{K,m},2})$ of the characteristic equation $D(z)=0$ in Eq. (3.39) associated with the eigenvalues $\lambda_{K,m}$ of the pinned Laplacian K, i.e.,

$$\sigma^* = \min_{\hat{\alpha},\beta_1,\beta_2} \left[\max_m(\bar{z}_m)|\right], \tag{3.52}$$

where $\bar{z}_m = \max(|z_{\lambda_{K,m},1}|, |z_{\lambda_{K,m},2}|)$.

3.2.3 Graphs with real spectrum

In general, using different gains for the momentum and outdated-feedback terms (i.e., different values of β_1, β_2) can yield better performance than using the same gains for each term. However, for graphs with real spectrum (which includes all undirected graphs), the momentum term is sufficient to yield fast convergence and balanced robustness, as shown below.

Assumption 2 (Real spectrum) *In this section, the pinned Laplacian K is assumed to have real eigenvalues, ordered as in Eq.* (3.20).

Stability given range of Laplacian eigenvalues

The application of Lemma 1 requires knowledge of all eigenvalues $\lambda_{K,m}$ of the pinned Laplacian K. The following corollary provides sufficient conditions for stability in terms of the range $[\underline{\lambda}\ \overline{\lambda}]$ of the eigenvalues $\lambda_{K,m}$ from Eq. (3.20). To begin, the stability condition for general A-DSR update in Eq. (3.43) is used to deduce stability for the other (Nesterov-update, momentum and outdated-feedback defined in Remark 2) methods for graphs with real spectrum.

Corollary 1 *The network update as in Eq.* (3.32)*, for the following accelerated methods, is stable if and only if $\hat{\alpha} > 0$, and the gains satisfy the following for each eigenvalue $\lambda_{K,m}$ of the pinned Laplacian K.*

1. *Nesterov-update method in Eq.* (3.28) *[52] with $\beta_1 = \beta_2 = \beta$:*

$$\frac{\hat{\alpha}\lambda_{K,m}}{2} - 1 < \beta(1 - \hat{\alpha}\lambda_{K,m}) < 1. \tag{3.53}$$

2. Momentum method ($\beta_1 = 0$):

$$\frac{\hat{\alpha}\lambda_{K,m}}{2} - 1 < \beta_2 < 1. \tag{3.54}$$

3. Outdated-feedback method ($\beta_2 = 0$):

$$-1 < \hat{\alpha}\lambda_{K,m}\beta_1 < 1 - \frac{\hat{\alpha}\lambda_{K,m}}{2}. \tag{3.55}$$

Proof For the Nesterov-update method ($\beta_1 = \beta_2 = \beta$), the stability condition in Eq. (3.43) becomes

$$\left[\hat{\alpha}\lambda_{K,m}(\beta + \frac{1}{2}) - 1\right] < \beta < (\hat{\alpha}\beta\lambda_{K,m} + 1)\,, \tag{3.56}$$

and subtracting $\hat{\alpha}\beta\lambda_{K,m}$ from both sides results in Eq. (3.53). For the momentum method, Eq. (3.43) becomes Eq. (3.54) with $\beta_1 = 0$. For the outdated-feedback method, with $\beta_2 = 0$, Eq. (3.43) becomes

$$\left[\hat{\alpha}\lambda_{K,m}(\beta_1 + \frac{1}{2}) - 1\right] \ < 0 < (\hat{\alpha}\beta_1\lambda_{K,m} + 1)\,. \tag{3.57}$$

The left inequality in Eq. (3.57) can be simplified to

$$\hat{\alpha}\lambda_{K,m}\beta_1 < 1 - \frac{\hat{\alpha}\lambda_{K,m}}{2} \tag{3.58}$$

and the right inequality becomes

$$\hat{\alpha}\lambda_{K,m}\beta_1 > -1, \tag{3.59}$$

resulting in the stability condition in Eq. (3.55). □

Corollary 2 *The network update as in Eq.* (3.32)*, for the following accelerated methods, is*

stable if and only if $\hat{\alpha} > 0$*, and the gains satisfy the following, where*

$$\lambda_* = \begin{cases} \underline{\lambda} & if \quad \beta_1 \leq -\frac{1}{2} \\ \overline{\lambda} & if \quad \beta_1 > -\frac{1}{2} \end{cases}$$
$$\lambda^* = \begin{cases} \overline{\lambda} & if \quad \beta_1 \leq 0 \\ \underline{\lambda} & if \quad \beta_1 > 0 \end{cases} \tag{3.60}$$

1. *Generalized A-DSR method:*

$$\left[\hat{\alpha}\lambda_*(\beta_1 + \frac{1}{2}) - 1\right] < \beta_2 < (\hat{\alpha}\beta_1\lambda^* + 1)\,. \tag{3.61}$$

2. *Nesterov-update method* ($\beta_1 = \beta_2 = \beta$)*:*

$$\left[\hat{\alpha}\lambda_*(\beta + \frac{1}{2}) - 1\right] < \beta < (\hat{\alpha}\beta\lambda^* + 1)\,. \tag{3.62}$$

3. *Momentum method* ($\beta_1 = 0$)*:*

$$\frac{\hat{\alpha}\lambda_*}{2} - 1 < \beta_2 < 1. \tag{3.63}$$

4. *Outdated-feedback method* ($\beta_2 = 0$)*:*

$$\left[\hat{\alpha}\lambda_*(\beta_1 + \frac{1}{2}) - 1\right] \quad < 0 < (\hat{\alpha}\beta_1\lambda^* + 1)\,. \tag{3.64}$$

Proof This follows from Lemma 1 and the proof of Corollary 1 since

$$\hat{\alpha}\lambda_{K,m}(\beta_1 + \frac{1}{2}) \leq \hat{\alpha}\lambda_*\beta_1, \quad \hat{\alpha}\lambda^*\beta_1 \leq \hat{\alpha}\lambda_{K,m}\beta_1$$

for all eigenvalues $\lambda_{K,m}$ of the pinned Laplacian K. Therefore, the conditions in this corollary

are more stringent that the conditions in Lemma 1 and Corollary 1. □

Optimal A-DSR for graphs with real spectrum

Fast convergence with structural robustness for A-DSR in networks with real spectrum is presented below, which is similar to the structurally-robust convergence without A-DSR in Section 3.1.2. Note that the characteristic equation in Eq. (3.39) with A-DSR for networks with real spectrum is equivalent to that of a standard second order system of the form,

$$D(z) = z^2 + 2\zeta_{\lambda_{K,m}}\omega_{\lambda_{K,m}} z + \omega^2_{\lambda_{K,m}} = 0, \tag{3.65}$$

where

$$\begin{aligned} \omega^2_{\lambda_{K,m}} &= (\beta_2 - \hat{\alpha}\beta_1\lambda_{K,m}), \\ \zeta_{\lambda_{K,m}} &= \frac{\hat{\alpha}(1+\beta_1)\lambda_{K,m} - (1+\beta_2)}{2\omega_{\lambda_{K,m}}}, \end{aligned} \tag{3.66}$$

with two roots ($z_{\lambda_{K,m},i}$, $i \in \{1,2\}$) associated with each real eigenvalue $\lambda_{K,m}$ of the pinned Laplacian K. As in the case without A-DSR, the goal is to select the roots ($z_{\underline{\lambda},i}, z_{\overline{\lambda},i}, i \in \{1,2\}$) of the characteristic equation in Eq. (3.39) for A-DSR, associated with the extremal eigenvalues $\lambda = \underline{\lambda}, \overline{\lambda}$ of the pinned Laplacian K, to be equidistant from origin (for similar structural robustness)

$$|z_{\underline{\lambda}}| = |z_{\underline{\lambda},1}| = |z_{\underline{\lambda},2}| = |z_{\overline{\lambda},1}| = |z_{\overline{\lambda},2}| = |z_{\overline{\lambda}}| \tag{3.67}$$

and be farthest away from the unit circle (for fast convergence), i.e., by choosing the A-DSR parameters $\hat{\alpha}, \beta_1, \beta_2$ to solve the following minimization problem

$$\min_{\hat{\alpha},\beta_1,\beta_2} \left[|z_{\underline{\lambda}}| = |z_{\overline{\lambda}}| \right]. \tag{3.68}$$

Furthermore, the roots of Eq. (3.39) associated with the dominant eigenvalue $\underline{\lambda}$ of the pinned

Laplacian are critically damped and positive, i.e.,

$$\zeta_{\underline{\lambda}} = -1, \qquad z_{\underline{\lambda},1} = z_{\underline{\lambda},2} > 0, \tag{3.69}$$

as in the case without A-DSR, which can help to reduce oscillations in the response.

Lemma 2 *[Parameter selection for Robust A-DSR] Let (i) the A-DSR parameter be chosen to be positive $\hat{\alpha} > 0$ to meet the stability condition in Eq.* (3.43)*, and (ii) the pinned Laplacian K have at least two distinct eigenvalues, i.e., $\overline{\lambda} \neq \underline{\lambda}$ in Eq.* (3.20)*. Then, the A-DSR parameters $(\hat{\alpha}, \beta_1, \beta_2)$*

$$\hat{\alpha} = \frac{4}{(\sqrt{\overline{\lambda}} + \sqrt{\underline{\lambda}})^2}, \quad \beta_1 = 0, \quad \beta_2 = \frac{(\sqrt{\overline{\lambda}} - \sqrt{\underline{\lambda}})^2}{(\sqrt{\overline{\lambda}} + \sqrt{\underline{\lambda}})^2} \tag{3.70}$$

result in

1. *balanced robustness of the extremal modes, i.e., satisfies Eq.* (3.67)*, the roots $z_{\underline{\lambda},i}, z_{\overline{\lambda},i}, i \in \{1, 2\}$ as in Eq.* (3.67)

2. *critical damping of the dominant mode, i.e., $\zeta_{\underline{\lambda}} = -1$ as in Eq.* (3.69)*, and*

3. *optimal convergence, i.e., achieves the minimization in Eq.* (3.68)*.*

Proof This is shown below in four steps.

Step 1 is to show that the roots of Eq. (3.39) associated with the extremal eigenvalue $\overline{\lambda}$ of the pinned Laplacian cannot be overdamped. Note that if the damping ratio $\zeta_{\overline{\lambda}}$ of the roots $z_{\overline{\lambda},1}, z_{\overline{\lambda},2}$ in Eq. (3.39) associated with the extremal eigenvalue $\overline{\lambda}$ is larger than one in magnitude, i.e., $|\zeta_{\overline{\lambda}}| > 1$, then the roots

$$\begin{aligned} z_{\overline{\lambda},1} &= -\left(\zeta_{\overline{\lambda}}\, \omega_{\overline{\lambda}}\right) + \omega_{\overline{\lambda}} \sqrt{\zeta_{\overline{\lambda}}^2 - 1} \\ z_{\overline{\lambda},2} &= -\left(\zeta_{\overline{\lambda}}\, \omega_{\overline{\lambda}}\right) - \omega_{\overline{\lambda}} \sqrt{\zeta_{\overline{\lambda}}^2 - 1}\ , \end{aligned} \tag{3.71}$$

are real and distinct and have different magnitudes $|z_{\overline{\lambda},1}| \neq |z_{\overline{\lambda},2}|$, which cannot satisfy the lemma's equidistant condition as in Eq. (3.67). Therefore, the roots $z_{\overline{\lambda},1}, z_{\overline{\lambda},2}$ of Eq. (3.39) associated with the extremal eigenvalue $\overline{\lambda}$ of the pinned Laplacian cannot be overdamped, i.e.,

$$|\zeta_{\overline{\lambda}}| \leq 1. \tag{3.72}$$

Step 2 is to show that the equidistant condition of the lemma, as in Eq. (3.67), leads to a zero outdated-feedback gain, $\beta_1 = 0$. Since the magnitude of the damping ratio is not more than one, $|\zeta_{\overline{\lambda}}| \leq 1$ from Eq. (3.72), the term $\zeta_{\overline{\lambda}}^2 - 1$ becomes non-positive in Eq. (3.71), and therefore its square root is either a complex number (when $|\zeta_{\overline{\lambda}}| < 1$) or zero (when $|\zeta_{\overline{\lambda}}| = 1$), and thus the magnitudes of the roots become

$$|z_{\overline{\lambda},1}| = |z_{\overline{\lambda},2}| = |z_{\overline{\lambda}}| = \omega_{\overline{\lambda}} = \sqrt{\beta_2 - \hat{\alpha}\beta_1\overline{\lambda}}\,. \tag{3.73}$$

Similarly, the magnitudes of the roots associated with the extremal value $\underline{\lambda}$ with damping ration $\zeta_{\underline{\lambda}} = -1$ in Eq. (3.69), are

$$|z_{\underline{\lambda},1}| = |z_{\underline{\lambda},2}| = |z_{\underline{\lambda}}| = \omega_{\underline{\lambda}} = \sqrt{\beta_2 - \hat{\alpha}\beta_1\underline{\lambda}}\,. \tag{3.74}$$

To satisfy the equidistant condition,

$$|z_{\underline{\lambda}}| = \sqrt{\beta_2 - \hat{\alpha}\beta_1\underline{\lambda}} = \sqrt{\beta_2 - \hat{\alpha}\beta_1\overline{\lambda}} = |z_{\overline{\lambda}}|,$$

and since $\hat{\alpha} > 0$ and $\underline{\lambda} \neq \overline{\lambda}$, $\beta_1 = 0$. Thus, the magnitude of the roots (associated with the extremal eigenvalues) are

$$|z_{\overline{\lambda}}| = |z_{\underline{\lambda}}| = \omega_{\overline{\lambda}} = \omega_{\underline{\lambda}} = \sqrt{\beta_2} \tag{3.75}$$

Step 3 is to show that the roots of Eq. (3.39) associated with the extremal eigenvalue $\overline{\lambda}$ are critically damped. Using the damping ratio definition for the extremal modes, $\zeta_{\overline{\lambda}}$ and $\zeta_{\underline{\lambda}}$ in

Eq. (3.66), with $\beta_1 = 0$ and $\zeta_{\underline{\lambda}} = -1$, and substituting for $\omega_{\overline{\lambda}}, \omega_{\underline{\lambda}}$ from Eq. (3.75), results in

$$\begin{aligned} -1 &= \frac{\hat{\alpha}\underline{\lambda} - (1+\beta_2)}{2\sqrt{\beta_2}} \\ \zeta_{\overline{\lambda}} &= \frac{\hat{\alpha}\overline{\lambda} - (1+\beta_2)}{2\sqrt{\beta_2}} \end{aligned} \tag{3.76}$$

Solving the two equations in Eq. (3.76) for the magnitude $\sqrt{\beta_2}$ of the extremal roots results in

$$\sqrt{\beta_2} = \frac{\hat{\alpha}(\overline{\lambda} - \underline{\lambda})}{2(1+\zeta_{\overline{\lambda}})}, \tag{3.77}$$

which is minimized over damping ratio $|\zeta_{\overline{\lambda}}| \leq 1$ by selecting

$$\zeta_{\overline{\lambda}} = 1. \tag{3.78}$$

Note that the magnitude of the roots (associated with the extremal eigenvalues) becomes, from Eqs. (3.75), and (3.77),

$$|z_{\overline{\lambda}}| = |z_{\underline{\lambda}}| = \sqrt{\beta_2} = \frac{\hat{\alpha}(\overline{\lambda} - \underline{\lambda})}{4}. \tag{3.79}$$

Step 4 is to find the optimal A-DSR gains $\hat{\alpha}$ and β_2. Substituting $\zeta_{\overline{\lambda}} = 1$ from Eq. (3.78) into Eq. (3.76), results in

$$\begin{aligned} \hat{\alpha}\overline{\lambda} &= (1+\beta_2) + 2\sqrt{\beta_2} \\ \hat{\alpha}\underline{\lambda} &= (1+\beta_2) - 2\sqrt{\beta_2}. \end{aligned} \tag{3.80}$$

Dividing the two equations to eliminate $\hat{\alpha}$ yields a quadratic equation for $\sqrt{\beta_2}$, the magnitude of the roots,

$$(\overline{\lambda} - \underline{\lambda})\beta_2 - 2(\overline{\lambda} + \underline{\lambda})\sqrt{\beta_2} + (\overline{\lambda} - \underline{\lambda}) = 0, \tag{3.81}$$

with solutions

$$\sqrt{\beta_2} = \frac{(\overline{\lambda} + \underline{\lambda}) \pm 2\sqrt{\overline{\lambda}\underline{\lambda}}}{(\overline{\lambda} - \underline{\lambda})}. \tag{3.82}$$

Since $\overline{\lambda} > \underline{\lambda} > 0$, the smaller root in Eq. (3.82) is chosen for maximizing structural robustness, resulting in

$$\sqrt{\beta_2} = \frac{(\overline{\lambda} + \underline{\lambda}) - 2\sqrt{\overline{\lambda}\underline{\lambda}}}{(\overline{\lambda} - \underline{\lambda})} = \frac{(\sqrt{\overline{\lambda}} - \sqrt{\underline{\lambda}})}{(\sqrt{\overline{\lambda}} + \sqrt{\underline{\lambda}})} \tag{3.83}$$

and from Eq. (3.79),

$$\hat{\alpha} = \frac{4}{(\overline{\lambda} - \underline{\lambda})}\sqrt{\beta_2} = \frac{4}{(\sqrt{\overline{\lambda}} + \sqrt{\underline{\lambda}})^2}. \tag{3.84}$$

□

Remark 4 (No outdated-feedback in Robust A-DSR) *As $\beta_1 = 0$ for Robust A-DSR (from Lemma 2 in Eq. (3.70)), the outdated-feedback term is zero for maximum robustness in A-DSR based approach for networks with real spectrum. Thus, only momentum term is found to be important for improving both robustness and convergence rate of general networks without loops.*

Stability with momentum term only

Lemma 3 *[Stability of Robust A-DSR] Let the A-DSR parameters $\hat{\alpha}$, β_1 and β_2 be selected as in Eq. (3.70) from Lemma 2 and let the extremal eigenvalues be distinct, i.e., $\overline{\lambda} \neq \underline{\lambda}$. Then, the resulting network with the general A-DSR is stable, i.e., the roots ($z_{\lambda_{K,m},i}$, $i \in \{1, 2\}$) of characteristic Eq. (3.65) (associated with each eigenvalue $\lambda_{K,m}$ of the pinned Laplacian K) have magnitude less than one.*

Proof With the optimal parameters in Eq. (3.70), the damping ratio $\zeta_{\lambda_{K,m}}$ of the roots ($z_{\lambda_{K,m},i}$, $i \in \{1, 2\}$) of Eq. (3.65) associated with each eigenvalue $\lambda_{K,m}$ of the pinned Laplacian K is given by

$$\zeta_{\lambda_{K,m}} = \frac{\hat{\alpha}\lambda_{K,m} - 1 - \beta_2}{2\sqrt{\beta_2}}, \tag{3.85}$$

which makes the damping ratio $\zeta_{\lambda_{K,m}}$ linear in the eigenvalue $\lambda_{K,m}$, and varying between $\zeta_{\underline{\lambda}} = -1$ to $\zeta_{\overline{\lambda}} = 1$. This implies that any eigenvalue between the extremal ones is underdamped,

i.e.

$$|\zeta_{\lambda_{K,m}}| < 1,\ \forall\ \underline{\lambda} < \lambda_{K,m} < \overline{\lambda} \tag{3.86}$$

As a result, the magnitude of the roots of the characteristic polynomial for $\lambda_{K,m}$ is

$$|z_{\lambda_{K,m},1}| = |z_{\lambda_{K,m},2}| = \sqrt{\beta_2} = \frac{\sqrt{\overline{\lambda}} - \sqrt{\underline{\lambda}}}{\sqrt{\overline{\lambda}} + \sqrt{\underline{\lambda}}} < 1,\ \forall\ \overline{\lambda} > \underline{\lambda} > 0, \tag{3.87}$$

which shows that the roots are strictly within the unit circle resulting in stability.

□

Remark 5 (Balanced structural robustness) *From Eq.* (3.87)*, all the roots of the characteristic equation in Eq.* (3.65)*, associated with the Robust A-DSR, have the same magnitude and lie on a circle centered at the origin. Therefore, the roots are equally structurally robust, i.e., they are equidistant from the unit circle. Thus, the A-DSR with optimal parameters, as in Eq.* (3.70) *from Lemma 2, leads to balanced structural robustness in networks with real spectrum.*

3.3 Results and Discussion

This section comparatively evaluates the Optimal no-DSR and the Robust A-DSR approaches using simulation results for an example network's structural robustness and convergence rate during transition. Additionally, the improvements in convergence rate with the Robust A-DSR are validated with an experimental system.

3.3.1 Simulation results

Example transition problem

The network considered here has four agents ($n = 4$) represented by nodes X_i, where $1 \leq i \leq 4$, with node connectivity represented by the graph in Figure 3.2. Note that the eigenvalues

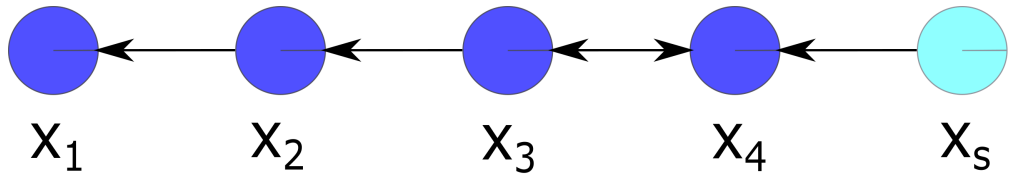

Figure 3.2: Graph of example network with four agents ($n = 4$). Non-source agents are $X_i, 1 \leq i \leq 4$, and the source agent is X_s. The edge between agents X_4 (the agent with source input) and X_3 is undirected, the others are directed.

of the given network's Laplacian are real, however the underlying graph is not strongly connected. Moreover, the graph (even without the source X_s) is not balanced.

The virtual source agent X_s determines the desired consensus value for the network and is connected to the agent X_4, i.e. the leader. The connecting edges are all directed in the non-source graph network, except for the undirected edge between the leader X_4 and follower agent X_3 which makes the graph Laplacian asymmetric. The system dynamics with no-DSR for the example network, is given by Eq. (3.7), with the pinned-Laplacian K and B given as

$$K = \begin{bmatrix} 1 & -1 & 0 & 0 \\ 0 & 1 & -1 & 0 \\ 0 & 0 & 1 & -1 \\ 0 & 0 & -1 & 2 \end{bmatrix} \quad B = \begin{bmatrix} 0 \\ 0 \\ 0 \\ 1 \end{bmatrix}. \tag{3.88}$$

As discussed in Section 3.2.1, the gradient of the asymmetric Laplacian potential $\Phi_{\mathcal{G}}(\hat{X}) = \hat{X}^T L \hat{X}$ in Eq. (3.24) does not lead to standard neighbor-based update in Eq. (3.7), where L is the graph Laplacian (from Eq. (3.3)) and $\hat{X}$ is the state vector including source agent.

Optimal no-DSR for example network

The optimal update gain α^* from Eq. (3.22), for minimum spectral radius $\sigma(P) = \sigma(P^*)$, is determined using the extremal eigenvalues $\overline{\lambda} = 2.618$ and $\underline{\lambda} = 0.382$ of the pinned-Laplacian

K in Eq. (3.88), using Eq. (3.22), as

$$\alpha^* = \frac{2}{\overline{\lambda} + \underline{\lambda}} = \frac{2}{2.6180 + 0.3820} = 0.6667. \tag{3.89}$$

The measure of structural robustness d^* with Optimal no-DSR is, from Eq. (3.18),

$$d^* = 1 - \sigma^* = 0.255, \tag{3.90}$$

with the optimal spectral radius $\sigma^* = 0.745$ (from Eq. (3.23)), as illustrated in Figure 3.3.

To assess the transition response, a simulation was performed with the virtual agent's state X_s changing from an initial value $X_s[k] = x_i$ for all $k < 0$ to a final value $X_s[k] = x_f$ for all $0 \leq k$. It was assumed that the non-source agents are initially at consensus, i.e., $X[0] = x_i \mathbf{1}_n$. With the update gain from Eq. (3.89), the simulated response of the Optimal no-DSR method for a change in virtual agent state X_s from $x_i = 0$ to $x_f = 100$ is shown in Figure 3.6. The settling time (T_s) of the network's response, defined as the time taken for all the agents' states to achieve and remain within 95% of the desired change $x_\Delta = x_f - x_i = 100$ in the consensus state was found to be 14 sampling time periods ($k = 14$) from the simulated response.

Remark 6 (Structural robustness with real spectrum) *The addition of edges (even with small edge weights) could lead to loss of the real spectrum property. Nevertheless, the stability will still be structurally robust (with or without A-DSR) since the roots of the any general polynomial (and the characteristic equations in particular) are continuous in its coefficients. To illustrate, the roots of the pinned-Laplacian with a perturbation term e*

$$K_e = \begin{bmatrix} 1 & -1 & 0 & 0 \\ e & 1-e & -1 & 0 \\ 0 & 0 & 1 & -1 \\ 0 & 0 & -1 & 2 \end{bmatrix} \tag{3.91}$$

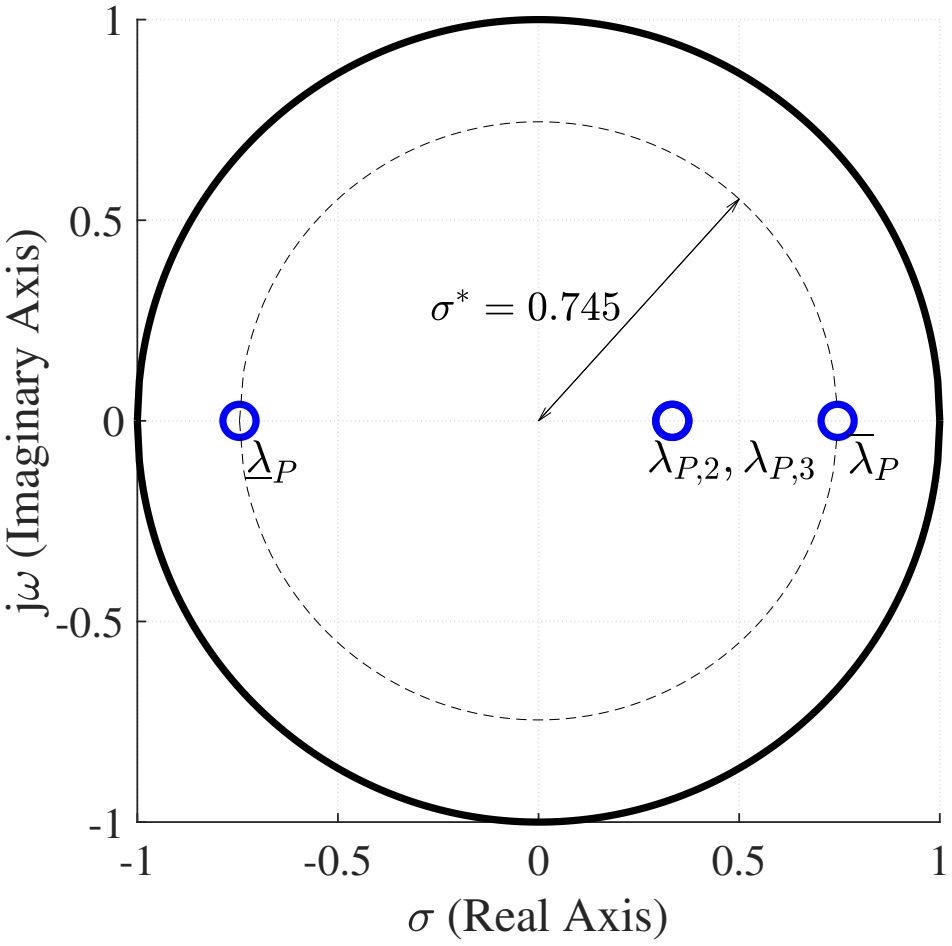

Figure 3.3: Optimal spectral radius (σ^*) for Optimal no-DSR. Location of the eigenvalues of matrix P, $\lambda_{P,m} = 1 - \alpha^* \lambda_{K,m}$ with optimal update gain α^* from Eq. (3.89). The spectral radius with Optimal no-DSR is $\sigma^* = 0.745$, as in Eq. (3.23)

are continuous with respect to e. The corresponding location of roots of $P_e = \boldsymbol{I}_4 - \alpha^* K_e$ *with Optimal no-DSR update gain* $\alpha^* = 0.6667$ *(obtained from Eq.* (3.89)*) are shown in Figure 3.4 for increasing perturbation e. Although, the resulting spectrum is no longer real, the stability is structurally robust, i.e., stability is maintained for small perturbations e.*

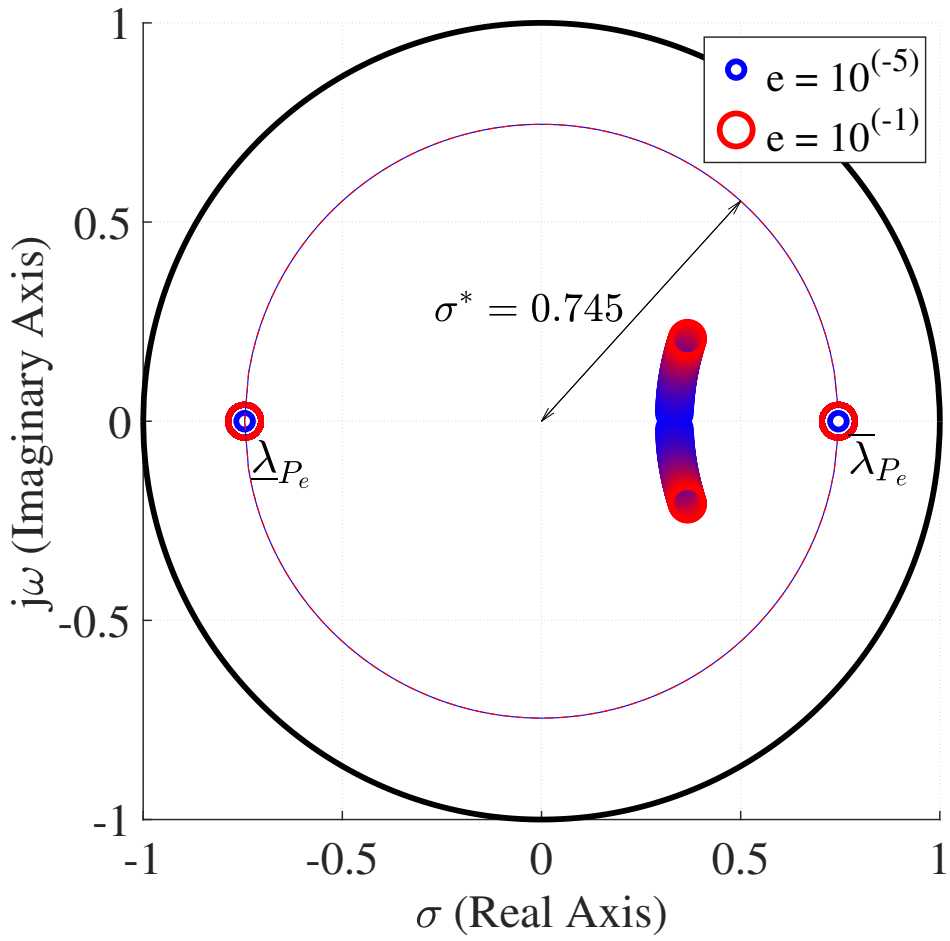

Figure 3.4: Perturbation e can lead to loss of real spectrum but stability is still structurally robust, i.e., stability is maintained for small perturbations e. Location of the eigenvalues $\lambda_{P_e} = 1 - \alpha^* \lambda_{K_e}$ of matrix $P_e = \mathbf{I}_4 - \alpha^* K_e$, where K_e from Eq. (3.91) has a perturbation term e, which varies from $10^{(-5)}$ (blue) to $10^{(-1)}$ (red).

A-DSR improves structural robustness

The A-DSR approach in Eq. (3.32) under Subsection 3.2.1 is used to improve the example network's structural robustness. The spectral radius of the network is minimized over the range of A-DSR parameters $\hat{\alpha}, \beta_1$ and β_2,

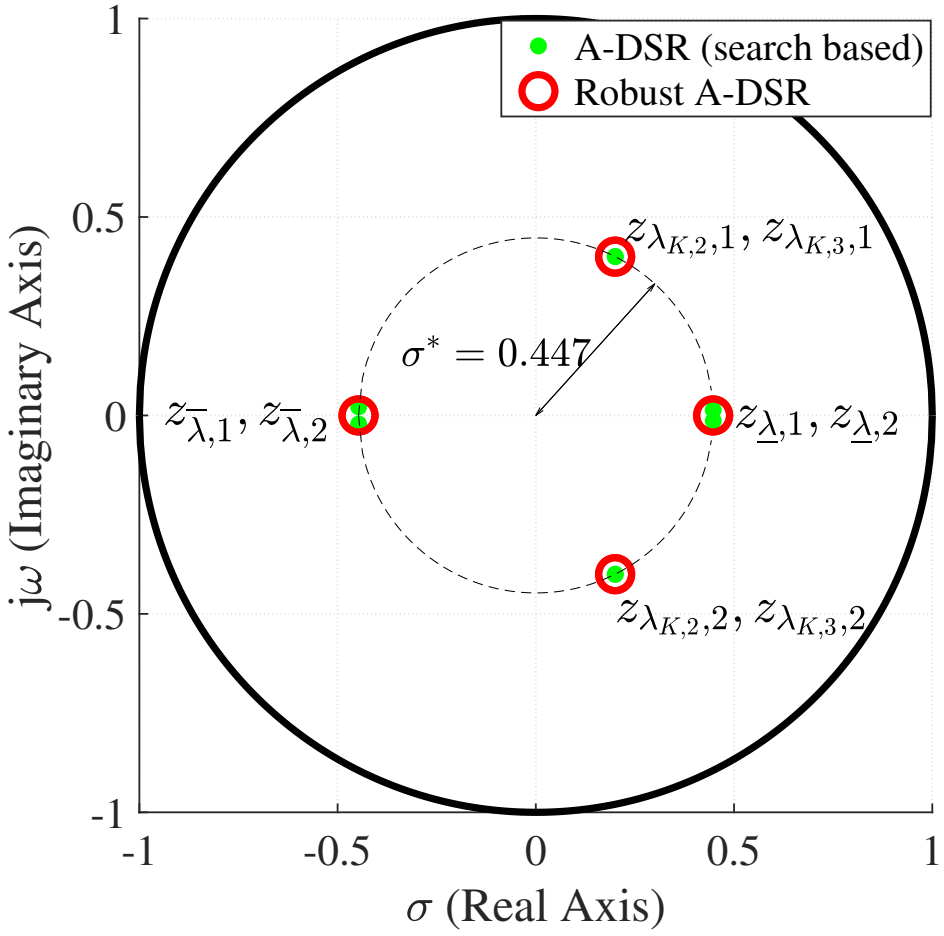

Figure 3.5: Optimal spectral radius (σ^*) with Robust A-DSR. Location of the roots of characteristic polynomials with Robust A-DSR as in Lemma 2 for each eigenvalue $\lambda_{K,m}$ of pinned-Laplacian K in Eq. (3.88). The spectral radius with Robust A-DSR is $\sigma^* = 0.447$, an improvement of 40% compared to Optimal no-DSR. The spectral radius with search-based A-DSR is similar to the Robust A-DSR, with similar root locations.

$$\sigma^* = \min_{\hat{\alpha},\beta_1,\beta_2} \left[\max_m \left(\max_{1 \le i \le 2} |z_{\lambda_{K,m},i}| \right) \right], \tag{3.92}$$

where $z_{\lambda_{K,m},i}$ with $i \in \{1, 2\}$ are the roots of the characteristic Eqs. (3.65) associated with eigenvalue $\lambda_{K,m}$ of the pinned-Laplacian K, and the search space is constrained by the sta-

bility conditions in Eq. (3.43). The optimum parameters for minimum spectral radius, found through a numerical search, and the resulting performance are tabulated in Table 3.1. With these optimal parameter selections, the corresponding roots of the characteristic polynomial with A-DSR, in Eq. (3.32), for each eigenvalue $\lambda_{K,m}$, are shown in Figure 3.5. The optimal spectral radius is given by $\sigma^* = 0.447$, which is a reduction of 40% when compared to the Optimal no-DSR case for this example network. For the same state transition from $x_i = 0$ to $x_f = 100$ in the consensus state, the corresponding 5% settling time is 7 sampling time periods ($k = 7$), which is a 50% improvement over the Optimal no-DSR case. Thus, the A-DSR approach improves both the structural robustness and the convergence rate when compared to the Optimal no-DSR case.

Robust A-DSR's performance similar to A-DSR

Instead of a numerical search to optimize the parameters as in the A-DSR case, the Robust A-DSR, proposed in Subsection 3.2.3, yields closed-form expressions for selection of its parameters as in Eq. (3.70). With the Robust A-DSR, the corresponding roots of the characteristic polynomials in Eq. (3.65), for each eigenvalue $\lambda_{K,m}$, are shown in Figure 3.5. Note that the roots corresponding to the extremal eigenvalues $\underline{\lambda}, \overline{\lambda}$ are real valued and critically damped, as in Lemma 2. Furthermore, the other roots of characteristic equation, for intermediate eigenvalues λ satisfying $\underline{\lambda} < \lambda < \overline{\lambda}$, lie on a circle with radius equal to magnitude of the critically damped extremal modes as shown in Figure 3.5, which follows from Lemma 3. Overall, the spectral radius σ^* of the example network, with Robust A-DSR, is equal to the magnitude of the roots, i.e., $\sigma^* = \sqrt{\beta_2} = 0.447$.

The performance of the Robust A-DSR is similar to the optimized search-based A-DSR (see Table 3.1). In particular, the spectral radius of $\sigma^* = 0.447$ with Robust A-DSR is smaller by 40% when compared to $\sigma(P^*) = 0.745$ with the Optimal no-DSR method (see Table 3.1), thus improving the structural robustness. Additionally, the settling time T_s with Robust A-DSR was found to be 7 sampling time periods from the simulation result (which corresponds to a 50% improvement in convergence rate) as shown in Figure 3.6.

Table 3.1: Simulation results for minimizing (min of) Spectral Radius (σ) and Settling Time (T_s): Comparison of robustness (σ) & convergence rates (T_s) of network responses using Optimal no-DSR (Eq. (3.7)), A-DSR (Eq. (3.32)), Nesterov-update (Eq. (3.28)), and the Outdated-feedback and the Momentum methods

Method	min of	$\hat{\alpha}$	β_1	β_2	σ	$T_s(k)$
Robust A-DSR		0.80	0	0.20	0.4472	7
A-DSR	σ	0.7997	0.0002	0.2005	0.4472	7
	T_s	0.6303	0.2376	0.3868	0.6634	6
Momentum	σ	0.7995	0	0.2006	0.4479	7
	T_s	0.8388	0	0.2347	0.4845	6
Nesterov -update	σ	0.4830	0.3992	0.3992	0.5706	11
	T_s	0.5212	0.4684	0.4684	0.7599	7
Outdated -feedback	σ	0.9638	-0.1414	0	0.5973	8
	T_s	1.0874	-0.1881	0	0.7318	6
Optimal no-DSR		0.6667	0	0	0.745	14

Remark 7 (Momentum term β_2 and settling time T_s) *For the Robust A-DSR approach, the settling time T_s can be estimated analytically in terms of the momentum term β_2. Since all the roots of the characteristic equation in Eq.* (3.87) *have the same magnitude, the dynamics associated with the under-damped roots of the Robust A-DSR converge faster than critically-damped, real-valued roots $\sqrt{\beta_2}$. The corresponding real-valued continuous-time roots s_{cont} are at $s_{cont} = (\ln\sqrt{\beta_2})/\delta_t$, which can be used to predict the 5% settling time T_s as (in number of sampling time periods)*

$$T_s \approx \frac{5}{|s_{cont}|\delta_t} \quad \frac{5}{|\ln\sqrt{\beta_2}|} = 6.2, \tag{3.93}$$

which matches the simulation-based value of 7 sampling time periods. Thus, a larger mo-

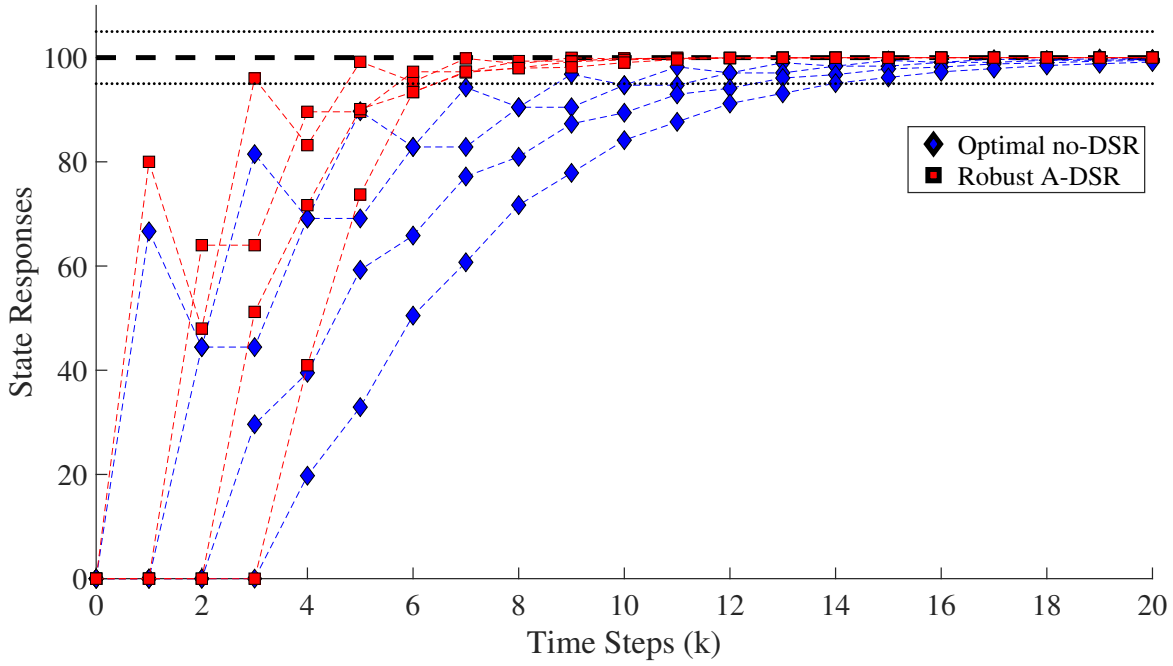

Figure 3.6: Simulated network state responses with Robust A-DSR (in red) and Optimal no-DSR (in blue, with $\alpha = \alpha^* = 0.6667$), where the Robust A-DSR parameters are chosen as $\hat{\alpha} = 0.80$, $\beta_1 = 0$ and $\beta_2 = 0.20$ from Eq. (3.70) for $\overline{\lambda} = 2.618$ and $\underline{\lambda} = 0.382$, showing the settling time $T_s = 7$ sampling time periods (50% improvement w.r.t. Optimal no-DSR method $T_s = 14$ sampling time periods)

mentum term β_2 results in faster settling.

In summary, the Robust A-DSR approach provides similar improvements as with the general A-DSR approach, in both the structural robustness and the convergence rate when compared to the Optimal no-DSR approach. The advantage of the Robust A-DSR approach is that it provides an analytical approach for selecting the control parameters instead of the numerical search with the general A-DSR.

Comparison of constrained accelerated approaches

Although constrained, the Robust A-DSR (with $\beta_1 = 0$) outperforms both the Nesterov-update method (with $\beta_1 = \beta_2 = \beta$) as well as the Outdated-feedback method (with $\beta_2 = 0$).

Optimal parameters for the Nesterov-update as well as the Outdated-feedback methods were also found using the same optimization in Eq. (3.92) with the additional constraints $\beta_1 = \beta_2 = \beta$ for Nesterov-update method and $\beta_2 = 0$ for Outdated-feedback method. The search space for parameters were constrained as in Corollary 1. The optimal parameters of Nesterov-update and Outdated-feedback methods and the performance are provided in Table 3.1. When compared to the Optimal no-DSR case, the Nesterov-update improves the spectral radius by 23.4% which is less than the improvement of 40% with the Robust A-DSR approach. The Outdated-feedback method also improves the spectral radius when compared to the no-DSR case, but the improvement (19.9%) is even smaller than the Nesterov-update case with 23.4%. Similarly, the settling time improvement of 50% with Robust A-DSR when compared to Optimal no-DSR is larger than the improvement of 21.43% with the Nesterov-update and 42.9% improvement with the Outdated-feedback. Thus, while the Robust A-DSR is constrained, it still matches the performance of the general optimal A-DSR, and outperforms both the Nesterov-update method as well as the Outdated-feedback method.

Remark 8 (Outdated-feedback versus momentum) *When simultaneously improving both the structural robustness and the convergence rate, of the two components of the A-DSR, the momentum component (associated with β_2) has more significant impact than the outdated-feedback component (associated with β_1).*

Convergence improvement without structural robustness

The above results focused on increasing both the structural robustness and convergence rate. However, the parameters of the accelerated update methods can be chosen purely for optimizing the convergence rate (i.e. minimizing the settling time T_s). The resulting optimized parameters (found through a numerical search) and the performance are quantified in Table 3.1.

The accelerated methods achieve smaller settling time T_s when the parameters are optimized for achieving a faster convergence rate. For instance, the settling time T_s with A-DSR

(search based) improves to 6 sampling time periods (see Table 3.1), which is faster than Robust A-DSR and Nesterov-update each taking 7 sampling time periods, and an improvement of 57.1% over the Optimal no-DSR case. However, this improvement in settling time T_s is accompanied by a decrease in structural robustness of the network. For example, with A-DSR parameters selected for fast convergence, the spectral radius σ increased to $\sigma = 0.6237$ from $\sigma = \sigma^* = 0.4472$ for the case when the parameters were selected to maximize bot the structural robustness and convergence rate. Among the other accelerated approaches, the Momentum method also achieves the same settling time of 6 sampling time periods as the A-DSR case, indicating the importance the momentum term in improving the convergence rate of the given example network. A similar loss in structural robustness is seen with the Momentum and Outdated-feedback approaches when the parameters are optimized purely for faster convergence rate, as seen in Table 3.1. The loss in structural robustness (for this example) is more with the Outdated-feedback than with the Momentum method.

The simulation results show that the network's convergence-rate alone can be improved with the general A-DSR further than that achieved with Robust A-DSR. However, this increase in convergence-rate alone involves a loss in structural robustness. Moreover, the A-DSR parameters are found using a numerical search method.

In contrast, the parameters of the Robust A-DSR can be found analytically and it achieves similar convergence rate as the A-DSR optimized for convergence-rate alone. Moreover, the performance improvement with the Robust A-DSR (as well as the A-DSR), in terms of both the structural robustness and the rapidity of transition, is better than the performance with the standard no-DSR consensus method.

3.3.2 Experimental results

A mobile-bot network is used for experimental evaluation of the proposed A-DSR approach.

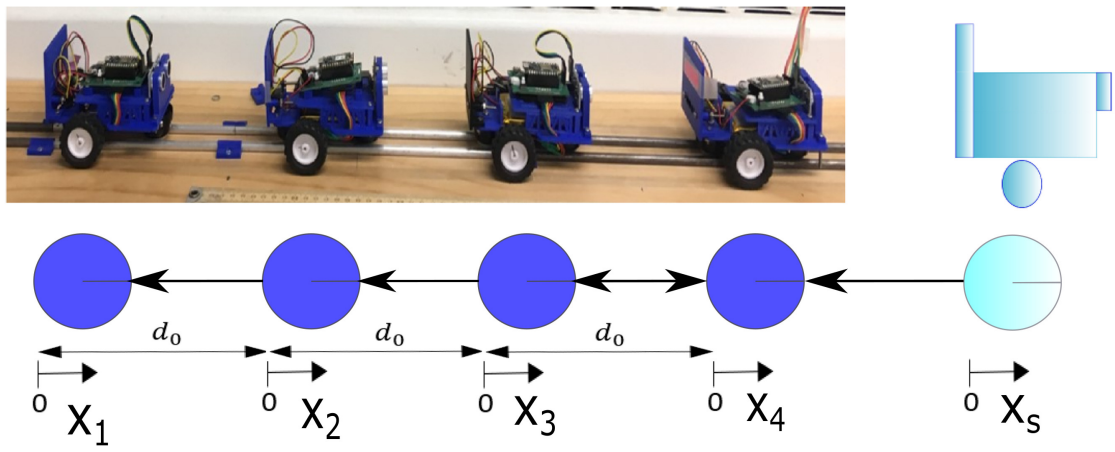

Figure 3.7: Experimental test bed consisting of four mobile-bot agents moving in a straight line, with the same connectivity as in the example simulation network in Figure 3.2. Each i^{th} agent's state is its displacement X_i from its initial position.

System description

The experimental setup consists of four mobile-bot agents that move in a straight line. The network connectivity is the same as in the simulation example. The bots aim to maintain a spacing of d_o between them, and the state X_i of each bot i is defined as the displacement from the initial equally-spaced configuration, as shown in Figure 3.7. The virtual source input X_s determines the desired position of the network.

Bot's update computation

The desired displacement $X_i[k+1]$ at the next time step $k+1$ is computed using local relative-distance measurements available at time step k by each bot i using distance sensors (Ultrasonic HC-SR04 to the front, and Infrared GP2Y0A21YK at the back). These measurements of each bot i include

$$X_{f,i}[k] = (X_{i+1}[k] - X_i[k]) + d_0, \tag{3.94}$$

the relative displacement w.r.t. the front bot $i+1$ (which is X_s for leader bot $i=4$), and

$$X_{b,i}[k] = d_0 - (X_{i-1}[k] - X_i[k]), \tag{3.95}$$

the relative displacement w.r.t. the back bot $i-1$ where $2 < i < 4$, and d_0 is the desired offset distance between the bots in the experimental setup. These relative-distance measurements $(X_{f,i}[k], X_{b,i}[k])$ are used to determine the neighbor information needed to evaluate the update law, i.e., to obtain $K_i X[k]$, where K_i is the i^{th} row of the pinned-Laplacian in Eq. (3.88). For example,

$$\begin{aligned} K_i X[k] &= K_{i,i+1}(X_i[k] - X_{i+1}[k]) \\ &\quad + K_{i,i-1}(X_i[k] - X_{i-1}[k]) \\ &= K_{i,i+1}(d_0 - X_{f,i}[k]) + K_{i,i-1}(X_{b,i}[k] - d_0). \end{aligned} \tag{3.96}$$

Thus, the relative-distance measurements $(X_{f,i}[k], X_{b,i}[k])$ at time step k enable each bot i to compute its update, i.e., to find the desired position $X_i[k+1]$ at the next time step according to Eq. (3.34), where parameters β_1 and β_2 are zero for the no-DSR case.

Bot's feedback control

Each i^{th} bot's controller aims to match its state (displacement) $X_i(t)$ to be the desired state $X_i[k+1]$ by the next time step, i.e., when time $t = t_{k+1}$. This is accomplished using a velocity-feedback inner-loop and a position-feedback outer-loop, as shown in Figure 3.8, using measurements of the agent state $X_i(t)$ from magnetic encoders on each bot i.
In particular, the desired velocity for the time period $[t_k, t_{k+1})$ is computed as

$$V_i[k] = \frac{X_i[k+1] - X_i[k]}{\delta_t}, \tag{3.97}$$

where δ_t is the discrete time step (in seconds) for the update method. The desired velocity $V_i[k]$ is then tracked using an inner-loop controller with gain k_v as shown in Figure 3.8.

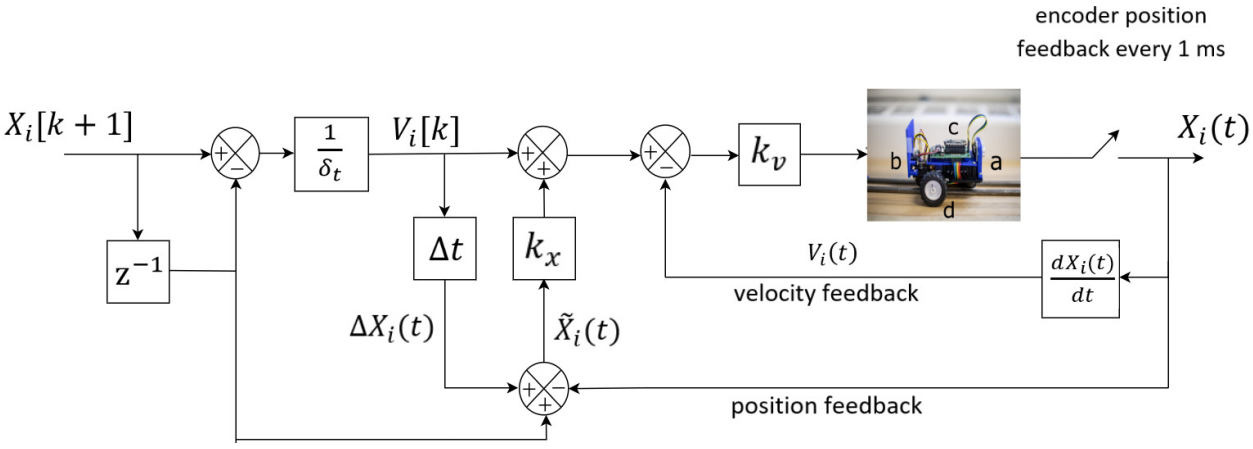

Figure 3.8: Each i^{th} bot's control system includes: a) distance sensors to the front and, b) back , c) micro-controller for on-board computation, and d) wheels with magnetic encoders on motors to estimate each bot's displacement, $X_i(t)$. To ensure that the bot achieves $X_i[k+1]$, an inner-loop controller with gain k_v to track desired velocity $V_i[k]$ in Eq. (3.97) and an outer-loop controller with gain k_x for position error ($\tilde{X}_i(t)$ in Eq. (3.98)) are implemented.

Additionally, an outer-loop feedback with gain k_x is used to correct for position error ($\tilde{X}_i(t)$) at any time $t \in [t_k, t_{k+1})$, determined as

$$\tilde{X}_i(t) = (X_i[k] + \Delta X_i(t)) - X_i(t), \tag{3.98}$$

where $\Delta X_i(t) = V_i[k](t - t_k) = V_i[k]\Delta t$, as shown in Figure 3.8.

The selection of position transition magnitude for the experiment was based on velocity limits of 20 cm/s for the bots. The initial position was $x_i = 0$, and the final position was $x_f = 100$ cm. Therefore the sampling time period δ_t was chosen as 4 s to ensure that the bots could meet the maximum position transitions of 80 cm in one sampling-time period δ_t, seen in simulations in Figure 3.6, with the bot's feedback gains $k_v = 5$ and $k_x = 1$.

Convergence rate improvement

The improvement in convergence rate of transition response in the example network with Robust A-DSR, over Optimal no-DSR, is evaluated through the experimental mobile-bot

Table 3.2: Experimental results. Comparison of convergence rate in position responses with Robust A-DSR and Optimal no-DSR for multi-agent network in Figure 3.7, using settling time T_s.

Method	Trial	$T_s(k)$
Robust A-DSR	Trial 1	11
	Trial 2	11
$(\hat{\alpha} = 0.80, \beta_1 = 0, \beta_2 = 0.20)$	Trial 3	10
	Trial 4	11
	Trial 5	11
	Trial 6	10
	Trial 7	9
Mean Response		**10**
Optimal no-DSR	Trial1	17
	Trial2	16
$(\alpha = \alpha^* = 0.67)$	Trial3	16
	Trial4	15
	Trial5	15
	Trial6	18
	Trial7	15
Mean Response		**16**

network.

A transition in desired position (defined using virtual source X_s) from $x_i = 0$ cm to $x_f = 100$ cm, similar to simulations, is implemented on the mobile-bot network. Each bot, initially in consensus with position zero, responds as the transition information propagates through the bot network (in Figure 3.7). This state transition is implemented using Optimal no-DSR and Robust A-DSR, with parameters given in Table 3.1, and the observations of convergence rates from seven trials (with both the approaches) are tabulated in Table 3.2. The position responses of the bots during the transition are plotted in Figure 3.9, for each of the seven trials with Optimal no-DSR (in light blue) and Robust A-DSR (in light red).

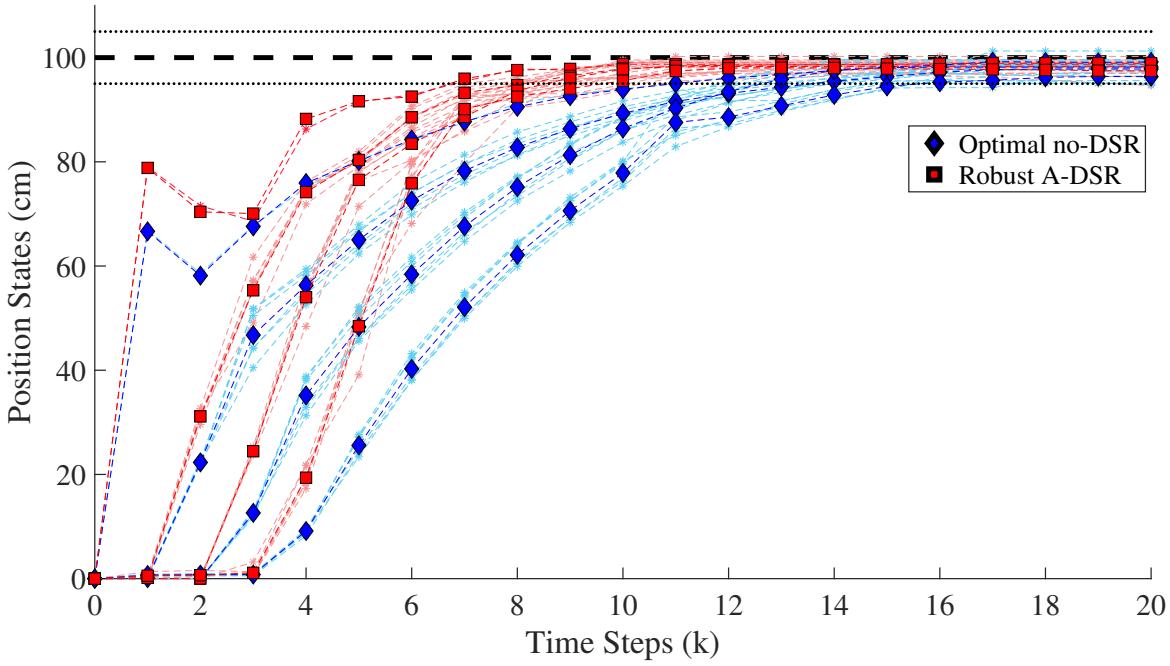

Figure 3.9: Experimental position responses over 7 trials (in lighter shade) and their mean (in dark lines) in the experiments comparing the Optimal no-DSR (in blue) and Robust A-DSR (in red) methods for fast convergence. The experiments on average show an improvement with Robust A-DSR of 37.5% in T_s (from 16 time steps to 10 time steps).

The mean responses for both approaches, obtained from averaging over the seven trials, are also shown in Figure 3.9.

Robust A-DSR shows improvement in convergence rate of the bot network's transition response, improving the settling time (within 5% of the final position) by 4 to 9 time periods (27% to 50%), when compared with Optimal no-DSR, similar to that observed in simulations. The mean response converges 6 time periods faster with Robust A-DSR (an improvement of 37.5%) when compared with Optimal no-DSR, see Table 3.2. Thus, the convergence rate improvements observed in simulations with Robust A-DSR, with analytically determined parameters, over Optimal no-DSR are verified with similar results from experimental studies of position transition in the mobile-bot network.

3.4 Chapter Conclusions

The chapter introduced an accelerated delayed self reinforcement (A-DSR) approach, based on local potential, for improving the structural robustness and convergence rate beyond the limits of standard consensus-based networks. Of the two terms in the accelerated approach, it was shown that the momentum term has substantially more impact when compared to the outdated-feedback term for improving convergence rate and robustness in networks with real spectrum. A Robust A-DSR approach was developed, with analytical expressions for its parameters, that closely matches the performance of the general A-DSR approach, which alleviates the need for numerical search when selecting parameters of the general A-DSR. Moreover, experimental results verified the improved convergence rate with Robust A-DSR over Optimal no-DSR.

Chapter 4

MC2.1: IMPROVING NETWORK'S TRANSITION COHESION BY APPROXIMATING STRONGLY DAMPED WAVES USING DELAYED SELF REINFORCEMENT.

This chapter forms the contribution **MC2.1** and has been presented as a conference article in [4]. The main contribution of this work is to show that DSR leads to a strongly-damped, wave-like propagation [18] of information at low frequencies, which improves cohesion during transitions. Furthermore, the wave-like-propagation formulation of DSR is used to show that the DSR approach implements consensus of agents in the network not only for the state information but also its time-derivative which provides a rationale for the low-dissipation propagation of information through networks that in turn leads to improved cohesion. This chapter is organized as follows. In Section 4.1 the standard consensus and the DSR based approaches are described and compared in terms of cohesion for an example system, and the research problem for the chapter is stated. Next in Section 4.2, the strongly damped wave formulation of the DSR approach is developed and the conclusions of chapter are presented in Section 4.3.

4.1 Cohesive Networks with DSR

This section describes the limits on cohesion with standard consensus-based method without DSR, introduces the DSR-based approach and then poses the research question addressed in the chapter.

4.1.1 Information transfer without DSR

The standard consensus-based method can be described as

$$I_i[k+1] = I_i[k] - \gamma\delta_t D_i[k], \tag{4.1}$$

where δ_t is the sampling time period, $I_i[k]$ is the information state of agent i, the index k represents time instant of the update $t = k\delta_t$, γ is the alignment strength and $D_i[k]$ is the average difference in the information states between the agent i and its neighbors, defined as,

$$D_i[k] = \frac{1}{|N_i|}\sum_{j\in N_i}\big[I_i[k] - I_j[k]\big], \tag{4.2}$$

where N_i is the set of neighbors (including a source agent s) of agent i and $|N_i|$ is the cardinal number of the set N_i. Let the number of non-source agents in the network be n, then the information dynamics for the network, using $n \times 1$ state vector $I[k]$, can be given as

$$I[k+1] = I[k] - \gamma\delta_t AI[k] + \gamma\delta_t BI_s[k], \tag{4.3}$$

where I_s is the information state of source agent s, and matrices A and B are defined as,

$$\begin{aligned} A(i,j) &= \frac{-1}{|N_i|}, && j \in N_i \text{ and } j \neq i \\ &= 1, && j = i \text{ and } |N_i| \neq 0 \\ &= 0, && \text{otherwise.} \end{aligned} \tag{4.4}$$

$$\begin{aligned} B(i) &= \frac{1}{|N_i|}, && s \in N_i \\ &= 0, && \text{otherwise.} \end{aligned} \tag{4.5}$$

Assumption 3 (Connectivity of the network structure) *It is assumed that the network structure of the agents is undirected, and that there is a path from the source agent s to each agent in the network $i \neq s$, which results in the Laplacian matrix A of the underlying graph to be symmetric and its eigenvalues $\lambda_{A,i},\ 1 \leq i \leq n$ lie in the open right half plane [14].* ■

Remark 9 (Continuous-time approximation) *The information dynamics without DSR in Eq.* (4.3) *can be considered as the discrete-time approximation of the following continuous-time consensus dynamics,*

$$\dot{I}(t) = -\gamma A I(t) + \gamma B I_s(t). \tag{4.6}$$

The continuous-time approximation is stable for positive alignment strength $\gamma > 0$ as the eigenvalues of $-A$ are in the open left half of the complex plane from Assumption 3. Further, the eigenvalues of the dynamics in Eq. (4.6) *are,*

$$\lambda_{c,i} = -\gamma \lambda_{A,i} \quad 1 \leq i \leq n. \tag{4.7}$$

The response speed of the continuous-time dynamics in Eq. (4.6) *can be improved without limits by increasing the alignment strength γ as it pushes the eigenvalues in Eq.* (4.7) *away from the imaginary axis.* ■

4.1.2 Metric for cohesion

The loss of cohesion is quantified by the maximum variance $\overline{\Delta}$ in the responses of each agent and its non-source neighbor agents, to a step change of magnitude $\bar{I}_s$ in the source agent

state I_s, from $I_s[0] = 0$ to $I_s[k] = \bar{I}_s$, $\forall 1 \leq k$. The maximum variance $\overline{\Delta}$ is defined as,

$$\overline{\Delta} = \max_i \left[\max_{j \in N_i, j \neq s} \left[\max_k \frac{\mid I_i[k] - I_j[k] \mid}{\bar{I}_s} \right] \right], \tag{4.8}$$

where $\mid . \mid$ represents the absolute value. A smaller value of $\overline{\Delta}$ represents more cohesive network responses, which is essential for applications such as minimizing deformation in flexible-object transport tasks [10].

4.1.3 Limit on cohesion without DSR

The cohesion of the network response without DSR can potentially be improved through faster response dynamics by optimizing the alignment strength for cohesion. The limits on the alignment strength γ for the stability of the information dynamics in Eq. (4.3) ($\overline{\gamma}$) are,

$$0 < \gamma < \overline{\gamma} \leq \frac{2}{\lambda_{A,i} \delta_t}, \tag{4.9}$$

for each eigenvalue $\lambda_{A,i}$ of the matrix A (see [60] for the proof), where,

$$\overline{\gamma} = \frac{2}{\overline{\lambda}_A \delta_t}, \tag{4.10}$$

where $\overline{\lambda}_A = \max_i \{\lambda_{A,i}\}$. Therefore, there exists a limit on the cohesiveness that can be achieved using the without DSR approach in Eq. (4.3), by optimizing the alignment strength γ for cohesion within the bounded range for stability.

Remark 10 (Smaller δ_t for cohesiveness without DSR) *Using Eq.* (4.10)*, it can be observed that the range of acceptable alignment strength γ can be increased by using a smaller sampling time δ_t. Thus better cohesiveness can potentially be achieved by increasing the sampling bandwidth.* ■

4.1.4 Delayed self reinforcement (DSR) approach

The DSR based approach is chosen as a discrete-time approximation of an ideal cohesive network. The continuous-time ideal cohesive network is based on each agent i having direct access to the source agent, i.e., in a centralized manner, which results in the following,

$$\dot{I}(t) = -\alpha I(t) + \alpha \mathbf{1}_n I_s(t), \tag{4.11}$$

where α can be chosen for a desired settling time of the ideal dynamics, and $\mathbf{1}_n$ is an $n \times 1$ vector of ones. Eq. (4.11) leads to an ideal cohesive network response, for instance, if the source state I_s is a unit step input, then each agent i in the network has the same state response $I_i(t) = (1 - e^{-\alpha t})$, assuming same zero initial conditions for each agent. The ideal dynamics is implemented in a decentralized manner by multiplying both sides of Eq. (4.11) by βA, substituting $A\mathbf{1}_n = B$ (from [60]) and adding $\dot{I}(t)$ on both sides of Eq. (4.11),

$$\dot{I}(t) = (\mathbf{I}_n - \beta A)\dot{I}(t) - \alpha\beta A I(t) + \alpha\beta B I_s(t) \tag{4.12}$$

$$\approx (\mathbf{I}_n - \beta A)\frac{I(t) - I(t-\tau)}{\tau} - \alpha\beta A I(t) + \alpha\beta B I_s(t), \tag{4.13}$$

where β is the DSR gain, $\mathbf{I}_n$ is an $n \times n$ identity matrix, and $\dot{I}(t)$ in the ideal dynamics on RHS of Eq. (6.8) is implemented using a delay-based approximation in Eq. (4.13) with time delay τ,

$$\dot{I}(t) \approx \frac{I(t) - I(t-\tau)}{\tau}. \tag{4.14}$$

Note that the DSR approach in Eq. (4.13) is a decentralized approximation of the ideal cohesive control law in Eq. (4.11), because it can be implemented using only current and prior information available from the network and only leaders (represented by nonzero terms in B) require access to the source information.

Remark 11 (Filter-like derivative approximation) *The delay-based approximation of*

$\dot{I}(t)$ in Eq. (4.14) *for the DSR approach in Eq.* (4.13) *acts like a filtered-derivative. For instance, this can be observed from the magnitude of $\mathcal{F}(s)$ defined as,*

$$\mathcal{F}(s) = \frac{1 - e^{-s\tau}}{\tau s}, \tag{4.15}$$

which is a ratio between the delay-based derivative in Eq. (4.14) *and the actual derivative in Laplace domain. The delay-based approximation in Eq.* (4.14) *is a good approximation of derivative at low frequencies as the magnitude $|\mathcal{F}(s)| \approx 1$. However, the magnitude $|\mathcal{F}(s)|$ tends to a small value as the frequency is increased, which means the delay-based derivative tends to zero in the DSR approach in Eq.* (4.13) *at higher frequencies. Therefore, the DSR approach in Eq.* (4.13) *approximates the ideal dynamics in Eq.* (6.8) *only at lower frequencies and simplifies to the without DSR approach at higher frequencies.* ■

The discrete-time DSR is obtained by discretizing Eq. (4.13) with sampling period δ_t using zero-order-hold (ZOH) on the input between updates and the time-delay chosen as $\tau = \delta_t$, as shown below,

$$\begin{aligned} I[k+1] = I[k] + (\mathbf{I}_n - \beta A)(I[k] - I[k-1]) \\ - \alpha\beta\delta_t A I[k] + \alpha\beta\delta_t B I_s[k]. \end{aligned} \tag{4.16}$$

The stability condition of the DSR approach in Eq. (4.16) (from [10] using Jury test) is given as,

$$0 < \beta < \frac{4}{\overline{\lambda}_A(\alpha\delta_t + 2)}, \quad 0 < \alpha. \tag{4.17}$$

Remark 12 (Network topology) *The DSR approach in Eq.* (4.16) *is applicable to general networks with directed underlying graph topology. However, an assumption of undirected graphs (Assumption 3) has been made in this paper to make the connection with wave dy-*

namics. ■

4.1.5 Example 1-D system simulations

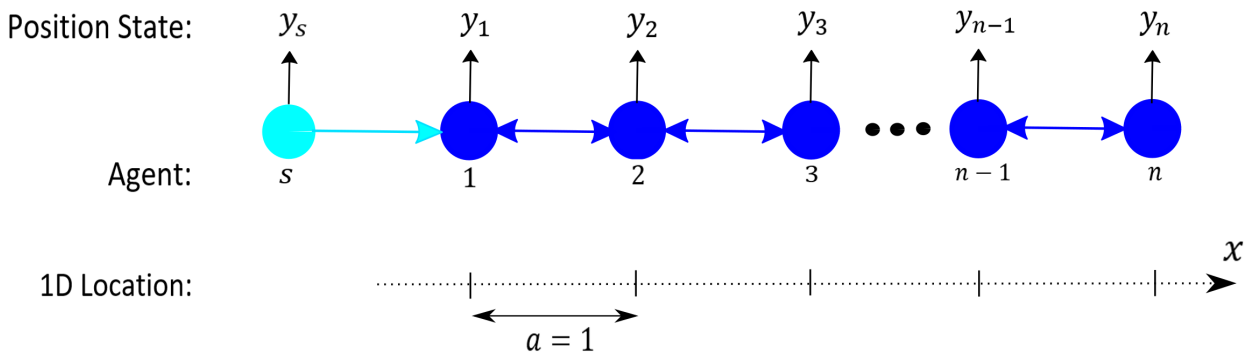

Figure 4.1: Schematic of the example system with n equally spaced ($a = 1$) non-source agents with an underlying undirected path graph network structure, with a source agent which specifies the desired position state y_s to agent $i = 1$ (leader).

The without DSR (in Eq. (4.3)) and DSR (in Eq. (4.16)) approaches are compared for their performance in maintaining cohesion on a network of $n = 20$ agents during a decentralized 1-D state transition task within a given time period $\mathcal{T} = 50$ seconds, where y_i is the position state of each agent i. The connectivity of the agents is given as an undirected path graph of n nodes, where only the first agent $i = 1$ has direct access to a virtual source agent s, as shown in Figure 4.1. Thus, each non-source agent i receives the average relative state information $D_i[k]$ w.r.t. it's neighbors, defined using Eq. (4.2) as,

$$D_i[k] = \begin{cases} (2y_i[k] - y_{i+1}[k] - y_s[k])/2 & i = 1 \\ (2y_i[k] - y_{i+1}[k] - y_{i-1}[k])/2 & 1 < i < n \\ (y_i[k] - y_{i-1}[k]) & i = n. \end{cases} \tag{4.18}$$

where agent $i = 1$ is connected to the virtual source with position defined as y_s. The loss of cohesion in the position state responses due to a unit step change in the source position, from $y_s[0] = 0$ to $y_s[k] = 1,\ 1 \leq k$, is compared for the with and without DSR approaches.

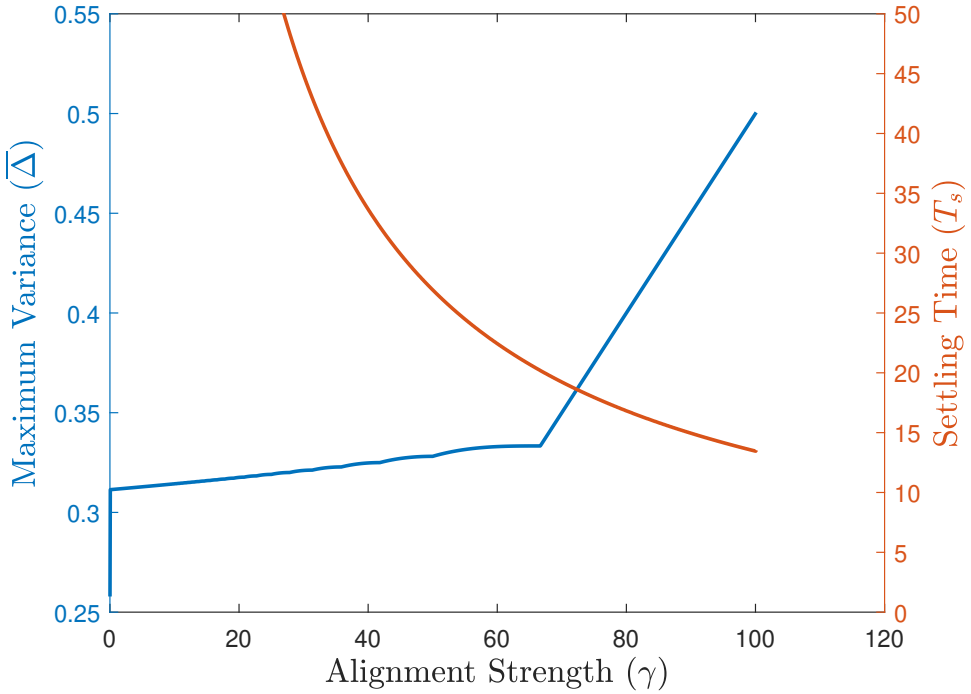

Figure 4.2: Simulated maximum variance $\overline{\Delta}$ in Eq. (4.8) of the position responses using the without DSR approach in Eq. (4.20) with $\delta_t = 0.01$ s of the example network in Figure 4.1 increases (i.e. cohesion decreases), and the settling time T_s decreases, with increasing alignment strength γ within the stability limit $\overline{\gamma} = 100.15$.

Without DSR

The discrete-time position update dynamics without DSR for each agent $1 \leq i \leq n$, using only local measurements is given as,

$$y_i[k+1] = y_i[k] - \gamma \delta_t D_i[k], \tag{4.19}$$

with the relative position measurements $D_i[k]$ is defined as in Eq. (4.18), γ is the alignment strength and δ_t is the sampling period. Therefore, the position update dynamics without

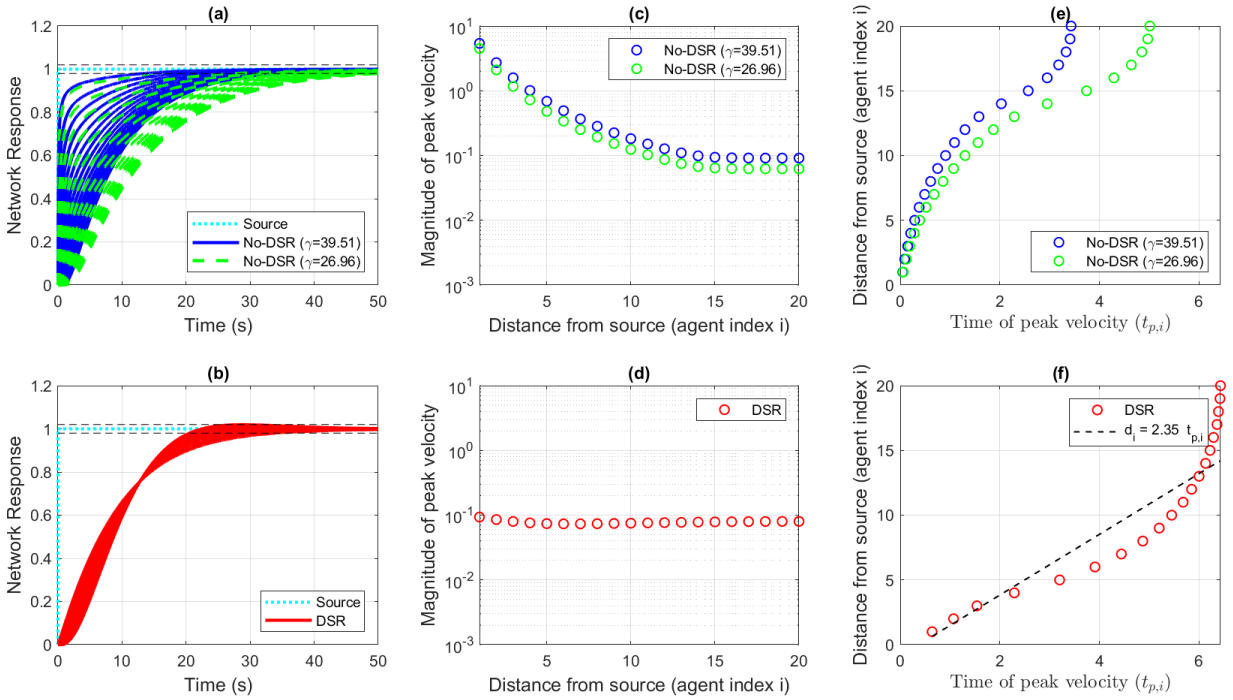

Figure 4.3: Simulated position responses of the example network in Figure 4.1 for $\delta_t = 0.01$ s **(a)** without DSR approach with $\gamma = 39.51$ in blue (for similar $T_s = 34.08$ s as the DSR case) and $\gamma = 26.96$ in green which maximizes the cohesion within the stability bound $\bar{\gamma} = 100.15$ with $T_s = 49.96$ s $< \mathcal{T} = 50$ s, and **(b)** with DSR approach ($\alpha = 0.11, \beta = 1$) which results in $T_s = 34.09$ s. The peak velocities $\bar{v}_i$ as a function of distance of agent i from the source shows **(c)** dissipation of velocity information in the without DSR approach, whereas **(d)** the velocity information propagates without dissipation with DSR. Further, agents' distance from source is shown as function of time of peak velocity ($t_{p,i}$) **(e)** without DSR and **(f)** with DSR to show the propagation speed of the information change through the network.

DSR for the overall network using Eq. (4.18) and Eq. (4.19) is given as,

$$Y[k+1] = (\mathbf{I}_n - \gamma\delta_t A)\, Y[k] + \gamma\delta_t B y_s[k], \tag{4.20}$$

where $Y[k] = \begin{bmatrix} y_1, & y_2, & \ldots, & y_n \end{bmatrix}^T$ is the position state of the $n = 20$ agents in the network, A and B are the Laplacian and source-connectivity matrices of dimensions $n \times n$ and $n \times 1$

respectively, defined as in Eq. (4.5) for the example network in Figure 4.1.

With DSR

The discrete-time position update dynamics with DSR, for each agent $1 \leq i \leq n$, using only local measurements from Eq. (4.18) is given as,

$$\begin{aligned} y_i[k+1] &= y_i[k] - \alpha\beta\delta_t D_i[k] + (y_i[k] - y_i[k-1]) \\ &- \beta(D_i[k] - D_i[k-1]) + \beta B_i(D_{i,s}[k] - D_{i,s}[k-1]), \end{aligned} \tag{4.21}$$

where B_i is the i^{th} row of source-connectivity matrix B, α determines the settling time T_s of the ideal dynamics in Eq. (6.8) which DSR approximates at low frequencies, β is the DSR gain, and $D_{i,s}$ is the relative measurement of agent i with the source s defined as,

$$D_{i,s}[k] = y_i[k] - y_s[k]. \tag{4.22}$$

Therefore, the position update dynamics with DSR for the overall network, using Eq. (4.18) and Eq. (4.21), is given as,

$$\begin{aligned} Y[k+1] &= Y[k] - \alpha\beta\delta_t AY[k] + \alpha\beta\delta_t By_s[k] \\ &+ (\mathbf{I}_n - \beta A)(Y[k] - Y[k-1]). \end{aligned} \tag{4.23}$$

Choice of parameters

The DSR parameters α and β for simulations are chosen for maximizing cohesion, quantified using $\overline{\Delta}$ in Eq. (4.8), for a given sampling period $\delta_t = 0.01$ s and a specified maximum transition time of $\mathcal{T} = 50$ s. The values of the DSR parameters were determined using a numerical search ensuring the stability conditions in Eq. (4.17) and that the settling time T_s of each networked agent is less than the maximum desired transition time of $\mathcal{T} = 50$ s. For the without DSR approach, two cases were considered to select the alignment strength

parameter γ. First, $\gamma = 39.51$ is chosen so that the settling time in the case without DSR is similar to the settling time with the DSR approach $T_s = 34.09$ s for the example network, from the data represented in Figure 4.2. Second, the alignment strength is chosen to be $\gamma = 26.96$, which optimizes cohesion for no-DSR while satisfying (i) the stability limit $\bar{\gamma} = 100.15$ from Eq. (4.10), and (ii) the settling time requirement of $T_s \leq \mathcal{T} = 50$ s, for the same sampling period of $\delta_t = 0.01$ s. In this example, increasing alignment strength γ does decrease the settling time for the case without DSR, however, it also decreases cohesion, i.e., increases the variance $\overline{\Delta}$ as shown in Figure 4.2.

Remark 13 (Loss of cohesion with higher γ) *Each agent dynamics in the case without DSR has first-order dynamics. Nevertheless, negative eigenvalues of the state-dependent update matrix* $(\mathbf{I}_n - \gamma\delta_t A)$ *in Eq.* (4.20) *can lead to oscillations in the velocity of the agents, and result in increased loss of cohesion as shown in Figure 4.2.* ■

DSR improves cohesion

DSR based approach in Eq. (4.23) has a maximum variance of $\overline{\Delta} = 0.0198$ with a settling time of $T_s = 34.09$ s, which is about 16 times more cohesive than the network response without DSR approach in Eq. (4.20) for similar settling time $T_s = 34.08$ s, as shown in Figures 4.3-a, 4.3-b and Table 4.1. The cohesion without DSR is maximized when the settling time is larger with the alignment strength at $\gamma = 26.96$, which results in a marginal improvement in cohesion with variance $\overline{\Delta} = 0.3199$. Therefore, as seen in this example system, the DSR approach can substantially improve the cohesion of the network response when compared to the standard consensus-based without DSR approach.

Transition information propagates without dissipation with DSR

The transition of the state, quantified in terms of the maximum rate of change i.e., peak velocity $\bar{v}_i$ of each agent i during the state transition, defined as, $\bar{v}_i = \max_k \dot{y}_i[k]$, is plotted as a function of the distance from the source (which is proportional to agent index i) without

Approach	**Parameters**	$\overline{\Delta}$	$\Delta\overline{v}$	$\mathbf{T_s}$ (s)
DSR	$\alpha = 0.11,\ \beta = 1$	0.0198	0.0202	34.09
Without DSR	$\gamma = 39.51$	0.3247	5.3050	34.08
	$\gamma = 26.96$	0.3199	4.4327	49.96

Table 4.1: Parameter values and comparison of DSR (α, β) and without DSR (γ) for cohesion ($\overline{\Delta}$ in Eq. (4.8)) & velocity dissipation ($\Delta\overline{v}$ in Eq. (4.24)) in the 1-D simulations.

DSR in Figure 4.3-c and with DSR in Figure 4.3-d. The dissipation of the velocity information is quantified using the maximum difference in the velocity peaks of agents, defined as,

$$\Delta\overline{v} = \max_{i,j} \left|\overline{v}_i - \overline{v}_j\right|. \tag{4.24}$$

It is observed that without DSR the peak velocity $\bar{v}_i$ is much higher for agents closer to the source than the agents farther away from the source with $\gamma = 39.51$, with the maximum difference in agent peak velocities as $\Delta\overline{v} = 5.305$. Further, upon changing the alignment strength for maximum cohesion without DSR to $\gamma = 26.96$, the peak velocities decrease for each agent i as shown in Figure 4.3-c and $\Delta\overline{v}$ decreases to 4.433, however the information still dissipates with increasing distance from the source. On the other hand the peak velocities remain approximately constant with DSR as shown in Figure 4.3-d with relatively negligible maximum peak velocity difference $\Delta\overline{v} = 0.02$, which shows that the DSR approach enables the velocity information to propagate without dissipation through the example network which is essential for similar response among the agents for cohesion.

4.1.6 Research question

The research question posed in this chapter is to provide a rationale for i) the improvement in cohesion with the DSR approach in Eq. (4.16) as compared to the standard consensus-based method in Eq. (4.3), and, ii) the propagation of the information about the change in the state (e.g., velocity) without dissipation through a network, without increasing the update bandwidth.

4.2 Analysis

This section shows that the DSR approach can be approximated as a strongly damped wave, which provides a rationale for the improved cohesion and dissipation free information transfer with DSR.

4.2.1 Strongly damped wave propagation with DSR

The DSR approach in Eq. (4.16) can be rearranged in the following form for each agent i,

$$\begin{aligned}&\frac{(I_i[k+1]-I_i[k])-(I_i[k]-I_i[k-1])}{\delta_t}\\&=-\beta A_i\frac{(I[k]-I[k-1])}{\delta_t}-\alpha\beta A_i I[k]+\alpha\beta B_i I_s[k],\end{aligned}\tag{4.25}$$

where A_i and B_i represent the i^{th} rows of the matrices A and B respectively, defined in Eq. (4.5). The Eq. (4.25) is then approximated with the following strongly damped wave equation [18] as the sampling period $\delta_t \to 0$,

$$\begin{aligned}&\delta_t\frac{\partial^2}{\partial t^2}I(t,X)=\\&\beta\frac{a^2}{2D}\left(\alpha\boldsymbol{\nabla}^2 I(t,X)+\frac{\boldsymbol{\nabla}^2 I(t,X)-\boldsymbol{\nabla}^2 I(t-\delta_t,X)}{\delta_t}\right),\end{aligned}\tag{4.26}$$

where, X is the spatial location of n agents, D is the number of dimensions of the spatial location of agents, a is the average distance between the neighbors, the Laplacian approximation

defined below is used from [1],

$$\boldsymbol{\nabla}^2 I(t,X) \approx -\frac{2D}{a^2} A_i I(t), \tag{4.27}$$

and the second term on RHS of Eq. (4.26) is approximated as

$$\frac{\boldsymbol{\nabla}^2 I(t,X) - \boldsymbol{\nabla}^2 I(t-\delta_t,X)}{\delta_t} = \boldsymbol{\nabla}^2 \frac{\partial}{\partial t} I(t,X). \tag{4.28}$$

Therefore, using Eq. (4.27) and Eq. (4.28), Eq. (4.26) is rewritten as a strongly damped wave propagation equation,

$$\frac{\partial^2}{\partial t^2} I(t,X) = \beta \frac{a^2}{2D\delta_t} \left(\alpha \boldsymbol{\nabla}^2 I(t,X) + \boldsymbol{\nabla}^2 \frac{\partial}{\partial t} I(t,X) \right), \tag{4.29}$$

which has an additional Laplacian term on the time-derivative of the information I, $\left(\boldsymbol{\nabla}^2 \frac{\partial}{\partial t} I(t,X)\right)$. The addition of this term promotes cohesion in information states of the agents during transitions with DSR, as each agent, in the limit of small sampling period δ_t, updates its state not only to reduce relative deviation in states w.r.t. to its neighbors (represented by $\boldsymbol{\nabla}^2 I(t,X)$), but also for any relative deviation in the derivative of the state ($\boldsymbol{\nabla}^2 \frac{\partial I(t,X)}{\partial t}$).

4.2.2 Wave equation for the 1-D example system

The strongly damped wave equation for the system in Figure 4.1 with one dimensional agent spatial locations $X = x$, i.e. $D = 1$, and unit inter-agent spacing $a = 1$, is considered. The information state for each agent is their y position, where $Y(t) = \begin{bmatrix} y_1 \; y_2 \; \ldots \; y_n \end{bmatrix}^T \in \mathcal{R}^n$ is state vector of non-source agents, and y_s is the virtual source position, as shown in Figure 4.1. Thus the Laplacian in Eq. (4.29) of the i^{th} agent's state $y_i(t)$ along the spatial dimension x

is found as,

$$\begin{aligned}\boldsymbol{\nabla}^2 y_i(t) &= \frac{\partial^2}{\partial x^2} y_i(t) \\ &= \frac{1}{a}\left(\frac{(y_{i+1}(t) - y_i(t))}{a} - \frac{(y_i(t) - y_{i-1}(t))}{a}\right) \\ &= \frac{y_{i+1}(t) - 2y_i(t) + y_{i-1}(t)}{a^2}. \end{aligned} \tag{4.30}$$

where a is the distance between the equally-spaced agents in the x direction. Assuming the Laplacian matrix A defined as in Eq. (4.5) for the underlying undirected path graph as in Figure 4.1, Eq. (4.30) is rewritten with $D = 1$ as,

$$\begin{aligned}\boldsymbol{\nabla}^2 y_i(t) &= -2\,\frac{(-0.5y_{i+1}(t) + y_i(t) - 0.5y_{i-1}(t))}{a^2}, \\ &= -\frac{2D}{a^2} A_i Y(t), \end{aligned} \tag{4.31}$$

where A_i is the i^{th} row of the matrix A. Therefore, the strongly damped wave propagation equation for the one dimensional case is,

$$\begin{aligned}\frac{d^2}{dt^2} y_i(t) &= \beta \frac{a^2}{2\delta_t}\left(\alpha \boldsymbol{\nabla}^2 y_i(t) + \boldsymbol{\nabla}^2 \frac{d}{dt} y_i(t)\right), \\ &= -\frac{\beta}{\delta_t}\left(\alpha A_i Y(t) + A_i \frac{d}{dt} Y(t)\right), \end{aligned} \tag{4.32}$$

where $Y(t)$ denotes the states of the non-source agents, which shows an additional consensus term on the velocity of the agents in the example network.

Remark 14 (Information propagation speed) *The speed of information propagation c from the second order wave-like equation in Eq.* (4.29) *can be found as,*

$$c = a\sqrt{\frac{\beta\alpha}{2D\delta_t}}\,, \tag{4.33}$$

which for the example network in Figure 4.1 is found to be $c = 2.35$ using $a = 1$, $D = 1$

and the parameters for DSR from Table 4.1. The actual speed of propagation using DSR is shown through a plot of distance of agents from source vs their time of velocity peak in Figure 4.3-f, which is compared with a straight line of slope $c = 2.35$*. It shows that the first* 4 *agents lie on the straight line showing linear propagation speed of information, however the actual propagation speed deviates more from the predicted value for agents farther away the source.* ■

4.3 Chapter Conclusions

This chapter showed that the DSR-based approach improves cohesion among networked agents during transitions under update bandwidth limits, and also allows the rate of change of information to propagate through the network without dissipation. Further, a strongly damped wave formulation of the DSR approach is developed, which shows that DSR promotes consensus on not only the information state, but also the rate of change of the information of the agents (i.e. both position and velocity consensus in the example system). This provides a rationale for the improved cohesion and relatively-lossless propagation of transition information through networks with DSR.

Chapter 5

MC2.2: LOW DISTORTION INFORMATION PROPAGATION WITH NOISE SUPPRESSION IN SWARM NETWORKS

This chapter forms the main contribution **MC2.2**, and is currently under review for publication in [5]. Motivated by swarms in nature, neighbor-based alignment rules have been proposed for a variety of engineered networks such as autonomous vehicles and robotic networks. Nevertheless, the information propagation with such neighbor-based update rules tends to be diffusive and do not capture the superfluid-like low-distortion response observed in nature that leads to to similar (cohesive) parallel turn maneuvers of swarms. The main contribution of the work is to show that self-reinforcement using already available prior information can substantially reduce the distortion during information propagation at low frequencies while suppressing unwanted, relatively-high-frequency noise that can otherwise lead to loss of information coherence. Thus, the current work enables improved cohesion of engineered networks and better models of biological swarm behavior.

5.1 Neighbor-based alignment approach

Each agent aligns its own information state using neighbor-averaged information as

$$I_i[k+1] \quad = I_i[k] + \delta_t U_i[k] \quad = I_i[k] - \delta_t \left(\gamma \Delta_i[k]\right), \tag{5.1}$$

where $I_i[k]$ is the information state of the i^{th} agent at periodic time instants $t = k\delta_t$, with $k = \{1, 2, 3, \ldots\}$ and update time period is δ_t. The input to each agent $U_i[k]$ is proportional

to $\Delta_i[k]$, the averaged information deviation from the neighbors, given by

$$\Delta_i[k] = \frac{1}{|N_i|} \sum_{j \in N_i} (I_i[k] - I_j[k]), \tag{5.2}$$

and $|N_i|$ is the number of neighbors of agent i in its set of neighbors N_i. The information propagation speed can be increased by increasing the alignment strength γ between the neighbor agents. Such consensus-based approaches lead to a diffusive information transfer in networks, i.e., a maneuver information starting from a leader agent will dissipate as it propagates to other agents in the network, which doesn't predict the superfluidic information transfer observed in biological flocking [8].

Self reinforcement with prior information

Convergence rates of the consensus-based information update in Eq. (5.1) can be improved using delayed self reinforcement (DSR) by each agent with prior information [99, 100],

$$\begin{aligned} I_i[k+1] - I_i[k] &= -\gamma \delta_t \Delta_i[k] - \beta_1(\Delta_i[k] - \Delta_i[k-1]) \\ &\quad + \beta_2(I_i[k] - I_i[k-1]) \\ &= \delta_t U_{sr,i}[k], \end{aligned} \tag{5.3}$$

where the added terms $\beta_1(\Delta_i[k] - \Delta_i[k-1])$ and $\beta_2(I_i[k] - I_i[k-1])$ in $U_{sr,i}[k]$ are referred to as the outdated-state feedback and momentum terms, respectively, in gradient-based optimization algorithms. For example, the addition of only the momentum term in Eq. (5.3) (i.e., $\beta_1 = 0$) leads to the momentum-method used in [13, 14]. Adding only the outdated-state feedback term (i.e., $\beta_2 = 0$) leads to the outdated-feedback approach pursued to speed up network convergence rates in [15]. The Nesterov-method uses both the outdated-state feedback and the momentum terms in a specific ratio, i.e., $\frac{\beta_1}{\gamma \delta_t} = \beta_2 = \beta$ [16]. The cohesive DSR approach [1], which approximates the decentralized implementation of the ideal cohesive centralized information broadcast, also uses both the outdated feedback and the momentum

terms, with the momentum term gain specified as $\beta_2 = 1$ and β_1 optimized for cohesion. (For derivation of the decentralized cohesive DSR approach, see SI Appendix, Section 1.)

5.2 Continuum-based analysis

The self-reinforcement based update in Eq. (5.3) can be rewritten as

$$\begin{aligned}\delta_t\beta_2\frac{1}{\delta_t}\left(\frac{I_i[k+1]-I_i[k]}{\delta_t}-\frac{I_i[k]-I_i[k-1]}{\delta_t}\right)\\ =-\gamma\Delta_i[k]-\beta_1\frac{\Delta_i[k]-\Delta_i[k-1]}{\delta_t}\\ -(1-\beta_2)\frac{I_i[k+1]-I_i[k]}{\delta_t},\end{aligned}\tag{5.4}$$

and the Laplacian ∇^2 can be approximated by the averaged information deviation $\Delta I_i[k]$, e.g., as in [8],

$$\nabla^2 I(t,x) \approx -\frac{2D}{a^2}\Delta I_i(t_k),\tag{5.5}$$

where a is the average distance to the neighbors (assumed to be small compared to the wavelength of the information variation), x represents the spatial location of agents, D is the number of dimensions of the spatial variable x over which the information I is varying, to yield the wave-like approximation

$$\begin{aligned}\frac{\partial^2}{\partial t^2}I(t,x)=\gamma\frac{a^2}{2D\beta_2\delta_t}\nabla^2 I(t,x)+\beta_1\frac{a^2}{2D\beta_2\delta_t}\nabla^2\left(\frac{\partial}{\partial t}I(t,x)\right)\\ -\frac{(1-\beta_2)}{\beta_2\delta_t}\frac{\partial}{\partial t}I(t,x).\end{aligned}\tag{5.6}$$

Note that this wave approximation has two damping terms. The first is the viscous damping term, proportional to $\frac{\partial}{\partial t}I(t,x)$ and scaled by $(1-\beta_2)/\beta_2\delta_t$, which seeks to reduce the rate of change of information. The second term, which depends on $\nabla^2\left(\frac{\partial}{\partial t}I(t,x)\right)$ and is proportional to β_1, does not seek to reduce the rate of change of information. Rather, it improves cohesion

by seeking to achieve a similar rate of change of information amongst neighboring agents, and is referred to as internal damping [101]. The internal damping term also appears in other areas of study, for instance, as Kelvin–Voigt damping in the description of vibrations in elastic media with energy dissipation [102], and in models of undamped heat wave propagation [103].

Remark 1 (Implementation of wave equation) *Agent updates based on direct discretization of the wave equation in Eq.* (5.6) *requires the exchange of the information's time-derivatives between neighbors (see SI Appendix, Section 3 for details), which might not be readily available. In contrast, the self-reinforcement method in Eq.* (5.3) *does not require additional information. Rather, it only needs delayed versions of already-available, prior information from the network.*

Remark 2 (Diffusive propagation without DSR) *Without the DSR terms (i.e., when* $\beta_1 = \beta_2 = 0$*), the continuum approximation reduces to, from Eq.* (5.4) *and Eq.* (5.5), $\frac{\partial}{\partial t} I(t,x) = \gamma \frac{a^2}{2D} \nabla^2 I(t,x)$*, which leads to diffusive information propagation with substantial decay over distance.*

Remark 3 (Effect of gains on damping) *Selection of gain* $\beta_2 = 1$ *leads to zero viscous damping in the wave approximation Eq.* (5.6) *of the discrete-time self-reinforcement method in Eq.* (5.3)*. A small stabilizing viscous damping can be added by selecting* β_2 *as slightly smaller than* 1*. The internal damping, on the other hand, is based on the selection* β_1*, where* $\beta_1 = 0$ *leads to zero internal damping in the wave approximation (Eq.* (5.6)*), and* $\beta_1 > 0$ *leads to higher levels of internal damping in the wave approximation.*

5.3 Low distortion information propagation conditions

To investigate the propagation of information from the source (for instance, from the first bird to initiate a turn maneuver in flocks as in [8]) in networks, the 1-dimensional case

$(D = 1)$ is considered, where Eq. (5.6) becomes

$$\frac{\partial^2}{\partial t^2} I(t,x) = c^2 \frac{\partial^2}{\partial x^2} I(t,x) + c^2 \frac{\beta_1}{\gamma} \frac{\partial^2}{\partial x^2} \left(\frac{\partial}{\partial t} I(t,x) \right) - \frac{(1-\beta_2)}{\beta_2 \delta_t} \frac{\partial}{\partial t} I(t,x). \tag{5.7}$$

and

$$c = \sqrt{\frac{\gamma a^2}{2D\beta_2 \delta_t}} \tag{5.8}$$

is the nominal wave speed without internal and viscous damping, i.e., with $\beta_1 = 0$, $\beta_2 = 1$. Substituting a general wave solution of the form,

$$I(t,x) = I_0 e^{i(kx+\omega t)} \tag{5.9}$$

into Eq. (5.7), where $i = \sqrt{-1}$, ω is the real-valued forcing frequency at $x = 0$, i.e., with the boundary condition

$$I(t,0) = I_0 e^{i(\omega t)} \tag{5.10}$$

and removing $I(t,x)$ from both sides results in

$$-\omega^2 = c^2(-k^2) + c^2 \frac{\beta_1}{\gamma}(-k^2)(i\omega) - \frac{(1-\beta_2)}{\beta_2 \delta_t}(i\omega), \tag{5.11}$$

which can be rewritten as

$$\omega^2 - \frac{(1-\beta_2)}{\beta_2 \delta_t}(i\omega) = k^2 c^2 \left[1 + \frac{\beta_1}{\gamma} \omega i \right]. \tag{5.12}$$

Thus,

$$k^2 = \frac{1}{c^2}\left[\omega^2 - \frac{(1-\beta_2)}{\beta_2\delta_t}(i\omega)\right]\frac{1-\frac{\beta_1}{\gamma}(i\omega)}{1+\frac{\beta_1^2\omega^2}{\gamma^2}}. \tag{5.13}$$

Remark 4 (Pure undamped wave condition) *Note that zero viscous damping ($\beta_2 = 1$) and zero internal damping ($\beta_1 = 0$) leads to the undamped wave propagation of information with the $\omega^2 = c^2k^2$ relationship between wave number k and frequency ω from Eq.* (5.13)*. Such purely undamped wave equation leads to marginal stability of the propagating information wave.*

Remark 5 (Waves in higher dimensional spaces) *The information wave equation from Eq.* (5.6) *is applicable to higher-dimensional networks such as in 2D and 3D. For instance, The wave equation for 2D information wave propagation is found from Eq.* (5.6) *as,*

$$\frac{\partial^2}{\partial t^2}I(t,x,y) = c^2\left(\frac{\partial^2}{\partial x^2}+\frac{\partial^2}{\partial y^2}\right)I(t,x,y) + c^2\frac{\beta_1}{\gamma}\left(\frac{\partial^2}{\partial x^2}+\frac{\partial^2}{\partial y^2}\right)\left(\frac{\partial}{\partial t}I(t,x,y)\right) - \frac{(1-\beta_2)}{\beta_2\delta_t}\frac{\partial}{\partial t}I(t,x,y). \tag{5.14}$$

Information wave decay rate and speed

The wave number k from Eq. (5.13) is complex valued and has the general form

$$k = \pm(k_r - ik_i). \tag{5.15}$$

Using the negative root, the information wave $I(t,x)$ in Eq. (5.9) becomes

$$I(t,x) = I_0 e^{-k_i x} e^{i(-k_r x+\omega t)} \tag{5.16}$$

where the negative sign associated with the real part k_r of the wave number k indicates information propagation along the positive x-direction. The complex part k_i of the wave

number k denotes the spatial decay rate of information as it propagates through the network. The speed of information propagation (c_ω) at frequency ω is found as,

$$c_\omega = \frac{\omega}{k_r}. \tag{5.17}$$

In the following, the wave-approximation-based spatial decay rates (k_i) and information propagation speeds (c_ω) are quantified for two cases: (Case 1) viscous damping without internal damping and (Case 2) internal damping without viscous damping.

Case 1: with viscous damping only

With non-zero viscous damping ($\beta_2 < 1$) and zero internal damping ($\beta_1 = 0$), the wave number k expression in Eq. (5.13) becomes,

$$c^2k^2 = \omega^2 - i\frac{(1-\beta_2)}{\beta_2\delta_t}\omega, \tag{5.18}$$

with solution (for information propagation along the positive x direction)

$$k = -\frac{\omega}{c\sqrt{2}}\left(\sqrt{|z_2|+1} - i\sqrt{|z_2|-1}\right) = -\left(k_r - ik_i\right), \tag{5.19}$$

where

$$|z_2| = \sqrt{1 + \left[\frac{(1-\beta_2)}{\beta_2\delta_t\omega}\right]^2}. \tag{5.20}$$

With viscous damping, the wave number k has a large complex component, especially for small frequencies due to the $1/\omega$ dependence of z_2 in Eq. (5.20), which results in distortion of information with distance x in the solution Eq. (5.9). Moreover, due to the $1/\omega$ dependence, the real part of the ratio k/ω, and therefore the wave speed, varies substantially at small frequencies leading to dispersion in the information propagation.

Case 2: with internal damping only

Rewriting Eq. (5.13) with zero viscous damping, i.e., $\beta_2 = 1$ results in

$$c^2k^2 = \frac{\omega^2}{1+\frac{\beta_1^2\omega^2}{\gamma^2}} - i\frac{\omega^3\frac{\beta_1}{\gamma}}{1+\frac{\beta_1^2\omega^2}{\gamma^2}}, \tag{5.21}$$

and taking the square root yields (for information propagation along the positive x direction)

$$k = -\frac{\omega}{c\sqrt{2}}\left(\sqrt{|z_1| + \frac{1}{1+\frac{\beta_1^2\omega^2}{\gamma^2}}} - i\sqrt{|z_1| - \frac{1}{1+\frac{\beta_1^2\omega^2}{\gamma^2}}}\right), \tag{5.22}$$

where

$$|z_1| = \frac{1}{1+\frac{\beta_1^2\omega^2}{\gamma^2}}\sqrt{1+\frac{\beta_1^2\omega^2}{\gamma^2}} = \frac{1}{\sqrt{1+\frac{\beta_1^2\omega^2}{\gamma^2}}}. \tag{5.23}$$

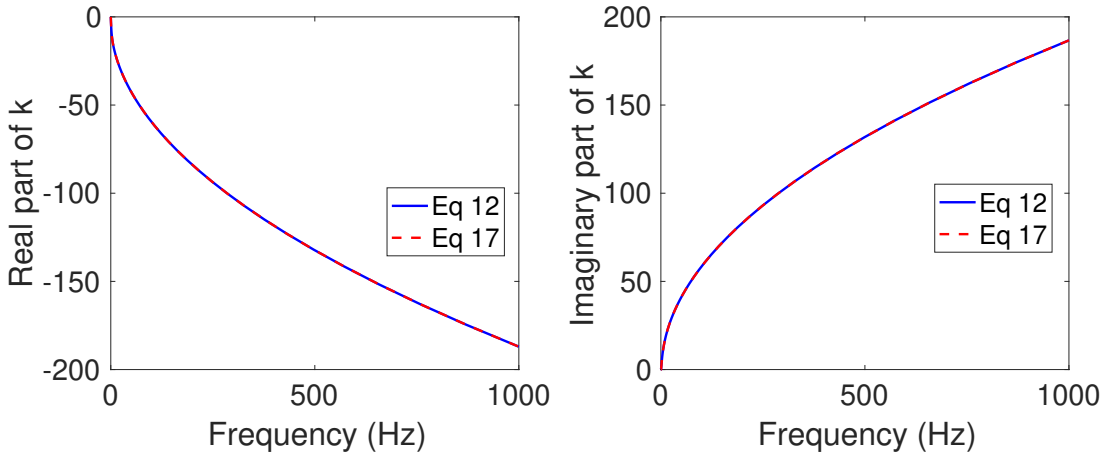

Figure 5.1: Comparing the real and imaginary part of k from Eq. (5.22) to the one from solving the root using Eq. (5.13) for the internal damping case.

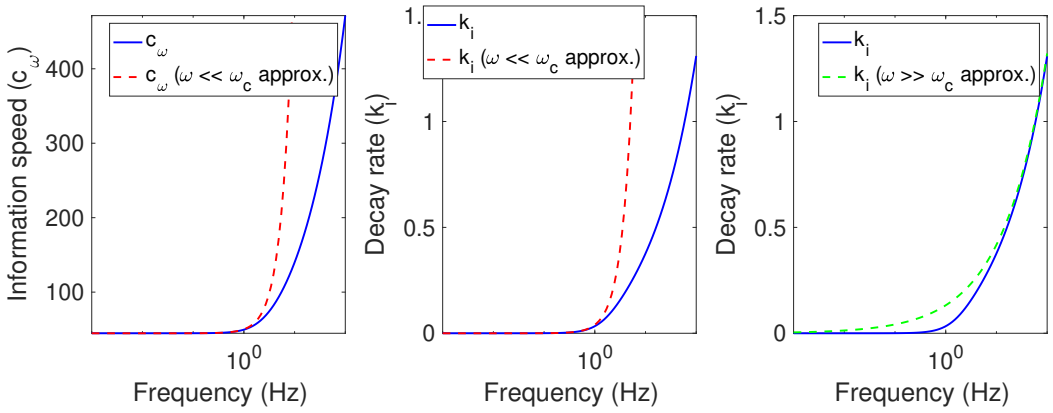

Figure 5.2: Checking the low frequency approximation (Eq. (5.30) for information propagation speed and Eq. (5.37) for decay rate) and high frequency approximation (Eq. (5.39) for decay rate) of the information propagation speed and decay rate theoretical predictions.

Low dispersion information propagation using only internal damping

The speed of information propagation is, from Eq. (5.17) and Eq. (5.22),

$$c_\omega = \frac{\omega}{k_r} = c\frac{\sqrt{2}}{\sqrt{\frac{1}{\sqrt{1+\frac{\beta_1^2\omega^2}{\gamma^2}}} + \frac{1}{1+\frac{\beta_1^2\omega^2}{\gamma^2}}}}, \tag{5.24}$$

The speed of information propagation can be written as,

$$c_\omega = \frac{\omega}{k_r} = \pm cF(x), \tag{5.25}$$

where

$$F(x) = \sqrt{2}\frac{1}{\sqrt{\frac{1}{\sqrt{1+x}} + \frac{1}{1+x}}}, \tag{5.26}$$

$$x = \frac{\beta_1^2\omega^2}{\gamma^2}. \tag{5.27}$$

$F(x)$ is approximated as a polynomial using Taylor series expansion, as follows,

$$F(x) \approx 1 + \frac{3}{8}x \tag{5.28}$$

$$= 1 + \frac{3}{8}\frac{\beta_1^2\omega^2}{\gamma^2}. \tag{5.29}$$

where higher order terms are dropped for $x \to 0$, which corresponds to small frequency values ($\omega \to 0$ in Eq. (5.27)), which can be approximated at small frequency ω as

$$c_\omega \approx c\left(1 + \frac{3}{8}\frac{\beta_1^2\omega^2}{\gamma^2}\right). \tag{5.30}$$

Note that the frequency knee point ω_c below which the wave frequency only changes by, say $\hat{P}_c\%$, from the nominal value c, i.e., $c_\omega = (1+\hat{P}_c/100)c$, can be found using the approximation in Eq. (5.30) as,

$$\omega_c = \frac{\gamma}{\beta_1}\sqrt{\frac{8}{3}\left(\frac{\hat{P}_c}{100}\right)}. \tag{5.31}$$

Therefore, the use of internal damping alone leads to low dispersion information transfer at small frequencies $\omega << \omega_c$.

Information decay rate and noise suppression with internal damping

The information dissipates exponentially $e^{-k_i x}$ with distance x and the decay rate depends on the imaginary component k_i of the wave number k given by, from Eq. (5.22),

$$k_i = \frac{\omega}{\sqrt{2}c}\sqrt{\frac{1}{\sqrt{1+\frac{\beta_1^2\omega^2}{\gamma^2}}} - \frac{1}{1+\frac{\beta_1^2\omega^2}{\gamma^2}}}. \tag{5.32}$$

The decay rate for the internal damping case is found from Eq. (5.22) as,

$$k_i = \frac{\omega}{\sqrt{2}c}\sqrt{G(x)}, \tag{5.33}$$

where,

$$G(x) = \frac{\sqrt{1+x}-1}{1+x}, \tag{5.34}$$

and x is from Eq. (5.27). $G(x)$ is approximated with a polynomial in x with Taylor series expansion, and dropping higher order terms for $x \to 0$ (which corresponds to low frequencies $\omega \to 0$ in Eq. (5.27)), as follows,

$$G(x) \approx \frac{1}{2}x, \tag{5.35}$$

$$= \frac{1}{2}\frac{\beta_1^2\omega^2}{\gamma^2}. \tag{5.36}$$

Therefore, using Eq. (5.36) and Eq. (5.33), the variation of decay rate w.r.t. the frequency for low frequencies can be approximated as,

$$k_i \approx \frac{\beta_1}{2\gamma c}\omega^2. \tag{5.37}$$

With internal damping, the complex part k_i of the wave number $k = \pm(k_r - ik_i)$ from Eq. (5.22) (that leads to information dissipation with increasing distance), can be rewritten as

$$\begin{aligned} k_i &= \frac{\omega}{\sqrt{2}c}\sqrt{\frac{1}{\sqrt{1+\frac{\beta_1^2\omega^2}{\gamma^2}}} - \frac{1}{1+\frac{\beta_1^2\omega^2}{\gamma^2}}}, \\ &= \frac{\omega}{\sqrt{2}c}\sqrt{\frac{\gamma\sqrt{\gamma^2+\beta_1^2\omega^2}-\gamma^2}{\gamma^2+\beta_1^2\omega^2}} \end{aligned} \tag{5.38}$$

and large frequency ω as,

$$k_i \approx \frac{1}{c}\sqrt{\frac{\gamma}{2\beta_1}}\sqrt{\omega}. \tag{5.39}$$

The frequency knee point for dissipation ω_i is defined as the frequency ω_i such that propagated information signal amplitude drop over the a desired distance $x = \hat{L}$, quantified by $e^{-\omega_i L}$, is smaller than some percentage, say $\hat{P}_i\%$, from the source amplitude for all frequency $\omega < \omega_i$, and can be estimated obtained using the approximation in Eq. (5.37) as,

$$\omega_i = \frac{1}{2\pi}\sqrt{\frac{2\gamma c}{\beta_1 \hat{L}}\log\left(\frac{1}{1-\hat{P}_i/100}\right)}. \tag{5.40}$$

Therefore, the use of internal damping alone results in small dissipation at small frequencies, e.g., when $\omega << \omega_i$ while enabling the suppression of large-frequency noise $\omega >> \omega_i$.

Remark 6 (Selection of network update gains) *Selecting the gain of the momentum term as $\beta_2 \approx 1$ in Eq.* (5.3) *for small viscous damping is needed for low distortion prop-*

agation of information through the network at small frequencies. In contrast, the outdated feedback $\beta_1 > 0$ (for internal damping) does not cause substantial dispersion or dissipation at small frequencies. Moreover, outdated feedback $\beta_1 > 0$ (for internal damping) is needed for suppressing noise at high frequencies.

5.4 Finite length networks

The information propagation in finite length discrete networks, unlike the infinitesimal continuum, includes interaction with boundary, which can lead to reflections and transient oscillations, which can persist in the network's response. The transition length (T-length) from non-oscillatory to oscillatory response can predicted for the internal damping case and can be increased using viscous damping, as shown below.

5.4.1 Damping in the response dynamics

Using separation of variable, $I(x,t) = X(x)T(t)$ in Eq. (5.7), where $X(x)$ and $T(t)$ represent the shape functions of position and time of the network response, results in,

$$X(x)\ddot{T}(t) = c^2 X''(x)T(t) + c^2\frac{\beta_1}{\gamma}X''(x)\dot{T}(t) - \frac{(1-\beta_2)}{\beta_2\delta_t}X(x)\dot{T}(t), \tag{5.41}$$

which can be rewritten as,

$$X(x)\left[\ddot{T}(t) + \frac{(1-\beta_2)}{\beta_2\delta_t}\dot{T}(t)\right] = c^2 X''(x)\left[T(t) + \frac{\beta_1}{\gamma}\dot{T}(t)\right], \tag{5.42}$$

and separated as

$$\frac{c^2 X''(x)}{X(x)} = \frac{\left[\ddot{T}(t) + \frac{(1-\beta_2)}{\beta_2\delta_t}\dot{T}(t)\right]}{\left[T(t) + \frac{\beta_1}{\gamma}\dot{T}(t)\right]} = -\Omega^2, \tag{5.43}$$

where Ω is the modal frequency. The solution of the position shape equation in Eq. (5.43),

$$X''(x) + \left(\frac{\Omega}{c}\right)^2 X(x) = 0, \tag{5.44}$$

depends on the boundary conditions. For a fixed boundary condition $I(0) = 0$ at one end $x = 0$ due to the leader agent (at $x = 0$), and free boundary condition with zero slope $\frac{\partial}{\partial x} I(L) = 0$ at the other end ($x = L$), the the position shape function for the m^{th} mode can be found as

$$X(x) = A \sin\left(\frac{\Omega_m}{c} x\right), \tag{5.45}$$

with fundamental mode frequency Ω_0

$$\Omega_m = (2m+1)\frac{\pi}{2L} c \ = (2m+1)\frac{\pi}{2L}\sqrt{\frac{\gamma a^2}{2\beta_2 \delta_t}}. \tag{5.46}$$

The time shape function in Eq. (5.43) becomes

$$\ddot{T}(t) + 2\zeta_m \Omega_m \dot{T}(t) + \Omega_m^2 T(t) \ = 0, \tag{5.47}$$

with mode-dependent damping ratio ζ_m given by

$$\zeta_m = \frac{(1-\beta_2)}{2\Omega_m \beta_2 \delta_t} + \frac{\beta_1}{2\gamma}\Omega_m \tag{5.48}$$

$$= \frac{(1-\beta_2)L}{(2m+1)\pi\beta_2\delta_t}\sqrt{\frac{2\beta_2\delta_t}{\gamma a^2}} + \frac{\beta_1}{4\gamma}\frac{(2m+1)\pi}{L}\sqrt{\frac{\gamma a^2}{2\beta_2\delta_t}} \tag{5.49}$$

obtained by using Eq. (5.55).

5.4.2 Position shape equation:

The position shape equation can be derived from Eq. (5.43), as follows,

$$X''(x) + \left(\frac{\Omega}{c}\right)^2 X(x) = 0, \tag{5.50}$$

Assuming the solution of the standard form,

$$X(x) = A\sin\left(\frac{\Omega}{c}x\right) + B\cos\left(\frac{\Omega}{c}x\right), \tag{5.51}$$

and applying the mixed boundary condition of,

$$X(0) = \kappa, \quad \frac{d}{dx}X(L) = 0, \tag{5.52}$$

for fixed boundary condition with the virtual source (at $x = 0$), and for slope to be zero at the free end ($x = L$), we get,

$$B = \kappa, \tag{5.53}$$

$$\left(\frac{\Omega_{n_x}}{c}\right) L = \frac{(2n_x + 1)}{2}\pi. \tag{5.54}$$

Therefore, the fundamental mode frequency, corresponding to $n_x = 0$, is found as,

$$\Omega_0 = \frac{\pi}{2L}c, \tag{5.55}$$

and therefore the position shape function for the fundamental mode is obtained as,

$$X(x) = A \sin\left(\frac{\pi}{2L}x\right). \tag{5.56}$$

5.4.3 Time shape equation:

The time shape function is derived from Eq. (5.43), as follows,

$$\ddot{T}(t) + \left[\frac{(1-\beta_2)}{\beta_2 \delta_t} + \frac{\beta_1}{\gamma}\Omega^2\right]\dot{T}(t) + \Omega^2 T(t) \ = 0. \tag{5.57}$$

5.4.4 Transition length

With internal damping alone ($\beta_2 = 1$), the smallest damping ratio ζ_0 corresponding to the first mode $m = 0$ decreases with length L, since from Eq. (5.49)

$$\zeta_0 \ = \frac{\beta_1}{4\gamma}\frac{\pi}{L}\sqrt{\frac{\gamma a^2}{2\delta_t}}. \tag{5.58}$$

Therefore, the transition length (T-length) L_T from non-oscillatory to oscillatory, becomes when the damping ratio $\zeta_0 = 1$ and is given by

$$L_T = \frac{\beta_1 \pi}{4\gamma}\sqrt{\frac{\gamma a^2}{2\delta_t}} \ = \frac{\beta_1 \pi}{4\gamma}c. \tag{5.59}$$

The damping ratio can be small for large networks beyond the T-length L_T, leading to sustained transient responses with reflections at boundary, since there is an upper bound β_1^* on the internal damping gain β_1 for stability (see SI Appendix, Section 4).

Remark 7 (Frequency-dependent response damping) *If the signal frequency ω is large,*

then the mode number m closest to the signal frequency ω is also large, since from Eq. (5.55)

$$\omega \approx \Omega_m = (2m+1)\frac{\pi}{2L}c = (2m+1)\Omega_0. \tag{5.60}$$

Therefore, the damping of the modes close to the signal frequency can be substantially higher than the first mode with internal damping alone, since from Eq. (5.49)

$$\zeta_m = (2m+1)\frac{L_T}{L} > 1 \tag{5.61}$$

for large m.

Remark 8 (Oscillation and cohesion trade-off) *If oscillations are undesired beyond the T-length limit, i.e., $L > L_T$, then some of the cohesion can be traded off by adding some viscous damping to keep the network critically damped, i.e., by selecting the momentum-term gain β_2 from Eq.* (5.49) *to achieve $\zeta_0 = 1$, as*

$$\beta_2 = \frac{\pi^2 a^2}{4L^2}\left(\sqrt{\frac{\gamma\delta_t}{2} + 4\frac{L^2}{\pi^2 a^2} + \frac{\beta_1}{2}} - \sqrt{\frac{\gamma\delta_t}{2}}\right)^2. \tag{5.62}$$

As the network length L increases the amount of viscous damping needed for avoiding oscillations becomes small, i.e., $\beta_2 \to 1$, from Eq. (5.62).

5.5 Discussion and conclusions

Simulation results are used to discuss the use of delayed self reinforcement (DSR) in networks. Results show that the use of DSR with already available information leads to low distortion wave-like information propagation with noise suppression. Moreover, the impact of using internal and viscous damping on cohesiveness and convergence of network responses is discussed.

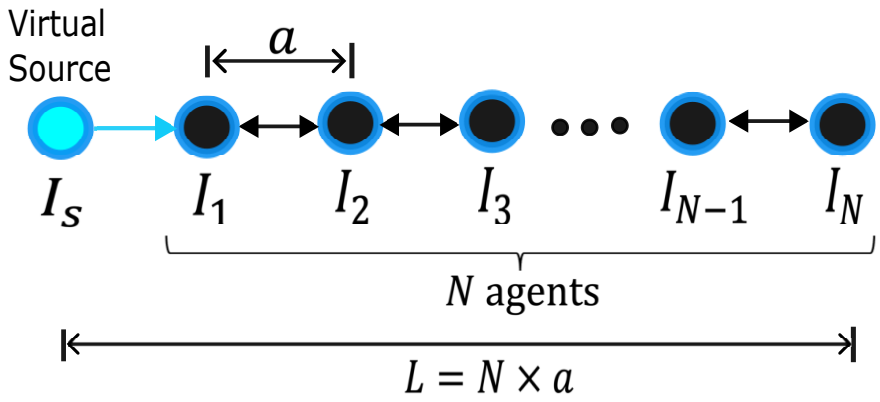

Figure 5.3: Example 1D network of N agents, with a virtual source (I_s) connected to the leader agent (I_1) and inter agent distance a. The set of neighbors (nearest agents to the left and right) for each agent is illustrated through the arrows.

5.5.1 DSR leads to wavelike information propagation

The low distortion wave-like information propagation with noise suppression in consensus-based networks by using outdated feedback $\beta_1 \neq 0$ (for internal damping) and selecting the momentum term as $\beta_2 = 1$ (to avoid viscous damping), as predicted from the continuum analysis of the DSR approach, is illustrated through a (temporally and spatially) discrete, 1D simulation example shown in (Figure 5.3).

Simulation example

The example network in the simulation in this subsection consists of a large number of agents ($N = 2000$) to assess the wave-like information propagation from the source on the left end, without the need to consider potential reflections from the boundary at the other end. The underlying undirected-path graph structure with inter-agent distances selected as $a = 0.2$ m, similar to the spacing of agents in the empirical model of starling flocks in [104], is shown in Figure 5.3. The left-most agent $i = 1$ is the leader agent connected to the information source $I_s(t)$, which propagates through the network due to the inter-agent connectivity. The response of each agent $I_i(t), \forall i \in [1, N]$ is computed according to the self-reinforcement

Cases	γ	β_1	β_2	Low distortion (small ω)	Noise suppression (large ω)
Case 0: Without damping	10	0	1	Yes	No
Case 1: With viscous damping	10	0	0.999	No	Yes
Case 2: With internal damping	10	$0.9\beta_1^*$	1	Yes	Yes

Table 5.1: Parameter choices $(\gamma, \beta_1, \beta_2)$ for comparison of damping cases and impact on low distortion at small frequencies ω and noise suppression at large frequencies. Case 2 with internal damping is the only case providing both low distortion at small frequencies and noise suppression at large frequencies.

approach in Eq. (5.3) for the example network in Figure 5.3, with different parameter (β_1, β_2) choices as in Table 5.1 to illustrate the effect of the viscous and internal damping terms, in Eq. (5.7), on information distortion during propagation through the network. The alignment strength γ, which determines the settling time of the network responses, is selected as $\gamma = 10$, and corresponds to a single agent's settling time of $T_s = 0.4$ s in the ideal cohesive dynamics (see SI Appendix, Section 1), and the update time period δ_t is selected to be small compared to the setting time, $\delta_t = T_s/4000 = 10^{-4}$ s.

Response matches wave-based predictions

The example-network's response matches the wave-like information propagation as predicted in Section 5.2 using only delayed self reinforcement of already available information (Eq. (5.3)) without the need for exchanging time-derivative information needed for discretized implementation of the wave equation (See SI text Section 3). In particular, the predicted information amplitude after unit distance propagation (i.e. e^{-k_i}) with k_i from Eq. (5.19) for the viscous damping (Case 1) and from Eq. (5.32) for the internal damping (Case 2) are shown in Figure 5.4(a). The wave-based analytical predictions are close to the values ob-

(a) Information amplitude after unit distance propagation (e^{-k_i})						
Freq. (Hz)	*Undamped*		*Viscous damping*		*Internal damping*	
	Pred.	Simul.	Pred.	Simul.	Pred.	Simul.
0.08	1	1	0.965	0.97	1	1
0.1	1	1	0.962	0.967	1	1
4	1	1	0.896	0.903	0.82	0.86
10	1	1	0.894	0.897	0.686	0.76
(b) Information propagation speed (c_ω)						
Freq. (Hz)	*Undamped Case 0*		*Viscous damping*		*Internal damping*	
	Pred.	Simul.	Pred.	Simul.	Pred.	Simul.
0.08	44.7	44.7	13.8	14.9	44.7	44.7
0.1	44.7	44.7	15.4	16.6	44.7	44.7
4	44.7	44.7	43.9	43.7	83	89
10	44.7	44.7	44.6	48	139.9	98.04

Table 5.2: (a) Information decay over unit distance (e^{-k_i}) and (b) propagation speed (c_ω) predictions from wave analysis match the simulation of discrete example with self-reinforcement (Eq. (5.3)), without the need for exchanging information time-derivatives among neighbor agents. The internal damping leads to low decay and low dispersion at small frequencies (0.08 Hz and 0.1 Hz), while dissipating larger frequencies (4 Hz and 10 Hz). On the other hand, viscous damping leads to distortion of small frequency signals due to high decay rate and different propagation speeds.

tained for the discrete network simulations (using Eq. (5.3)) as marked in the same figure as diamonds, both before and after the frequency knee point $\omega_i = 0.5$ Hz for an amplitude drop of less than $\hat{P}_i = 99\%$ over unit length $\hat{L}_i = 1$ from Eq. (5.40). Additionally, predictions of wave speed ($c_\omega = \omega/k_r$) using the analytical expression in Eq. (5.19) for the viscous damping (Case 1) and Eq. (5.24) for the internal damping (Case 2) are shown in Figure 5.4(b). The information propagation speeds obtained from discrete simulations using self-reinforcement matches the analytical predictions from the wave-based analysis, for both the internal and viscous damping cases, at smaller frequencies before the frequency knee $\omega < \omega_c$, and larger frequency $\omega > \omega_c$ where $\omega_c = 0.91$ Hz from Eq. (5.31) for a 10 % change in the speed.

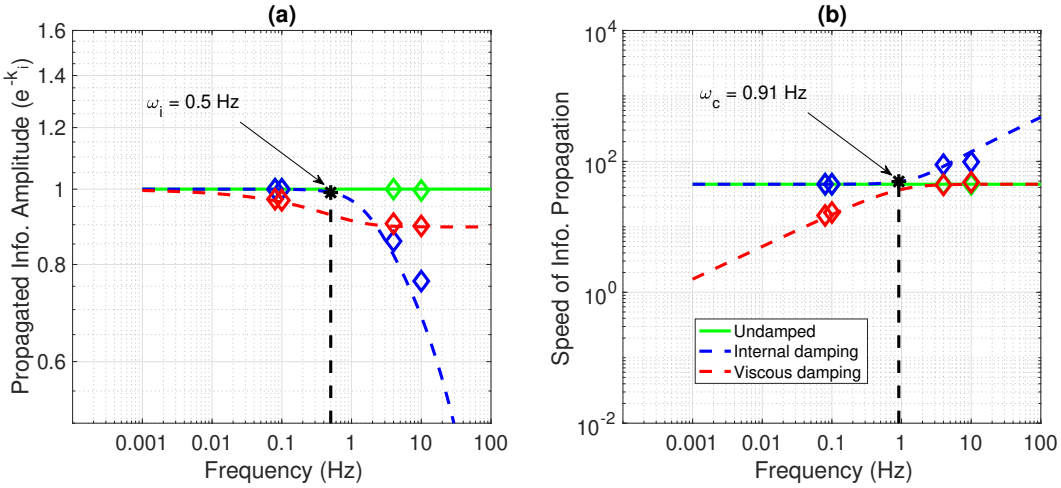

Figure 5.4: Comparision of information decay and speed characteristics under different damping conditions in Table 5.1. **(a)** Information amplitude dissipation over a unit length (i.e. e^{-k_i}) and **(b)** speed of information propagation (c_ω from Eq. (5.17). The results from simulating the network in Eq. (5.3) (shown as diamonds) matches the analytical predictions (shown as lines) at both small frequencies $f_1 = 0.08$ Hz and $f_2 = 0.1$ Hz, and at large frequencies $f_3 = 4$ Hz and $f_4 = 10$ Hz. The frequency knee point for transition in decay rate (ω_i from Eq. (5.40)) and in propagation speeds (ω_c from Eq. (5.31)) are depicted with vertical dashed lines. Internal damping (blue lines) leads to low distortion information propagation, i.e., when $\omega << \min\{\omega_i, \omega_c\}$and noise suppression at large frequencies $\omega >> \omega_i$. Viscous damping leads to distortion of small frequency signals due to high decay rate (red in **(a)** and different propagation speeds (red in **(b)**, while the associated dissipation saturates at large frequencies (red in **(a)** limiting noise suppression.

The information propagation with internal damping (blue line in Figure 5.4) is close to the results of the distortion-free ideal wave propagation (green line) with no damping at small frequencies, i.e., it has low dispersion (speed variations) and low dissipation (amplitude decay). In contrast, the information propagation with viscous damping (red line) shows substantial deviation from the distortion-free ideal wave propagation (green line) in Figure 5.4. This prediction of distortion-free information propagation when using internal damping compared to the substantial distortion with viscous damping is observed in the network simulations using Eq. (5.3), as depicted by diamonds in Figure 5.4, and illustrated in Figure 5.5, and tabulated in Table 5.2. Furthermore, the network simulations at large

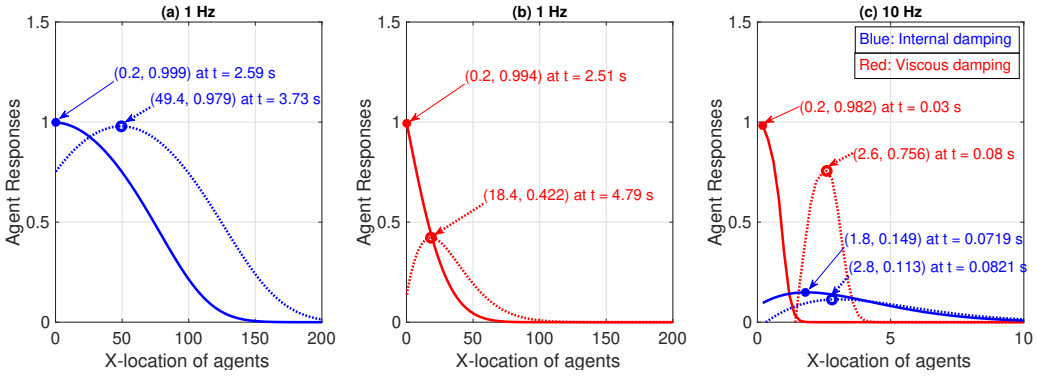

Figure 5.5: Simulated small and large frequency propagation results with internal and viscous damping based parameter selections for Eq. (5.3). Signal propagation in the example network in Section 5.5.1 is used to calculate (using peak amplitude information) the dissipation over unit distance (e^{-k_i}) and propagation speeds (c_ω) in Table 5.2. Dissipation with internal damping (blue in **(a)**) is significantly lower at small frequency (0.1 Hz) when compared to viscous damping (red in **(b)**). Moreover, internal damping enables substantially more noise suppression at large frequencies 10 Hz (blue in **(c)**) compared to viscous damping (red in **(c)**).

frequency (10 Hz) match the predicted substantial noise suppression with internal damping when compared to viscous damping and the no-damping cases, as seen in Figures 5.4 and 5.5, and tabulated in Table 5.2.

Noise-suppressed information propagation

The ability to transmit small frequency signals with low distortion while suppressing noise substantially at large frequency using internal damping is illustrated in Figure 5.6. The source signal $I_s = I_{s,s} + I_{s,l}$ has both small frequency(0.1 Hz) component $I_{s,s}$ and large frequency (10 Hz) component $I_{s,l}$ as shown in Figure 5.6 (a-c). With internal damping alone (Case 2 in Table 5.1) only the large frequency component is dissipated, while propagating the smaller frequency component with low distortion as seen in Figure 5.6 (f). On the other hand, agent responses with no damping (Figure 5.6 (d)) show propagation of both small and large frequencies without any noise suppression behavior. The viscous damping

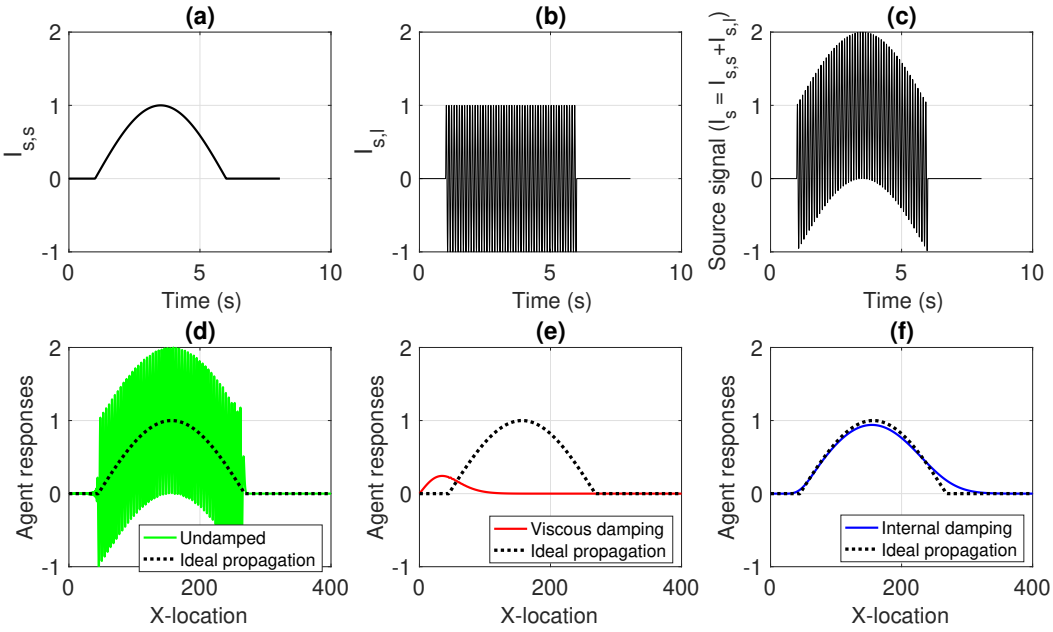

Figure 5.6: Information distortion and noise suppression for different damping conditions in Table 5.1 on propagation of small ($I_{s,s}$ 0.1 Hz in **(a)**) and large frequency noise ($I_{s,l}$ 10 Hz in **(b)**) components of a source signal $I_s = I_{s,s} + I_{s,l}$ shown in **(c)**. Agent responses over the network length (x) are compared at the same time instant $t = 7$ s with parameters selected as in Table 5.1 for **(d)** Case 0 undamped, **(e)** Case 1 viscous damping and **(f)** Case 2 internal damping. The undamped case does not suppress the high frequency noise **(d)**, while viscous damping dissipates both noise and the small frequency information content **(e)**. In contrast, the internal damping case **(f)** leads to propagation of small frequency content with low distortion and substantial suppression of larger frequency noise content (see Movie S1 for the three in the supplementary material).

case (Figure 5.6 (e)) dissipates both the small and large frequency signals leading to high distortion of the small-frequency source information as it propagates through the network. Furthermore, the viscous damping case does not sufficiently suppress large frequency signals as the internal damping case, leading to oscillations in the response, as predicted by the decay rates in Figure 5.4 and Table 5.2 (see Movie S1 in the supplementary material).

Remark 9 (General noise) *The impact of noise was studied using a high-frequency noise signal at the source. The larger exponential decay with distance* e^{-k_i}*) of the source noise with*

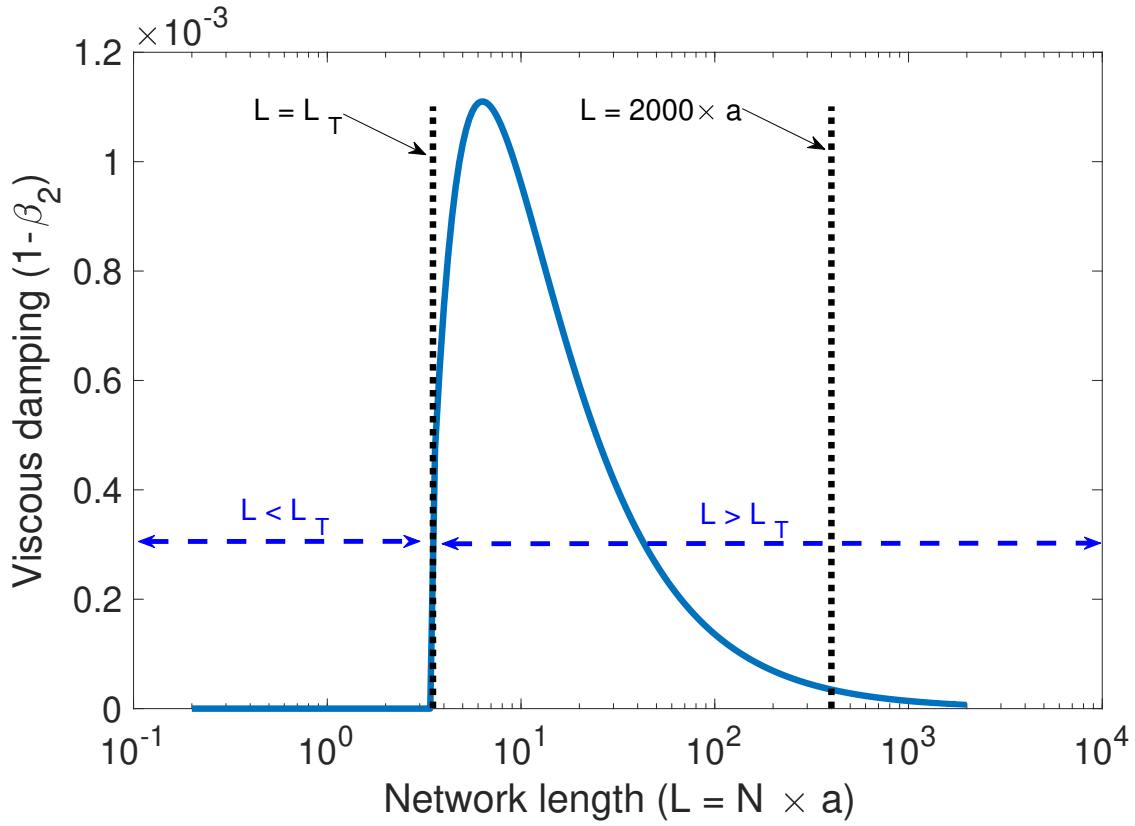

Figure 5.7: Quantifying the amount of viscous damping needed for critical damping of networks with different lengths according to Eq. (5.58). Viscous damping is not needed below the transition length ($L < L_T$), and the amount of viscous damping $1 - \beta_2 > 0$ needed decreases with increasing network length L.

internal damping in Figure 5.4(a) also implies that the summation of noise from all agents (at varying distances) will be smaller as well for the internal damping case when compared to viscous damping and undamped cases.

Remark 10 (Selection of internal damping parameters) *Internal damping leads to distortion-free information propagation in the example network at low frequencies, while also dissipating out high frequency signals, as shown in this section. Moreover, the transition point in frequency for the internal damping case, from distortion-free information propagation at low frequencies to dispersion of higher frequency signals, can be predicted and designed using the*

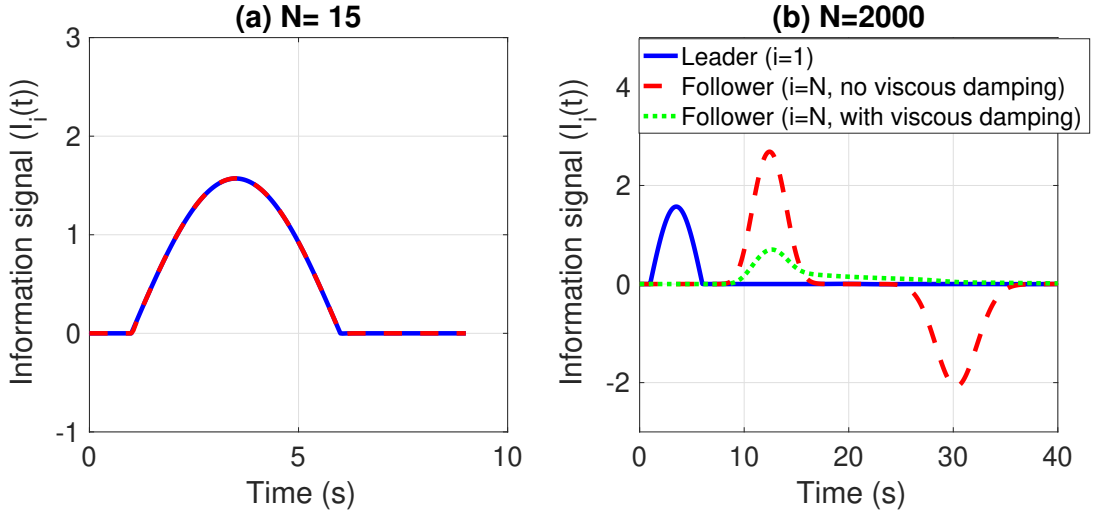

Figure 5.8: Non-zero viscous damping is needed for non-oscillatory behaviour of networks longer than the transition length $L > L_T$. **(a)** Short networks below the transition length $L < L_T$ are non-oscillatory without viscous damping, however, **(b)** large networks require viscous damping for non-oscillatory response but lead to information decay. The source information signal used is $I_{s,s}$ in Figure 5.6 (a).

update parameters.

5.5.2 Impact on cohesion of networks

The impact of cohesion on networks with internal damping is shown for networks of length L shorter and longer than the transition length L_T from Eq. (5.59). The parameter β_1 in Eq. (5.3), which signifies the level of internal damping in the wave approximation Eq. (5.6), is selected to critically damp the fundamental temporal dynamics mode of the shorter network ($L < L_T$), according to Eq. (5.58) with $\zeta_{\Omega_0} = 1$. However, longer networks with length $L > L_T$ cannot be critically damped with internal damping only, which leads to oscillatory responses. Therefore, some viscous damping, with $\beta_2 < 1$ according to Eq. (5.62) and shown in Figure 5.7, is needed to avoid oscillations for longer networks ($L > L_T$).

Internal damping leads to cohesive short networks

A cohesive network, where all agents respond in a similar manner, is achieved using the internal damping approach for networks of length $L < L_T = 17.55a$. For instance, information signal $I_{s,s}$ (Figure 5.6 (a)) propagates with low distortion, and without oscillations, in the example network (Figure 5.3) with $N = 15$ agents and length $L = 15 \times a$, which is smaller than the transition length L_T (Figure 5.7), as shown in Figure 5.8 (a).

Underdamped longer networks using internal damping only

Some viscous damping, with $\beta_2 < 1$ according to Eq. (5.62) (Figure 5.7), is required for critically damping the first mode of wave dynamics (Eq. (5.57)) for networks of length greater than transition length ($L > L_T$). This is illustrated for network of length $L = 2000 \times a$ in Figure 5.8. The orientation response of the last follower agent, with index $i = N$ (Figure 5.3), is oscillatory, and amplified as shown in Figure 5.8. The amount of viscous damping required for achieving critical damping in longer networks approaches zero with increasing length L, as discussed in Remark 8 and illustrated in Figure 5.7, where $1 - \beta_2 \to 0$ as $L \to \infty$. Therefore, adding a small amount of viscous damping, according to Eq. (5.62), removes the oscillation of the information signal, however, with increased signal dissipation, as shown in Figure 5.8.

Coherent turning maneuvers using only internal damping

Internal damping leads to coherent turning maneuvers in networks, even in presence of noise, because of noise suppression, as shown in Figure 5.6. The coherence of the turning maneuver is evaluated through an example network, with underlying graph structure as in Figure 5.3 with $N = 15$. Each agent in the network has the velocity state $\vec{v}_i = v_0\, e^{iI_i}$ and 2D location on the X-Y plane (x_i, y_i), where $v_0 = 1$ is a constant velocity magnitude, and I_i is the orientation information. The velocities of the agents are determined at each time step k using orientation information state $I_i[k]$, which is updated by each agent using neighbor information according to Eq. (5.3), and the resulting location at the next time step is found

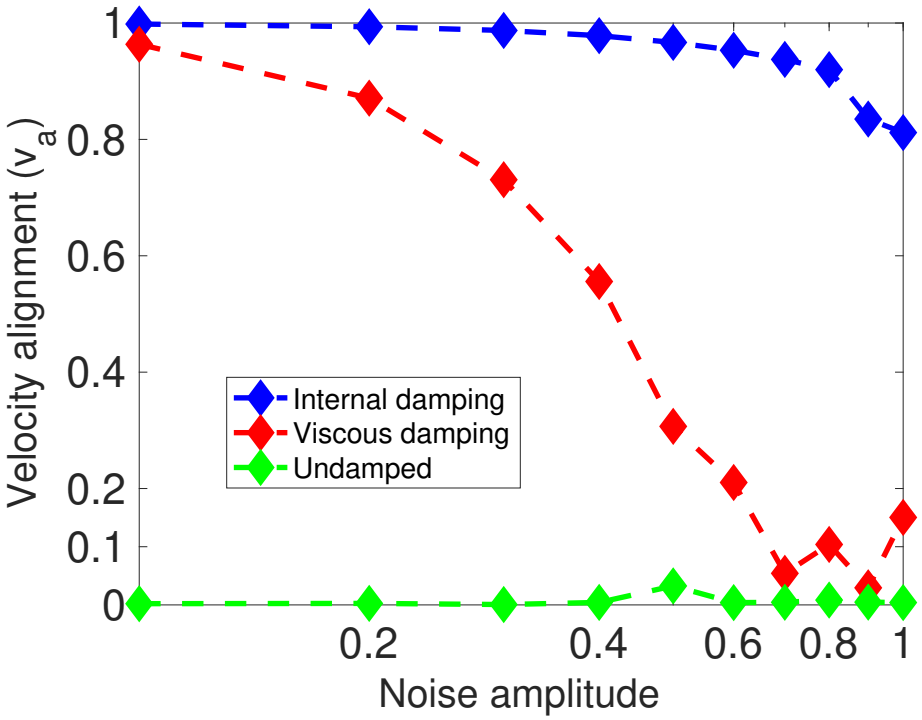

Figure 5.9: Velocity coherence (v_a from Eq. (5.66)) for different damping conditions in Table 5.1 during turning for a network of $N = 15$ agents with increasing noise amplitude n_l in Eq. (5.65). (see Movie S2 in the supplementary material for turning maneuvers with noise level $n_l = 0.5$). Use of internal damping leads to substantial increase in velocity coherence in the presence of noise compared to the viscous and undamped cases.

as,

$$x_i[k+1] = x_i[k] + \delta_t \mathrm{Re}(\vec{v}_i) = x_i[k] + \delta_t v_0 \cos\left(I_i[k]\right), \tag{5.63}$$

$$y_i[k+1] = y_i[k] + \delta_t \mathrm{Im}(\vec{v}_i) = y_i[k] + \delta_t v_0 \sin\left(I_i[k]\right). \tag{5.64}$$

The desired orientation response, I_s for the turning maneuver is chosen as $I_s = (\pi/2) \times I_s$,

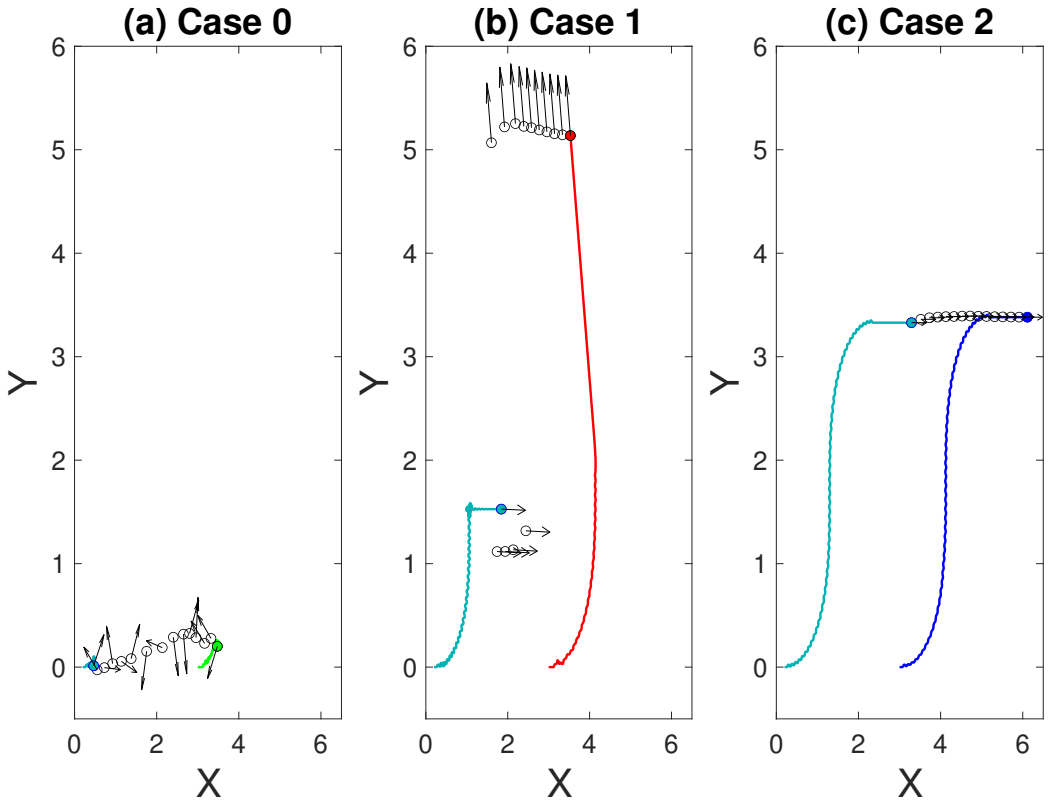

Figure 5.10: Comparison of different damping conditions in Table 5.1 when propagating orientation information in the presence of large frequency noise. Source orientation information with small frequency (0.1 Hz, $I_{s,s}$ in Figure 5.6 (a)) component, and large frequency (10 Hz, $I_{s,l}$ in Figure 5.6 (b)) component with amplitude of the larger frequency signal as $n_l = 0.5$ leads to **(a)** approximately zero velocity coherence without damping (Case 0), **(b)** network splitting due to loss of velocity coherence using viscous damping (Case 1), and **(c)** parallel turns due to low distortion and noise suppression using internal damping (Case 2) for a network with $N = 15$ agents (see Movie S2 in supplementary material for the entire trajectory).

where

$$I_s = I_{s,s} + n_l I_{s,l} \tag{5.65}$$

with $I_{s,s}$ from Figure 5.6 (a) and $I_{s,l}$ from Figure 5.6 (b), where n_l is the amplitude of the

high-frequency noise. The velocity coherence is quantified using

$$v_a = \min_k \left[\frac{1}{N v_0} \sum_{i=1}^{N} \vec{v}_i[k] \right], \tag{5.66}$$

with the minimum value taken to quantify the worst-case loss of coherence during a maneuver. The measure v_a is similar to the averaged velocity alignment of the agents in [81], and is used to assess the orientation alignment during the transition for the different damping cases in this study. Note that for perfect velocity coherence $v_a \to 1$, whereas, smaller values represent increasing decoherence.

Internal damping leads to higher velocity coherence, in the presence of noise as compared to other methods. For example, the velocity coherence of the example network with $N = 15$ agents (and length $L < L_T$) is compared in Figure 5.9 for the different cases in Table 5.1. Internal damping leads to higher velocity coherence, as compared to other methods, which is necessary for maintaining formation during the turning maneuver, as shown for noise level $n_l = 0.5$ in Movie S2 in the supplementary material, where a network is considered broken if the distance between neighbors becomes larger than twice the nominal spacing of $2 \times a$ (Figure 5.3). The noise suppression with internal damping enables maintaining formation during the turning maneuver, as opposed to the viscous damping and undamped cases with similar noise levels.

In conclusion, the use of delayed self reinforcement (DSR) by the agents in the network with prior information (e.g., using short-term memory) can lead to the wave-like information propagation at low-frequencies without the need for additional information sharing (e.g., of higher-order time derivative information) between the agents. Moreover, the DSR can be designed to enable suppression of larger-frequency noise transmission while limiting the dissipation and dispersion of (smaller-frequency) information content leading to similar (cohesive) behavior of agents and improved coherence — even in the presence of substantial noise.

5.6 Chapter Conclusions

In this article it is shown that delayed self reinforcement (DSR) by the agents in the network with prior information (e.g., using short-term memory) can lead to the wave-like information propagation at low-frequencies without the need for additional information (such as higher-order time derivatives) sharing between the agents. Moreover, it is shown that the DSR can be designed to enable suppression of larger-frequency noise transmission while limiting the dissipation and dispersion of (smaller-frequency) information content leading to similar (cohesive) behavior of agents. Thus, the work provides a potential model for the super-fluid like information transfer and parallel maneuvers observed in natural swarms, and the improved information transfer can improve performance of engineered networked systems.

Chapter 6

MC3: COHESIVE TRANSITIONS IN PRESENCE OF NETWORK DELAYS.

This chapter forms the contribution **MC3** of the dissertation, enabling cohesive transitions under network delays, which can be due to sensing or communication between neighbors. This chapter has been published as an article in [6].

6.1 Problem Formulation

This section provides the description of each agent's higher-order dynamics, the derivation of the ideal higher-order network dynamics and the DSR-based implementation for cohesive tracking of a desired response $x_s(t)$ given as the state of a source agent s. Then the DSR approach in networks with delay is presented, which leads to the problem statement of the chapter.

6.1.1 DSR Background

Agent's higher-order dynamics

A network of N heterogeneous n_i dimensional agents is considered, where each i^{th} agent's dynamics is in the output-tracking form (through appropriate input and state transformation [105]) as,

$$x_i^{(r_i)}(t) = u_i(t), \tag{6.1}$$

$$\frac{d}{dt}\eta_i(t) = A_{\eta,i}\eta_i(t) + A_{x,i}X_i(t), \tag{6.2}$$

where $x_i(t) \in \mathbb{R}$ is the output of the i^{th} agent, r_i is the relative degree (the difference between the number of poles and number of zeros of the i^{th} agent's transfer function), $x_i^{(r_i)}(t)$ is the r_i^{th} time-derivative of $x_i(t)$, $X_i(t) \in \mathbb{R}^{r_i}$ is a vector of the observable states consisting of the output $x_i(t)$ and its derivatives $x_i^{(k)}(t)$ for $1 \leq k \leq r_i - 1$ and $\eta_i(t) \in \mathbb{R}^{n_i - r_i}$ is the vector of the non-observable internal states of the system.

Assumption 4 (Relative degree and minimum phase) *All agents are assumed to have the same relative degree $r_i = r$, with strictly proper transfer functions i.e. $1 \leq r \leq n$, and minimum phase dynamics i.e., i.e. $A_{\eta,i}$ is Hurwitz.* □

Remark 15 (Heterogeneous agents) *The agents, although having same relative degree r, can have different matrices, $A_{\eta,i}, A_{x,i}$, governing the internal state dynamics in Eq.* (6.2) *as well as different state and input transformations to bring them to the output tracking form.*

Ideal cohesive network dynamics

If each agent i in the network, defined in Subsection 6.1.1, has direct access to the desired response $x_s(t)$, then the control input u_i in Eq. (6.1) can be chosen as,

$$x_i^{(r)}(t) = u_i(t) = x_s^{(r)}(t) - \sum_{k=0}^{r-1} \hat{\alpha}_k (x_i^{(k)}(t) - x_s^{(k)}(t)), \tag{6.3}$$

where the error gains $\hat{\alpha}_k > 0$ are chosen to place the roots of the tracking dynamics at $-\alpha < 0$, with $\hat{\alpha}_r = 1$, as given below,

$$\sum_{k=0}^{r} \hat{\alpha}_k s^k = (s + \alpha)^r = \mathcal{P}(s), \tag{6.4}$$

where $\mathcal{P}(s)$ is the characteristic equation polynomial of the tracking dynamics in Eq. (6.3), which will lead to cohesive output response among the agents of the network, assuming same

initial conditions of the agents [1]. The cohesive tracking dynamics for the entire network is shown below,

$$\begin{aligned} X^{(r)}(t) &= -\sum_{k=0}^{r-1} \hat{\alpha}_k X^{(k)}(t) + \mathbf{1}_N \sum_{k=0}^{r} \hat{\alpha}_k x_s^{(k)}(t), \\ &= -\sum_{k=0}^{r-1} \hat{\alpha}_k X^{(k)}(t) + \mathbf{1}_N x_s^*(t), \end{aligned} \tag{6.5}$$

where,

$$x_s^*(t) = \sum_{k=0}^{r} \hat{\alpha}_k x_s^{(k)}(t). \tag{6.6}$$

However, the cohesive tracking network dynamics in Eq. (6.5) requires a centralized network architecture where each agent i is connected directly to the source agent s.

Decentralized cohesive network dynamics

A decentralized implementation of the cohesive tracking network dynamics in Eq. (6.5), which doesn't require each agent being connected to the source agent, is derived. Upon multiplying Eq. (6.5) with βK, where β is the DSR gain and K is the pinned Laplacian matrix of the non-source agents in the network with dimensions $N \times N$, defined as in [85],

$$\begin{aligned} K(i,j) &= -w_{ij}, && j \in N_i \text{ and } j \neq i \\ &= \sum_{m=1}^{N} w_{im}, && j = i \\ &= 0, && \text{otherwise}, \end{aligned} \tag{6.7}$$

where the edge weights $w_{ij} > 0$ if $j \in N_i$, N_i is the set of neighbors (including a source agent s) of agent i. and using $K\mathbf{1}_N = B$ from [60], where $B = \begin{bmatrix} w_{1s} \, w_{2s} \, \dots \, w_{Ns} \end{bmatrix}^T$ is the source connectivity vector (i.e. $B_i = w_{is} > 0$ if agent i is connected to the source and $B_i = 0$ otherwise) and $\mathbf{1}_N$ is an $N \times 1$ vector of all ones, we get,

$$\beta K X^{(r)}(t) = -\beta \sum_{k=0}^{r-1} \hat{\alpha}_k K X^{(k)}(t) + \beta B x_s^*(t). \tag{6.8}$$

Adding and subtracting $X^{(r)}(t)$ on the left hand side of Eq. (6.8) and rearranging the terms, the cohesive tracking dynamics in Eq. (6.5) can be written in a decentralized form as

$$\begin{aligned} X^{(r)}(t) = (\mathbf{I}_N - \beta K) X^{(r)}(t) - \beta \sum_{k=0}^{r-1} \hat{\alpha}_k K X^{(k)}(t) \\ + \beta B x_s^*(t), \end{aligned} \tag{6.9}$$

where $\mathbf{I}_N$ is an $N \times N$ identity matrix. The network dynamics obtained in Eq. (6.9) is a decentralized implementation of the cohesive tracking dynamics in Eq. (6.5). However, Eq. (6.9) has the r^{th} derivative of the states ($X^{(r)}(t)$) on both sides of the equation, which implies each agent requires the r^{th} derivative of both its own state and the relative information from its neighboring agents to compute its r^{th} derivative, which is difficult to implement [1]. Therefore, a decentralized approach for cohesive tracking which doesn't require r^{th} derivative information as in Eq. (6.9) is required.

DSR-based cohesive network dynamics

Delayed self reinforcement (DSR) [1], which provides a decentralized approximation of the cohesive tracking network dynamics in Eq. (6.5), is derived below. The derivative $s^r X(s)$ on RHS in the ideal dynamics Eq. (6.9) is approximated with $\hat{X}^{(r)}(s, \tau)$ using with delayed

state information as shown below,

$$s^r X(s) \approx \hat{X}^{(r)}(s,\tau) = \left(f(s) \frac{1-e^{-s\tau}}{\tau} \right)^r X(s)$$
$$= \mathcal{F}(s) X(s), \tag{6.10}$$

where $f(s)$ is a low pass filter with cut-off frequency as $\omega > 0$,

$$f(s) = \frac{\omega}{s+\omega}, \tag{6.11}$$

which results in the DSR-based implementation of cohesive tracking dynamics in Eq. (6.5), by replacing $X^{(r)}(t)$ on RHS in Eq. (6.9) with the Laplace inverse of $\hat{X}^{(r)}(s,\tau)$, as follows,

$$X^{(r)}(t) = (\mathbf{I}_N - \beta K)\hat{X}^{(r)}(t,\tau) - \beta K \sum_{k=0}^{r-1} \hat{\alpha}_k X^{(k)}(t)$$
$$+ \beta B x_s^*(t). \tag{6.12}$$

Remark 16 (Standard consensus-based approach) *The standard consensus based approaches can be recovered from DSR approach in Eq.* (6.19)*, by removing the term* $(\boldsymbol{I}_N - \beta K)\, \hat{X}^{(r)}(t,\tau)$ *and setting* $\beta = 1$ *on the RHS, which results in,*

$$X^{(r)}(t) = \; -K \sum_{k=0}^{r-1} \hat{\alpha}_k X^{(k)}(t) + \beta B x_s^*(t). \tag{6.13}$$

Assumption 5 (Connected to source node) *It is assumed that every non-source agent in the network lies on at least one directed path starting from the source agent s. Therefore, by the Matrix-Tree-Theorem [106], the network's pinned Laplacian K is invertible, i.e. its*

eigenvalues satisfy $\mathcal{R}e(\lambda_{K,i}) > 0$*, which, using Matrix-Tree-Theorem [106], can be bounded as* $\lambda_{K,i} = m_i e^{j\phi_i}$*,* $\forall\, 1 \leq i \leq N$ *of the pinned Laplacian* K*,*

$$0 < \underline{m} \leq m_i \leq \overline{m}, \quad |\phi_i| \leq \overline{\phi} < \frac{\pi}{2} \tag{6.14}$$

where $j = \sqrt{-1}$*.* □

Lemma 4 (Exponential stability of DSR [1]) *Let the the DSR gain* $\beta > 0$ *in Eq.* (6.12) *be chosen to be sufficiently large, i.e.,*

$$\beta > \max_{1 \leq i \leq N} \frac{1}{\mathcal{R}e\{\lambda_{K,i}\}}. \tag{6.15}$$

where $\lambda_{K,i}$ *are the eigenvalues of the pinned Laplacian* K*. Then, under Assumptions 4-5, the delayed differential equation (DDE) of the DSR approach in Eq.* (6.12) *is exponentially stable if*

$$\sup_{\mathcal{R}e(s) \geq 0} \left| f(s)(1 - e^{-\tau s}) \right| \leq (\epsilon_\lambda)^{1/r} \alpha \tau, \tag{6.16}$$

where

$$\epsilon_\lambda = \frac{\beta \overline{m}}{\sqrt{\beta^2 \overline{m}^2 - 2\beta \overline{m} \cos \overline{\phi} + 1}}, \quad \textit{if } r > 1, \tag{6.17}$$

$$= \frac{\beta \underline{m} \cos \overline{\phi}}{\sqrt{\beta^2 \overline{m}^2 - 2\beta \overline{m} \cos \overline{\phi} + 1}}, \quad \textit{if } r = 1. \tag{6.18}$$

Proof See [1]. □

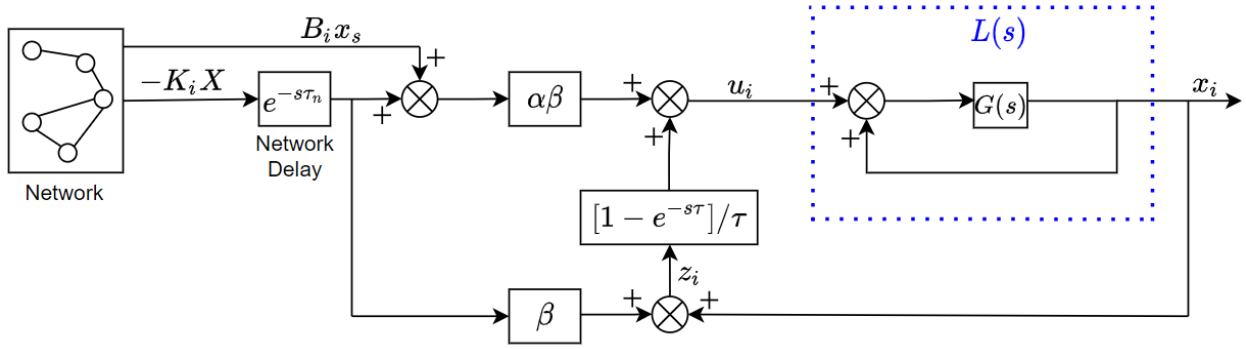

Figure 6.1: Dynamics of agent i with delayed self reinforcement using network information $K_i X$ with network delay τ_n.

6.1.2 Research problem: stability of DSR with network delay

With all agents having the same constant network delay τ_n, the network dynamics with the DSR approach in Eq. (6.12) becomes modified as shown in Figure 6.1, and can be described by

$$X^{(r)}(t) = \hat{X}^{(r)}(t,\tau) - \beta K \hat{X}^{(r)}(t-\tau_n,\tau) - \beta K \sum_{k=0}^{r-1} \hat{\alpha}_k X^{(k)}(t-\tau_n) + \beta B x_s^*(t). \tag{6.19}$$

The research problem is to develop conditions for stability of DSR with network delay τ_n as in Eq. (6.19), by predicting a lower bound on the network delay margin (DM) for stable cohesive network transitions using DSR.

6.2 Estimating DSR Network Delay Margin

The DSR approach with network delay τ_n in Eq. (6.19) is stable if the roots of the characteristic equation $C_{\tau_n}(s) = 0$ in Eq. (6.21) lie in the open left half of the complex plane, which is obtained by taking the Laplace transform of Eq. (6.19) (with $x_s^*(t) = 0$ as it doesn't

influence stability), and equating the determinant to zero,

$$\det \left| s^r \mathbf{I}_N - (\mathbf{I}_N - \beta K e^{-s\tau_n})\mathcal{F}(s) + e^{-s\tau_n}\beta K \sum_{k=0}^{r-1} \hat{\alpha}_k s^k \right| = 0, \tag{6.20}$$

which simplifies to the following characteristic equation through Jordan decomposition (using arguments from Lemma 2 of [1]),

$$\begin{aligned} \mathcal{C}_{\tau_n}(s) = \; & s^r - (1 - \beta\lambda_{K,i} e^{-s\tau_n})\mathcal{F}(s) \\ & + e^{-s\tau_n}\beta\lambda_{K,i} \sum_{k=0}^{r-1} \hat{\alpha}_k s^k = 0, \end{aligned} \tag{6.21}$$

where the DSR gain is β, the pinned Laplacian eigenvalues are $\{\lambda_{K,i}\}_{i=1}^{N}$, the intentional DSR delay terms are $e^{-sm\tau},\ m \in [1, r]$ and the network delay term is $e^{-s\tau_n}$. The characteristic polynomial with network delay $\mathcal{C}_{\tau_n}(s)$ in Eq. (6.21) can be rewritten as the sum of the original characteristic polynomial $\mathcal{C}(s)$ with no network delay, defined as,

$$\mathcal{C}(s) = s^r - (1 - \beta\lambda_{K,i})\mathcal{F}(s) + \beta\lambda_{K,i} \sum_{k=0}^{r-1} \hat{\alpha}_k s^k, \tag{6.22}$$

and network delay dependent perturbation term $g(s, \tau_n)$, by adding and subtracting $\mathcal{C}(s)$ in Eq. (6.21), as

$$\mathcal{C}_{\tau_n} = \mathcal{C}(s) + g(s, \tau_n), \tag{6.23}$$

where,

$$\begin{aligned} g(s,\tau_n) &= \mathcal{C}_{\tau_n}(s) - \mathcal{C}(s) \\ &= (e^{-s\tau_n} - 1)\beta\lambda_{K,i}\left(\mathcal{F}(s) + \sum_{k=0}^{r-1}\hat{\alpha}_k s^k\right). \end{aligned} \tag{6.24}$$

The following lemma shows that any roots of the characteristic equation in Eq. (6.21) lie in a bounded region in the closed right half of the complex plane, irrespective of the network delay.

Lemma 5 *The roots of* $C_{\tau_n}(s) = 0$ *in Eq.* (6.21) *on the closed right half of the complex plane* ($\overline{\mathbb{C}}_+$)*, if any, are bounded within the region* $\overline{\Omega}$ *for any network delay* $\tau_n \in [0, \infty)$*, where* $\overline{\Omega}$ *is defined as,*

$$\overline{\Omega} = \{s \in \overline{\mathbb{C}}_+ \ : \ |s| < R^*\}, \tag{6.25}$$

where for a given $0 < \epsilon < 1$*,*

$$R^* = \max\{1, R_1, R_2\}, \tag{6.26}$$

$$R_1 = \left(\frac{1 + 3\beta\overline{\lambda}_K}{\epsilon\beta\overline{\lambda}_K \sum_{k=0}^{r-1}\hat{\alpha}_k}\right)^{1/(r-1)}\left(\frac{2}{\tau}\right)^{r/r-1}, \tag{6.27}$$

$$R_2 = (3+\epsilon)\beta\overline{\lambda}_K \sum_{k=0}^{r-1}\hat{\alpha}_k, \tag{6.28}$$

$$\overline{\lambda}_K = \max_i |\lambda_{K,i}|. \tag{6.29}$$

Proof Since $|\mathcal{C}_{\tau_n}(s)| \geq |\mathcal{C}(s)| - |g(s,\tau_n)|$ from Eq. (6.23), there can be no root of $\mathcal{C}_{\tau_n}(s) = 0$ at s if $|\mathcal{C}(s)| > |g(s,\tau_n)|$. In the following, it is shown that, for large magnitude complex numbers s in the closed right half of the complex plane, the perturbation $|g(s,\tau_n)|$ in Eq. (6.24) is upper bounded by a polynomial in $|s|$ of degree $r-1$, and the original characteristic polynomial $|\mathcal{C}(s)|$ is lower bounded by a polynomial of $|s|$ of degree r resulting in $|\mathcal{C}(s)| > |g(s,\tau_n)|$ for large $|s|$. Specifically, from Eq. (6.24),

$$|g(s,\tau_n)| \leq |\beta\lambda_{K,i}(e^{-s\tau_n} - 1)| \left(\sum_{k=0}^{r-1} \hat{\alpha}_k |s|^k + |\mathcal{F}(s)| \right). \tag{6.30}$$

Moreover, on the closed right half of the complex plane ($\overline{\mathbb{C}}_+$),

$$|\beta\lambda_{K,i}(e^{(-s\tau_n)} - 1)| \leq 2\beta|\lambda_{K,i}| \leq 2\beta\overline{\lambda}_K, \tag{6.31}$$

and if $s \neq 0$

$$|\mathcal{F}(s)| = \left| \frac{\omega}{(s+\omega)} \frac{(1-e^{-s\tau})}{\tau} \right|^r < \left| \frac{(1-e^{-s\tau})}{\tau} \right|^r \leq \left(\frac{2}{\tau} \right)^r. \tag{6.32}$$

Then, if

$$s \in \hat{\Omega} = \left\{ \overline{\mathbb{C}}_+ - \ \overline{\Omega} \right\}, \tag{6.33}$$

substituting the bounds in Eq. (6.31) and Eq. (6.32), into Eq. (6.30), results in $|g(s,\tau_n)|$ upper bounded by a polynomial in $|s|$ of degree $r-1$, $\overline{g}(|s|)$, as

$$\begin{aligned} |g(s,\tau_n)| &< 2\beta|\lambda_{K,i}| \left(\sum_{k=0}^{r-1} \hat{\alpha}_k |s|^k + \left(\frac{2}{\tau} \right)^r \right) \\ &\leq 2\beta\overline{\lambda}_K \left(|s|^{r-1} \sum_{k=0}^{r-1} \hat{\alpha}_k + \left(\frac{2}{\tau} \right)^r \right) \\ &= \overline{g}(|s|), \end{aligned} \tag{6.34}$$

since $\hat{\alpha}_k > 0$ and $|s| \leq |s|^k$ for $k > 1$ when $|s| \geq 1$. Similarly, if $s \in \hat{\Omega}$, $|\mathcal{C}(s)|$ is lower bounded by $\underline{\mathcal{C}}(|s|)$, a polynomial in $|s|$ of degree r.

$$\begin{aligned}
|\mathcal{C}(s)| &= \left| s^r + \beta\lambda_{K,i} \sum_{k=0}^{r-1} \hat{\alpha}_k s^k - (1 - \beta\lambda_{K,i})\mathcal{F}(s) \right| \\
&\geq |s|^r - \beta|\lambda_{K,i}| \sum_{k=0}^{r-1} \hat{\alpha}_k |s|^k - |1 - \beta\lambda_{K,i}||\mathcal{F}(s)| \\
&> |s|^r - \beta\overline{\lambda}_K |s|^{r-1} \sum_{k=0}^{r-1} \hat{\alpha}_k - (1 + \beta\overline{\lambda}_K) \left(\frac{2}{\tau}\right)^r \\
&= \underline{\mathcal{C}}(|s|). \qquad (6.35)
\end{aligned}$$

Next to show that $|\mathcal{C}(s)| > |g(s, \tau_n)|, \forall s \in \hat{\Omega}$,

$$\begin{aligned}
&|\mathcal{C}(s)| - |g(s, \tau_n)| \\
&> \underline{\mathcal{C}}(|s|) - \overline{g}(|s|) \\
&= |s|^r - 3\beta\overline{\lambda}_K |s|^{r-1} \sum_{k=0}^{r-1} \hat{\alpha}_k - (1 + 3\beta\overline{\lambda}_K) \left(\frac{2}{\tau}\right)^r, \\
&= |s|^{r-1} \left[|s| - 3\beta\overline{\lambda}_K \sum_{k=0}^{r-1} \hat{\alpha}_k - \frac{(1 + 3\beta\overline{\lambda}_K|)}{|s|^{r-1}} \left(\frac{2}{\tau}\right)^r \right], \\
&\geq |s|^{r-1} \left[|s| - 3\beta\overline{\lambda}_K \sum_{k=0}^{r-1} \hat{\alpha}_k - \epsilon\beta\overline{\lambda}_K \sum_{k=0}^{r-1} \hat{\alpha}_k \right], \\
&\qquad \text{from Eqs. (6.26) and (6.27)} \\
&\geq 0, \qquad \text{from Eqs. (6.26) and (6.28).} \qquad (6.36)
\end{aligned}$$

The result follows since

$$\begin{aligned}
|\mathcal{C}_{\tau_n}(s)| &\geq |\mathcal{C}(s)| - |g(s, \tau_n)| \\
&> \underline{\mathcal{C}}(|s|) - \overline{g}(|s|) \geq 0 \qquad (6.37)
\end{aligned}$$

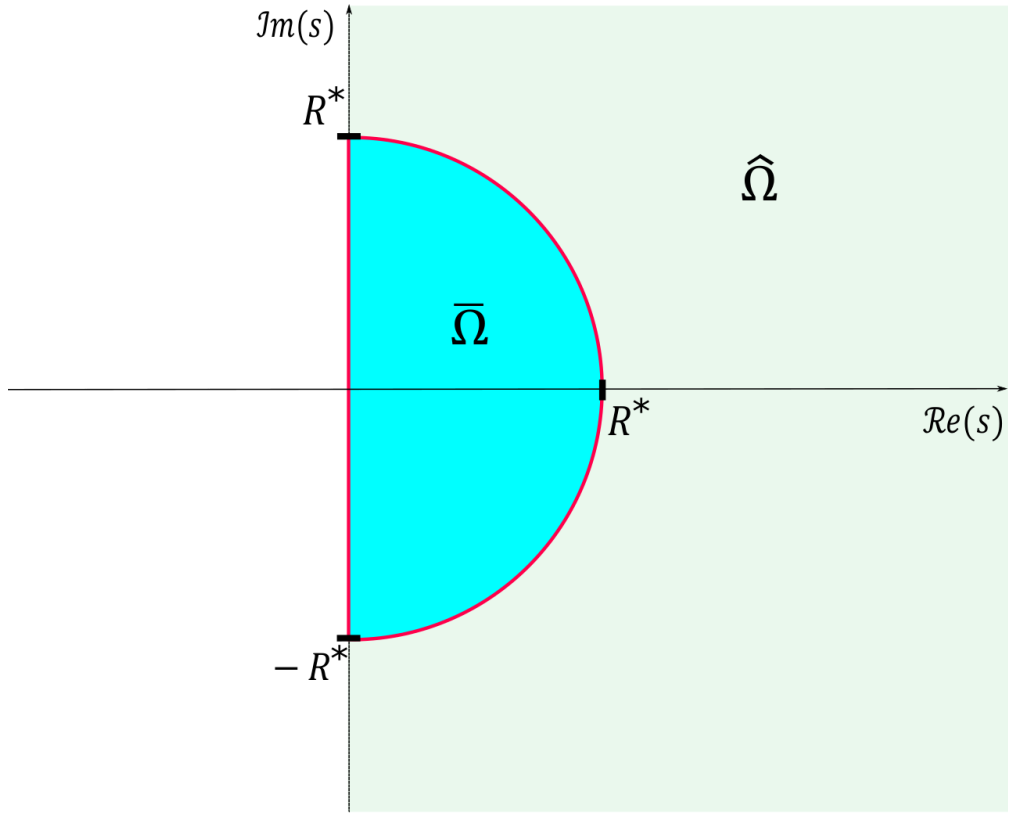

Figure 6.2: Complex plane representing the region $\overline{\Omega}$ (Eq. (6.25)) with its boundary $\partial\overline{\Omega}$, and the outer unbounded region of $\hat{\Omega}$ (Eq. (6.33)).

when $s \in \hat{\Omega} = \{\overline{\mathbb{C}}_+ - \ \overline{\Omega}\}$. □

The stability condition for the DSR approach with network delay is developed in the following theorem.

Theorem 1 (Exponential stability of DSR with network delay) *Under Assumptions 4-5, and assuming that the nominal DSR without network delay is stable (e.g., stability condition in Eq.* (6.16) *of Lemma 4 is satisfied), the DSR approach with a given network delay* $\tau_n \geq 0$ *is stable, i.e., no roots of* $C_{\tau_n}(s) = \mathcal{C}(s) + g(s, \tau_n)$ *(Eq.* (6.23)*) lie in the closed right*

half complex plane $\overline{\mathbb{C}}_+$*, if*

$$|\mathcal{C}(j\omega)| > |g(j\omega, \tau_n)|, \quad \forall \ \ \omega \in [0, R^*], \tag{6.38}$$

where R^* *is defined in Eq.* (6.26)*.*

Proof Consider the boundary $\partial\overline{\Omega}$ of the set $\overline{\Omega}$ is a closed contour. If $|\mathcal{C}(s)| > |g(s, \tau_n)|$ for each s on the boundary $\partial\overline{\Omega}$, then $\mathcal{C}(s) = 0$ and $C_{\tau_n}(s) = \mathcal{C}(s) + g(s) = 0$ have the same number of roots, counting multiplicities, in the region bounded by $\partial\overline{\Omega}$ by Rouché's theorem (Section 5.2. in [19]). In particular, if $|\mathcal{C}(s)| > |g(s, \tau_n)|$ on the boundary $\partial\overline{\Omega}$ and if the nominal DSR without network delay is stable, i.e., $\mathcal{C}(s) = 0$ has no roots in $\overline{\Omega}$ then the characteristic equation $C_{\tau_n}(s) = 0$ of the DSR with network delay τ_n also does not have roots in $\overline{\Omega}$. Moreover, the DSR with network delay τ_n cannot have roots outside of $\overline{\Omega}$ in the closed right half complex plane $\overline{\mathbb{C}}_+$ from Lemma 5, which ensures stability of the DSR with network delay τ_n. The condition $|\mathcal{C}(s)| > |g(s, \tau_n)|$ is satisfied by the curved part of the boundary $\partial\overline{\Omega}$ from the proof of Lemma 5, e.g., see Eq. (6.36), so the condition only needs to be checked on the bounded interval along the imaginary axis portion of the boundary $\partial\overline{\Omega}$, as stated in Condition (6.38) of the theorem. □

The DSR with network delay is structurally stable, i.e., stable for a sufficiently small network delay, as shown next.

Corollary 1 (Structural stability of DSR) *Under assumptions of Theorem 1, there exists some nonzero network time delay* $\tau_n^* > 0$ *such that the DSR with any time delay* τ_n*, such that* $0 \leq \tau_n < \tau_n^*$*, is stable.*

Proof This follows from Theorem 1, since $C(s)$ is continuous and $\mathcal{C}(j\omega) > 0$ in the bounded interval $\omega \in [0, R^*]$ and therefore has a nonzero minima $\mathcal{C}(j\omega) > c > 0, \ \ \forall \omega \in [0, R^*]$. Moreover, $g(s)$ is continuous and $g(j\omega, 0) = 0$ without network delay. Therefore, by continuity there exists some network time delay $\tau_n^* > 0$ such that $g(j\omega, \tau_n) < c, \ \ \forall \omega \in [0, R^*]$ and $0 \leq \tau_n < \tau_n^*$. □

6.3 Simulation Results

Simulation results are provided to show the application of the stability conditions of the DSR approach (Eq. (6.19)) derived in Theorem 1. The estimated delay margin ($\overline{\tau}_{n,est}$) is compared with the actual delay margin value ($\overline{\tau}_n$) to assess the efficacy of the proposed approach. Furthermore, the DSR approach is comparatively evaluated with the standard consensus method without DSR (Eq. (6.13) with the same network delay) to assess (i) the robustness to network delay, and (ii) response cohesiveness. The cohesion is quantified using the maximum deformation $\overline{\Delta}$ of the network response $X(t)$, defined as

$$\overline{\Delta} = \max_i \left[\max_t |x_i(t) - \overline{x}(t)| \right], \tag{6.39}$$

where $|\cdot|$ is the absolute value, and, $\overline{x}$ is the mean response

$$\overline{x}(t) = \frac{1}{N} \sum_{i=1}^{N} x_i(t), \tag{6.40}$$

and a smaller $\overline{\Delta}$ implies more cohesive response.

6.3.1 Example network

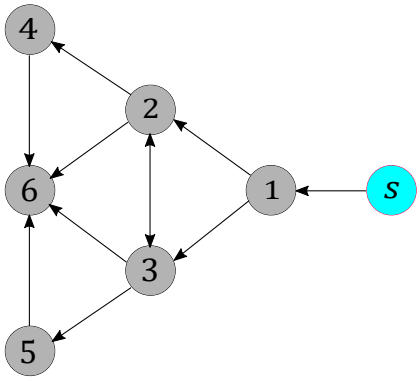

Figure 6.3: Example network from [1] used for simulations with $N = 6$ non-source agents.

The example network considered is from [1] with second-order agent dynamics as shown in Figure 6.3. The network delay margin is estimated for an example network with $N = 6$ agents with graph structure as in Figure 6.3 and DSR parameters $\alpha = 1.195, \beta = 2$, taken from [1] (Table 6.1). The effect of the DSR gain β on both cohesion and network-delay is shown by increasing the gain to $\beta = 20$.

Remark 17 (Not strongly-connected) *The example network in Figure 6.3 is not strongly connected, which is needed for standard methods of stability with delay as developed in [83], [84], and discussed in the Introduction.*

The pinned Laplacian matrix K for the example network in Figure 6.3, with weights w_{ij} either 0 or 1 in Eq. (6.7), is

$$K = \begin{bmatrix} 1 & 0 & 0 & 0 & 0 & 0 \\ -1 & 2 & -1 & 0 & 0 & 0 \\ -1 & -1 & 2 & 0 & 0 & 0 \\ 0 & -1 & 0 & 1 & 0 & 0 \\ 0 & 0 & -1 & 0 & 1 & 0 \\ 0 & -1 & -1 & -1 & -1 & 4 \end{bmatrix} \tag{6.41}$$

whose eigenvalues are $\lambda_{K,1} = \lambda_{K,2} = \lambda_{K,3} = \lambda_{K,4} = 1$, $\lambda_{K,5} = 3$ and $\lambda_{K,6} = 4$. The example network's second order dynamics, with network delay τ_n, is given as,

$$\begin{aligned} X^{(2)}(t) =& \hat{X}^{(2)}(t,\tau) - \beta K \hat{X}^{(2)}(t-\tau_n,\tau) \\ & -\beta K(2\alpha X^{(1)}(t-\tau_n) + \alpha^2 X(t-\tau_n)) + \beta B x_s^*(t). \end{aligned} \tag{6.42}$$

Remark 18 (Delays in non-exponential form) *The characteristic equation of the ex-*

ample network with DSR approach in Figure 6.3, is

$$s^2 + \beta\lambda_{K,i}e^{-s\tau_n}(2\alpha s + \alpha^2) - (1 - e^{-s\tau_n}\beta\lambda_{K,i})\mathcal{F}(s) = 0, \tag{6.43}$$

where, $\mathcal{F}(s) = \{\omega(1 - e^{-s\tau})/(\tau(s + \omega))\}^2$. *The characteristic equation has the delay* τ *in the denominator and is thus not is the standard exponential-only form, needed to use the methods in [87], [88], as discussed in the Introduction.*

6.3.2 DSR delay margin of the example network

The DSR delay margin estimate $\overline{\tau}_{n,est}$ is determined by increasing the network delay τ_n and checking when the condition in Eq. (6.38) of Theorem 1 fails for the example network in Figure 6.3. This results in the estimated network delay margin $\overline{\tau}_{n,est}$ for stability of the DSR approach, with parameter values from [1]. In particular, the network delay dependent $|g(i\omega, \tau_n)|$ is computed for increasing network delay values τ_n, until $|\mathcal{C}(i\omega)| > |g(i\omega, \tau_n)|$ is satisfied, where $\omega \in [0, R^*]$ with $R^* = 582.04$ found using Eq. (6.26). The estimated network delay margin $\overline{\tau}_{n,est}$ of 75.9 ms (Table 6.1) is less than (but close to) the "actual" delay margin of $\overline{\tau}_n = 83.5$ ms found using numerical simulations, as shown in Figures 6.4 and 6.5.

6.3.3 Effect of DSR gain β *on delay margin*

Cohesion increases with larger DSR gain β but the delay margin for stability decreases. For example, increasing the DSR gain β from $\beta = 2$ (as in [1]) to $\beta = 20$ does decrease the delay margin from $\overline{\tau}_n = 83.5$ ms at $\beta = 2$ to $\overline{\tau}_n = 8.25$ ms with $\beta = 20$ (Table 6.1). The estimate of the DSR delay margin $\tau_{n,est} = 7.7$ ms (which is smaller but close to the actual value of 8.25 ms) is found using the condition in Eq. (6.38) in Theorem 1, where $R^* = 1221.8$ is found using Eq. (6.26). Nevertheless, even for increased DSR gain $\beta = 20$, which tends to increase cohesion, as seen in Figure 6.6 (for $\tau_n = 7.7$ ms) and Figure 6.7, but reduces the delay robustness of the DSR approach, Theorem 1 provides a sufficient stability condition in Eq. (6.38).

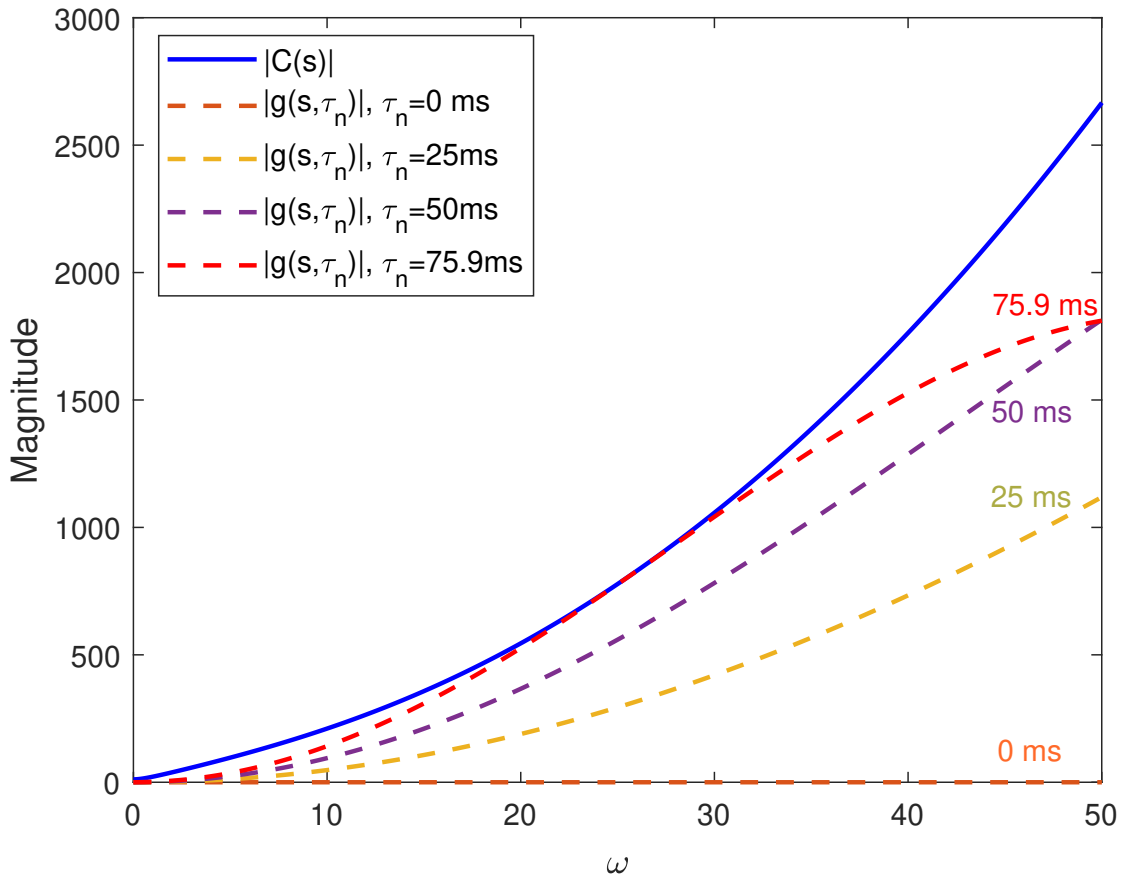

Figure 6.4: The $|g(i\omega, \tau_n)|$ magnitude for increasing τ_n values shows that $|\mathcal{C}(i\omega)| > |g(i\omega, \tau_n)|$ for DSR approach with $\alpha = 1.195, \beta = 2$, is satisfied until 75.9 ms, where $\omega \in [0, R^*]$ with $R^* = 582.04$ found using Eq. (6.26), which provides $\tau_{n,est} = 75.9$ ms.

6.3.4 Comparing with and without DSR approaches

The network responses, with and without the DSR approach, are compared in terms of the achieved cohesion and robustness to the presence of network delay for unit step changes in the overall network response. The without DSR approach (from Eq. (6.13)), but with network delay, for the second order example network in Figure 6.3 is given as,

$$X^{(2)}(t) = -K(2\alpha X^{(1)}(t - \tau_n) + \alpha^2 X(t - \tau_n)) + Bx_s^*(t), \tag{6.44}$$

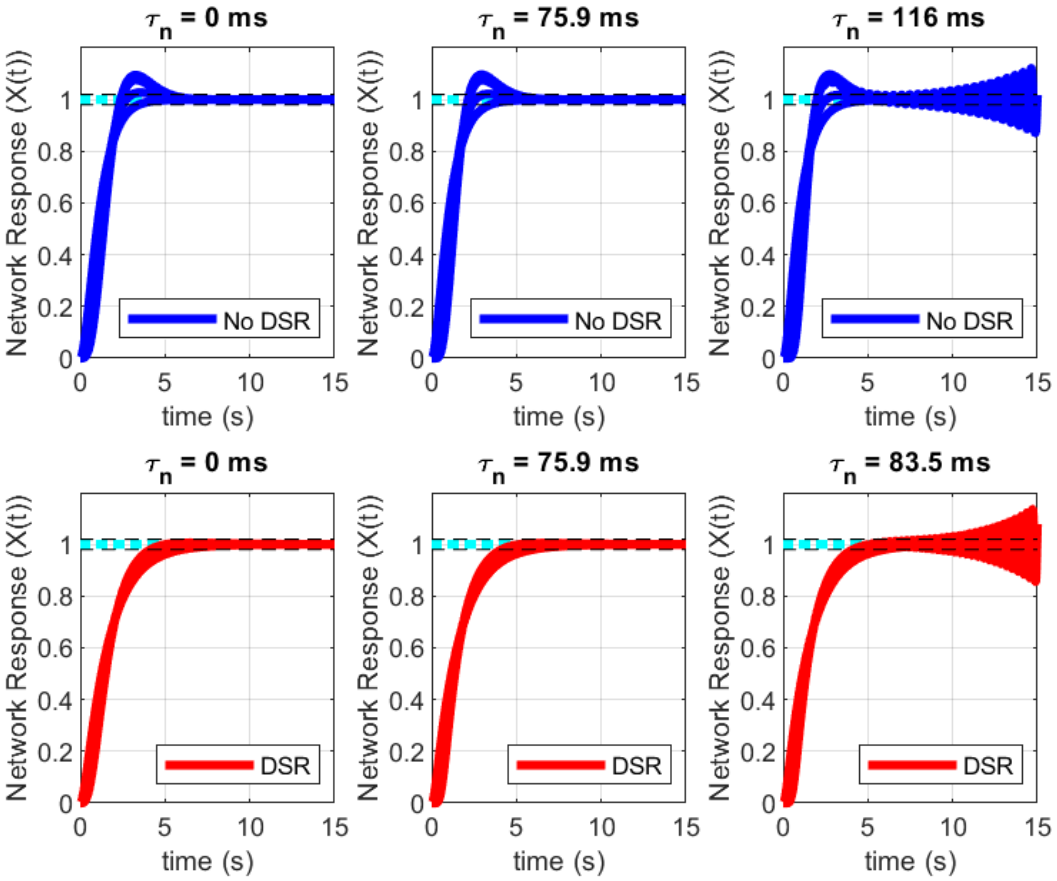

Figure 6.5: Simulated responses of the example network in Figure 6.3 with DSR (Eq. (6.42), with parameter values $\alpha = 1.195, \beta = 2$ obtained from [1]) and without DSR ($\alpha = 1.69$), for increasing network delay values of $\tau_n = 0$ ms, DSR delay margin estimate $\overline{\tau}_{n,est} = 75.9$ ms, and actual delay margins with DSR $\overline{\tau}_n = 83.5$ ms and without DSR at $\overline{\tau}_n = 116$ ms.

where the only parameter $\alpha = 1.69$, from [1], is chosen to achieve the same network settling time as the DSR-based case.

The DSR approach with $\beta = 2$ improves the cohesion performance compared to the case without DSR in the example network. For example at low network delay values ($\tau_n < 0.01$s) the maximum deformation $\overline{\Delta}$ decreases by 37.5% from about $\overline{\Delta} = 0.16$ without DSR to $\overline{\Delta} = 0.1$ with DSR, as shown in Figure 6.7. Even for a relatively large network delay of

Method	**Parameters**	$\overline{\tau}_{n,est}$ (ms)	$\overline{\tau}_n$ (ms)
DSR ($\tau = 75$ ms)	$\alpha = 1.195,\ \beta = 2$	75.9	83.5
	$\alpha = 1.195,\ \beta = 20$	7.7	8.25
No DSR	$\alpha = 1.69$	–	116

Table 6.1: Parameter values for with and without DSR approaches, for the example network (Figure 6.3) with second-order dynamics from [1] and comparison of the estimated delay margin ($\overline{\tau}_{n,est}$) and actual margin ($\overline{\tau}_n$) for stability.

$\tau_n = \overline{\tau}_{n,est} = 75.9$ ms, which is the delay margin estimate and close to instability for the DSR approach, cohesion is still maintained with DSR ($\overline{\Delta} = 0.13$), as shown in Figure 6.5, when compared to the case without DSR ($\overline{\Delta} = 0.20$). Increasing the DSR gain to $\beta = 20$ in the DSR approach leads to further improvement in cohesion performance, by about 90%, compared to without DSR, decreasing $\overline{\Delta}$ to about $\overline{\Delta} = 0.015$ for the corresponding DSR delay margin, as shown in Figure 6.7, and in Figure 6.6 for $\tau_n = \tau_{n,est} = 7.7$ ms which is close to instability for the DSR approach. Therefore, the example network is much more cohesive with the DSR approach compared to the case without DSR. Nevertheless, even with a reduction in the robustness to network delays, the proposed approach results in a close estimate of the delay margin in the presence of network delays.

6.4 Chapter Conclusion

A method for estimating the stability network delay margin for cohesive networks was developed using Rouchè's theorem. The DSR approach, with intentional delays, improves cohesion, but leads to reduced robustness to unintentional network delays. Therefore, there is a need to determine the network delay margin for ensuring stability. The usefulness of

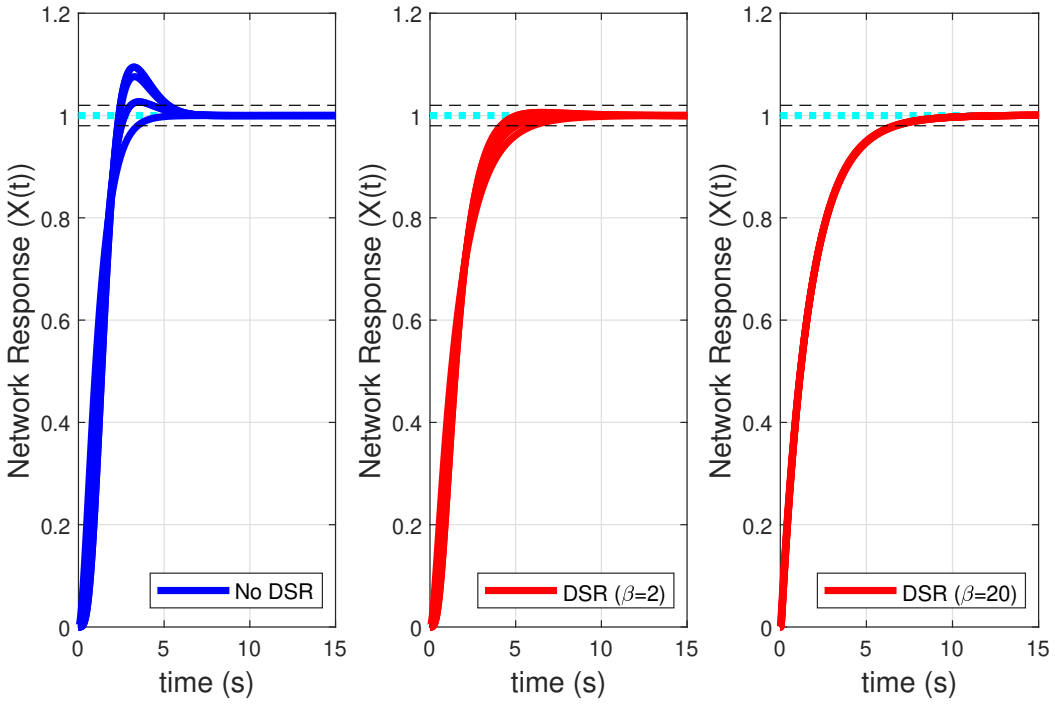

Figure 6.6: Simulated responses of the example network in Figure 6.3 with network delay $\tau_n = 7.7$ ms, for without DSR approach (Eq. (6.44) with $\alpha = 1.69$) and with DSR approach (Eq. (6.42) with $\alpha = 1.195$, $\beta = 2$ and 20). Cohesiveness is improved by DSR, by decreasing maximum deformation $\overline{\Delta} = 0.16$ achieved without DSR, to $\overline{\Delta} = 0.1$ with DSR $\beta = 2$, and even further to $\overline{\Delta} = 0.015$ with DSR $\beta = 20$ even with network delay as large as the estimated DM for the $\beta = 20$ case.

the proposed approach in predicting the delay margin for the DSR approach was illustrated using an example network, which also showed that the DSR approach improves network cohesion when compared with the standard no-DSR approach, even in the presence of network delays.

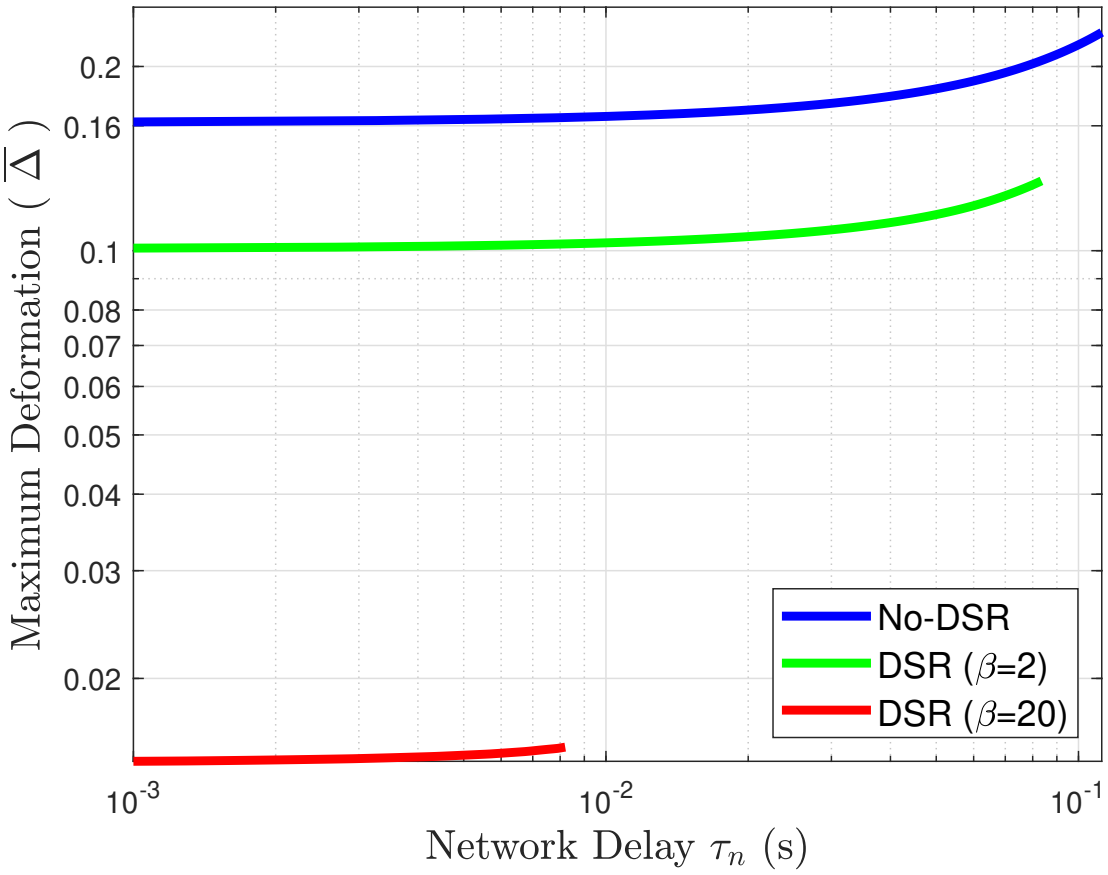

Figure 6.7: Simulated maximum deformation ($\overline{\Delta}$ in Eq. (6.39)) for the range of delay margin of without DSR ($\overline{\tau}_n = 116$ ms), with DSR for $\beta = 2$ ($\overline{\tau}_n = 83.5$ ms), and with DSR for higher $\beta = 20$ ($\overline{\tau}_n = 8.25$ ms).

Chapter 7
NETWORKS WITH AGENT DELAYS.

This chapter briefly introduces the last research problem addressed in the dissertation of handling agent delays (τ_a) in networks for cohesive transitions using DSR.

7.1 Problem statement formulation using an example network.

The problem statement is formulated using an example network from [1], also used in Chapter 6 with network structure as shown in Figure 6.3, with second order agents in presence of uniform agent delays τ_a.

7.1.1 Agent's second-order dynamics with agent delay

The $n = 6$ second-order agents in the considered example network (Figure 6.3) are modeled according to the following state equation

$$\ddot{X}(t) = -a\dot{X}(t) + aU(t - \tau_a), \tag{7.1}$$

where $X(t) \in \mathbb{R}^n$ is the position state vector for the agents, a is the damping coefficient of each agent, $U(t-\tau_a)$ is the control input at time t with τ_a as the agent delay, and $\dot{x}$ signifies time derivative (first order) of x w.r.t. time. The input $U(t)$ is chosen as

$$U(t) = \dot{X}(t) + \frac{1}{a}\hat{U}(t), \tag{7.2}$$

where $\dot{X}(t)$ helps in cancelling (approximately for small τ) the damping term $-a\dot{X}(t)$ in Eq. (7.1). $\hat{U}(t)$ is chosen to improve cohesion in the agent-network, as in [1], using cohesive delayed-self-reinforcement (DSR).

7.1.2 Ideal dynamics

The cohesive DSR input $\hat{U}(t)$ is derived from the ideal dynamics of the second-order agent-network for cohesion, as given by

$$\ddot{X}(t) = \mathbf{1}_n \ddot{x}_d(t) - \hat{\alpha}_1(\dot{X}(t) - \mathbf{1}_n \dot{x}_s(t)) - \hat{\alpha}_0(X(t) - \mathbf{1}_n x_s(t)), \tag{7.3}$$

where $x_s(t)$ is the desired virtual source position trajectory for the agents, $\mathbf{1}_n$ is a vector of ones, $\hat{\alpha}_1 = 2\alpha$, and $\hat{\alpha}_0 = \alpha^2$ for some $\alpha > 0$, such that the characteristic equation of the ideal dynamics in Eq. (7.3) is given by $\mathcal{P}(s)$,

$$\mathcal{P}(s) = (s + \alpha)^2. \tag{7.4}$$

The ideal dynamics in Eq. (7.3) can be rewritten as [1]

$$\begin{aligned} \ddot{X}(t) &= (\mathbf{I}_n - \beta K)\ddot{X}(t) - \beta K(\hat{\alpha}_1 \dot{X}(t) + \hat{\alpha}_0 X(t)) + \beta B x_s^*(t), \\ &= \hat{U}(t) \end{aligned} \tag{7.5}$$

where K is the pinned-Laplacian of the non-source agents in the example network in Figure 6.3, B is the source-connectivity vector, and $x_s^*(t) = \ddot{x}_s(t) + \hat{\alpha}_1 \dot{x}_s(t) + \hat{\alpha}_0 x_s(t)$.

7.1.3 Ideal dynamics with agent delay

The ideal dynamics input $\hat{U}(t)$ from Eq. (7.5) is substituted in the control input Eq. (7.2), which makes the agent-network dynamics from Eq. (7.1) as following

$$\begin{aligned} \ddot{X}(t) &= -a\dot{X}(t) + a\left(\dot{X}(t - \tau_a) + \frac{1}{a}\hat{U}(t - \tau_a)\right), \\ &= (\mathbf{I}_n - \beta K)\ddot{X}(t - \tau_a) - \beta K(\hat{\alpha}_1 \dot{X}(t - \tau_a) + \hat{\alpha}_0 X(t - \tau_a)) \\ &\quad + \beta B x_s^*(t - \tau_a) - a(\dot{X}(t) - \dot{X}(t - \tau_a)). \end{aligned} \tag{7.6}$$

7.1.4 Cohesive DSR with agent delay

The ideal dynamics with agent delay in Eq. (7.6) can be implemented by approximating $\ddot{X}(t-\tau_a)$ using delayed (with DSR delay τ) versions of the state as follows

$$\begin{aligned} e^{-s\tau_a}\ddot{X}(s) &\approx e^{-s\tau_a}\left(\frac{\omega}{(s+\omega)}\frac{(1-e^{-s\tau})}{\tau}\right)^2 X(s), \\ &= e^{-s\tau_a}\ddot{\hat{X}}(s) = e^{-s\tau_a}F(s)X(s). \end{aligned} \tag{7.7}$$

Taking the Laplace transform of Eq. (7.6) and using the delay-based approximation from Eq. (7.7), we get the following

$$\begin{aligned} s^2X(s) = e^{-s\tau_a}(\mathbf{I}_n - \beta K)F(s)X(s) - \beta K e^{-s\tau_a}(\hat{\alpha}_1 s + \hat{\alpha}_0)X(s) \\ + \beta B x_s^*(s) - as(1-e^{-s\tau_a})X(s). \end{aligned} \tag{7.8}$$

Remark 19 (Standard consensus approach) *The standard consensus approach can be obtained from Eq.* (7.6) *by omitting the* $(\mathbf{I}_n - \beta K)\ddot{X}(t-\tau_a)$ *on RHS and setting* $\beta = 1$*, resulting in,*

$$\ddot{X}(t) = -K(\hat{\alpha}_1\dot{X}(t-\tau_a) + \hat{\alpha}_0 X(t-\tau_a)) + Bx_s^*(t-\tau_a) - a(\dot{X}(t) - \dot{X}(t-\tau_a)). \tag{7.9}$$

7.1.5 Network response in presence of agent delay

The example network's response is shown in Figure 7.1, using the standard consensus approach (Eq. (7.9)) and DSR approach (Eq. (7.8)) for a unit step virtual source position input $x_s = 1$, where the agent delay is taken as $\tau_a = 0.2$ s. It is seen in Figure 7.1 that the DSR approach, although showing improvement over the consensus approach, still remains non-cohesive during the transition. Therefore, presence of the agent delay leads to loss of cohesion in the DSR approach.

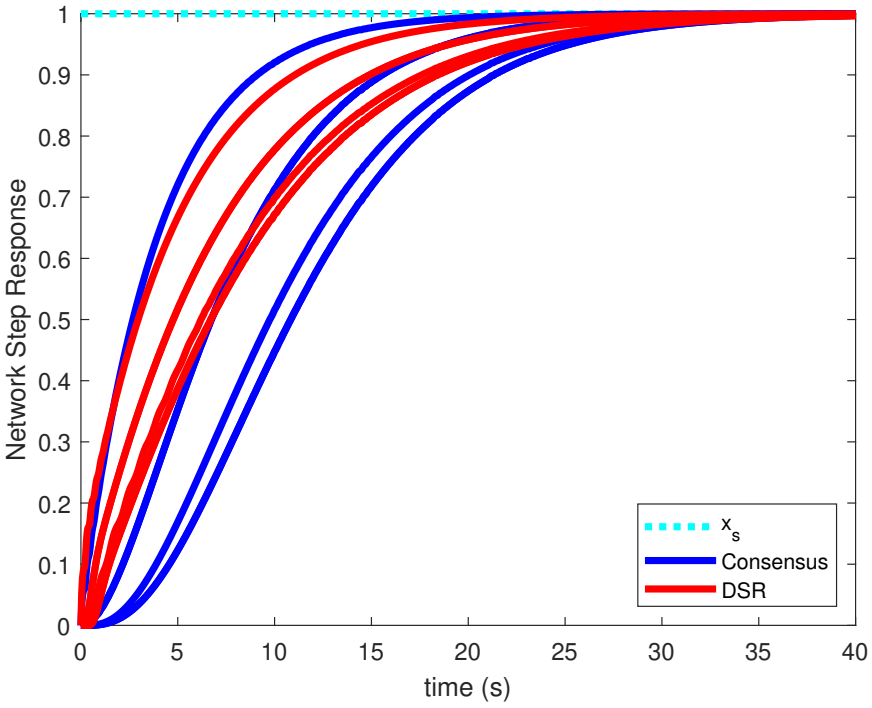

Figure 7.1: Response of the example network in Figure 6.3 with consensus (Eq. (7.9)) and DSR approach (Eq. (7.8)) in presence of agent delay $\tau_a = 0.2$ s.

7.1.6 Problem statement

The proposed research for the main contribution of the chapter is to derive the stability conditions of the DSR approach for networks with agent delay τ_a. Furthermore, unlike network delays, agent delays lead to loss of cohesion during transitions with DSR, therefore a method needs to be developed to enable cohesiveness in presence of agent delays.

7.2 Proposed method for handling agent delays.

The development of stability conditions and methods for improving cohesion for networks with agent delays are discussed below, using the example network Figure 6.3 with second-order agents.

7.2.1 Proving stability in presence of input delays

The network of second-order agents with agent delay τ_a is stable if all the roots of the following characteristic equation ($\mathcal{C}_{\tau_a}(s) = 0$), obtained from Eq. (7.8) through Jordan decomposition using arguments from Lemma 2 of [1], lie in the open left half of the complex plane,

$$\mathcal{C}_{\tau_a}(s) = s^2 + \beta\lambda_{K,i}e^{-s\tau_a}(\hat{\alpha}_1 s + \hat{\alpha}_0) - e^{-s\tau_a}\left(\mathbf{I}_n - \beta\lambda_{K,i}\right)F(s) + as(1 - e^{-s\tau_a}). \tag{7.10}$$

It is assumed that the network with zero agent delay $\tau_a = 0$ is stable, i.e., the following characteristic equation $\mathcal{C}(s)$, obtained by substituting $\tau_a = 0$ in Eq. (7.10), has all its roots in the open left half plane,

$$\mathcal{C}(s) = s^2 + \beta\lambda_{K,i}(\hat{\alpha}_1 s + \hat{\alpha}_0) - (\mathbf{I}_n - \beta\lambda_{K,i})F(s) = 0. \tag{7.11}$$

Then, $C_{\tau_a}(s)$ from Eq. (7.10) can be rewritten as a summation of $\mathcal{C}(s)$ (Eq. (7.11)) and an agent delay dependent perturbation term $g(s, \tau_a)$,

$$\mathcal{C}_{\tau_a}(s) = \mathcal{C}(s) + g(s, \tau_a), \tag{7.12}$$

where,

$$g(s, \tau_a) = \mathcal{C}_{\tau_a}(s) - \mathcal{C}(s). \tag{7.13}$$

The proposed approach for estimating the agent delay margin τ_a^*, such that $C_{\tau_a}(s)$ has all its roots in open left half complex plane for all $0 \leq \tau_a < \tau_a^*$, is using the continuity of

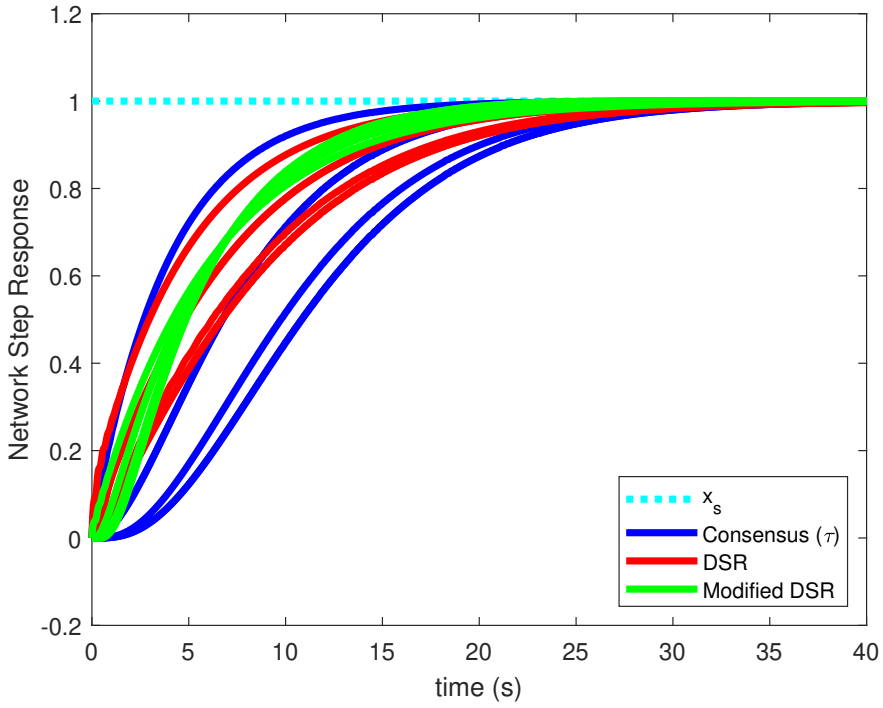

Figure 7.2: Response of the example network in Figure 6.3 with consensus (Eq. (7.9)), DSR approach (Eq. (7.8)) and the modified DSR approach proposed in Eq. (7.14), which improves cohesion in presence of agent delay $\tau_a = 0.2$ s.

$|g(s, \tau_a)|$ with τ_a and the Rouchè's theorem, similar to the approach for network delays in Chapter 6.

7.2.2 Improving cohesion during transitions in networks with agent delays

It is shown in Figure 7.1 that presence of agent delays can lead to loss of cohesion. Upon investigating Eq. (7.6) using time domain simulations, it is observed that the damping error term $a(\dot{X}(t) - \dot{X}(t - \tau_a))$ is the major factor towards the loss of cohesion during transitions.

The damping error can be compensated by increasing the gain of the term $\ddot{X}(t - \tau_a)$ in Eq. (7.6) adaptively by $a\tau$, assuming the DSR delay τ to be approximately equal to the agent delay τ_a, as shown below in the modified version of the DSR approach for the example

network,

$$\ddot{X}(t) = ((1+a\tau)\mathbf{I}_n - \beta K)\ddot{\hat{X}}(t-\tau_a) - \beta K(\hat{\alpha}_1\dot{X}(t-\tau_a) + \hat{\alpha}_0 X(t-\tau_a)) + \beta B x_s^*(t-\tau_a) - a(\dot{X}(t) - \dot{X}(t-\tau_a)), \tag{7.14}$$

where $\ddot{\hat{X}}(t-\tau_a)$ is the approximation from Eq. (7.7). A comparison of the example network response using consensus approach (Eq. (7.9)), DSR (Eq. (7.8)) and the modified DSR approach in Eq. (7.14), given in Figure 7.2, shows that the proposed modification in the DSR approach can potentially lead to improved cohesion during transitions even in presence of agent delays.

7.3 Chapter Conclusions

A method for guaranteeing stability and maintaining cohesion with the DSR approach in presence of agent delays is presented in this chapter. The stability in presence of delays can be provided using Rouchè's theorem, similar to the approach for network delays in Chapter 6. Finally, the cohesion in presence of the agent delays is maintained by compensating for the damping error.

Chapter 8

SUMMARY AND FUTURE WORK.

This chapter briefly provides a summary of the main contributions, and discusses some of the future works which can be pursued based on the results of the thesis.

8.1 Summary of the main contributions

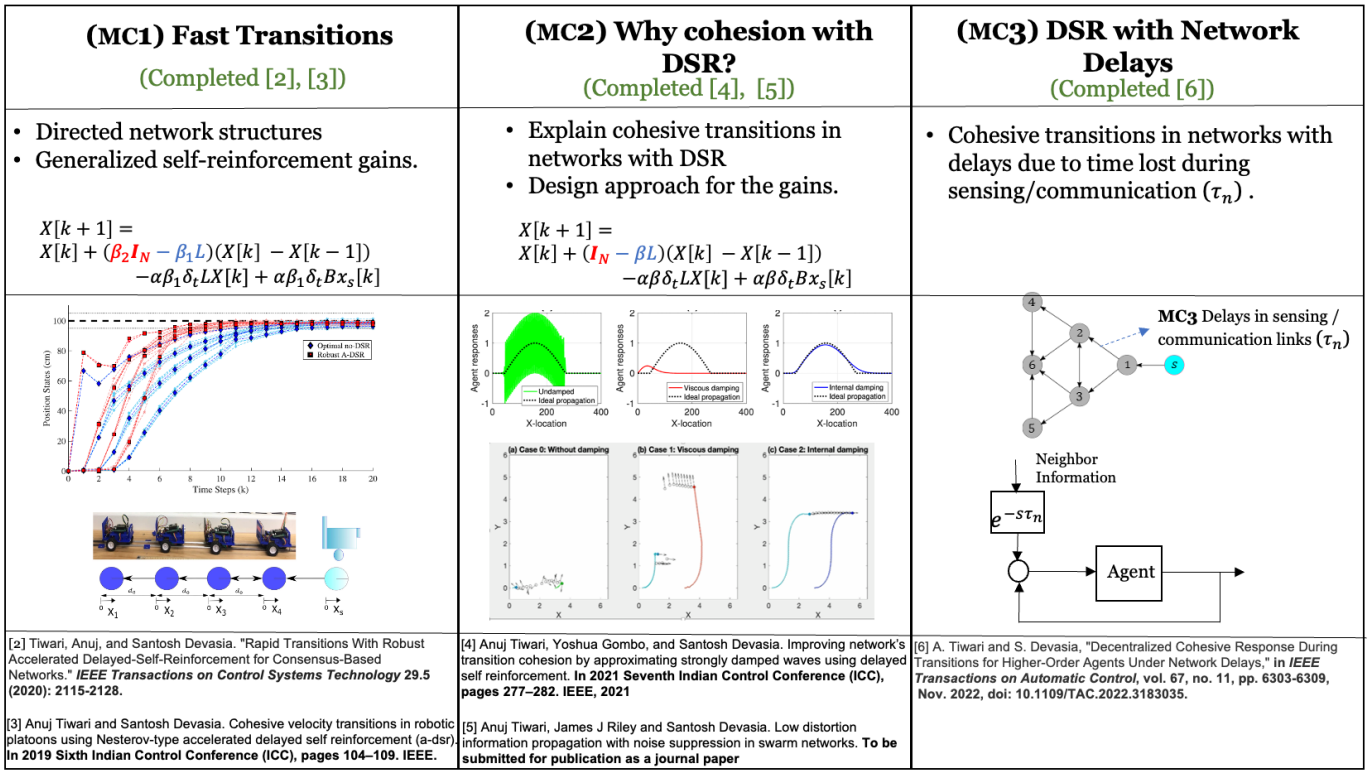

Figure 8.1: Figure highlighting main contributions of the thesis, and resulting publications [2,3], [4], [5], [6].

The main contributions from the thesis have been summarized in Figure 8.1. Cohesive

transitions in decentralized networks, where each agent responds similarly, are important for several engineering applications such as truck platooning, and cooperative object transportation tasks using robots. Furthermore, current consensus-based control algorithms do not maintain cohesion in decentralized networks.

1. Chapter 3 introduces a method for faster information propagation through networks using accelerated approaches [2,3], where each agent responds to changes in their neighbor agents faster, which leads to faster transitions in networks. This chapter forms the contribution **MC1** of this dissertation, and is published as an article in [2]. The main contribution of this chapter is to design a Nesterov-type accelerated update for general graph networks using a local potential function for each agent. However, the resulting update law does not necessarily reduce the overall Laplacian potential [55] because each agent's update is in the negative gradient direction of its own local potential. Therefore, the convergence studies from optimization methods cannot be used to establish stability [46, 47] of accelerated update derived using local potential functions. Moreover, while Lyapunov functions can be found to study stability for general directed graphs [55], the gradient of these Lyapunov functions does not lead to the control update law, and hence accelerated methods cannot be directly applied using these Lyapunov functions. Prior methods that use either the momentum term alone or the outdated-feedback term alone also do not address the stability when both terms are used for general directed graphs. In this context, a contribution of this chapter is to develop stability conditions for the proposed generalized accelerated approach, with both the momentum and outdated-feedback terms. The current chapter expands on our prior work in [52], which used a fixed ratio between the momentum and outdated-feedback terms, by (i) proposing the general case with varying ratios between the momentum and outdated-feedback terms; (ii) developing a stability condition for the generalized approach, (iii) designing the A-DSR to achieve fast response while maximizing structural robustness, (iv) illustrating the importance of momentum term over

the outdated-feedback term for graph networks with real spectrum and (v) presenting experimental results to comparatively evaluate the performance, with and without A-DSR.

2. Chapter 5 proposes a new model, which adds delayed self-reinforcement (DSR) terms to current alignment based models [8], not only predicts the low-distortion information propagation through networks, including turning information in bird flocks, but also shows noise suppression behavior during the information propagation that is not seen in the earlier models [14, 62]. Such DSR-based models suppresses unwanted motions, such as higher frequency movements of neighbors (say, due to flapping of wings), and prevents such noise from spreading across the network leading to loss of coherence. In contrast, prior works do not allow such suppression of noise. For example, prior works in [8, 62] have introduced a behavioral inertia, in addition to the neighbor-based social force, in a new microscopic model to explain the propagation of turning information through bird flocks. The parameters of the model can be tuned to achieve undamped propagation of information without dissipation. Similar results are obtained in [14], where self-reinforcement of the alignment based algorithms with additional momentum term [13] leads to a wave-like information propagation in networks. However, these models also lead to undamped propagation of noise without dissipation. Adapting the network structure which leads to maximal robustness to external disturbances can be another approach, such as in [82] which shows certain structures are more robust to perturbations than others. However, changing the network structure for noise suppression might not always be feasible.

3. The current DSR approach [1] assumes instantaneous access to neighbor information and could become unstable in the presence of network delays. Such unavoidable delays can arise due to the time needed for sensing and/or communication between the agents [85], as well as computation of control actions. As the third main contribution (**MC3**), Chapter 6 develops stability conditions for the DSR-based approach in the presence

of network delays, and provides a computational method to estimate a lower bound $\overline{\tau}_{n,est} \leq \overline{\tau}_n$ on the delay margin (DM) $\overline{\tau}_n$, such that the DSR-based approach is stable when the network delay τ_n is less than the DM, i.e., $0 \leq \tau_n < \overline{\tau}_n$.

8.2 Future work

The section discusses some of the future works that can be pursued based on the results obtained in the thesis.

1. The A-DSR approach, presented in Chapter 3, assumes scalar gains for the outdated-feedback and momentum terms, which can be extended in future work by using different, possibly nonlinear or time-varying gains for each agent in the network. Further, the proposed Robust A-DSR approach in Chapter 3, can be used to accelerate convergence and improve performance of networks with uncertainty, for instance, distributed sensing in presence of communication delays, operation of multi-agent networks with a human-in-the-loop where the human or network model is uncertain, and transporting flexible structures with uncertain stiffness values using mobile bots. Further work is needed to explore the suitability of the Robust A-DSR for these applications.

2. The proposed method for maintaining cohesion in presence of agent delays in Chapter 7 can be applied to robotic systems with second-order dynamics. However, certain applications with higher-order networked systems require further investigation in terms of the techniques which can be used to compensate for the delays for maintaining cohesion during transitions. Experimental studies with varying time delays can be used to evaluate the effectiveness of the proposed delay handling strategies in physical networked systems.

BIBLIOGRAPHY

[1] Santosh Devasia. Cohesive networks using delayed self reinforcement. *Automatica*, 112:108699, 2020.

[2] Anuj Tiwari and Santosh Devasia. Rapid transitions with robust accelerated delayed-self-reinforcement for consensus-based networks. *IEEE Transactions on Control Systems Technology*, 2020.

[3] Anuj Tiwari and Santosh Devasia. Cohesive velocity transitions in robotic platoons using nesterov-type accelerated delayed self reinforcement (a-dsr). In *2019 Sixth Indian Control Conference (ICC)*, pages 104–109. IEEE, 2019.

[4] Anuj Tiwari, Yoshua Gombo, and Santosh Devasia. Improving network's transition cohesion by approximating strongly damped waves using delayed self reinforcement. In *2021 Seventh Indian Control Conference (ICC)*, pages 277–282. IEEE, 2021.

[5] Anuj Tiwari, Santosh Devasia, and James J Riley. Low distortion information propagation with noise suppression in swarm networks. *To be submitted for publication as a journal paper*.

[6] Anuj Tiwari and Santosh Devasia. Decentralized cohesive response during transitions for higher-order agents under network delays. *IEEE Transactions on Automatic Control*, 2022.

[7] Mehran Mesbahi and Magnus Egerstedt. *Graph Theoretic Methods in Multiagent Networks*. Princeton University Press, stu - student edition edition, 2010.

[8] A. Attanasi, A. Cavagna, L Del Castello, I. Giardina, T.S. Grigera, A. Jelic, S. Melillo, L. Parisi, O. Pohl, E. Shen, and M. Viale. Information transfer and behavioural inertia in starling flocks. *Nature Physics*, 10(9):615–698, Sep 1 2014.

[9] Assad Al Alam, Ather Gattami, and Karl Henrik Johansson. An experimental study on the fuel reduction potential of heavy duty vehicle platooning. In *13th international IEEE conference on Intelligent Transportation Systems*, pages 306–311. IEEE, 2010.

[10] Yoshua Gombo, Anuj Tiwari, and Santosh Devasia. Communication-free cohesive flexible-object transport using decentralized robot networks. In *2021 American Control Conference (ACC)*, pages 106–111, 2021.

[11] M Hafez M Ariffin, Mohd Azizi Abdul Rahman, and Hairi Zamzuri. Effect of leader information broadcasted throughout vehicle platoon in a constant spacing policy. In *2015 IEEE International Symposium on Robotics and Intelligent Sensors (IRIS)*, pages 132–137. IEEE, 2015.

[12] Simon Parkinson, Paul Ward, Kyle Wilson, and Jonathan Miller. Cyber threats facing autonomous and connected vehicles: Future challenges. *IEEE Transactions on Intelligent Transportation Systems*, 18(11):2898–2915, 2017.

[13] Ning Qian. On the momentum term in gradient descent learning algorithms. *Neural networks*, 12(1):145–151, 1999.

[14] Santosh Devasia. Rapid information transfer in swarms under update-rate-bounds using delayed self-reinforcement. *Journal of Dynamic Systems, Measurement, and Control*, 141(8), 2019.

[15] Yongcan Cao and Wei Ren. Multi-agent consensus using both current and outdated states with fixed and undirected interaction. *Journal of Intelligent and Robotic Systems*, 58(1):95–106, 2010.

[16] Yurii E Nesterov. A method for solving the convex programming problem with convergence rate o (1/kˆ 2). In *Dokl. akad. nauk Sssr*, volume 269, pages 543–547, 1983.

[17] Wei Ren. Multi-vehicle consensus with a time-varying reference state. *Systems & Control Letters*, 56(7-8):474–483, 2007.

[18] G. F. Webb. Existence and asymptotic behavior for a strongly damped nonlinear wave equation. *Canadian Journal of Mathematics*, 32(3):631–643, 1980.

[19] Lars Ahlfors. *Complex Analysis : An Introduction to The Theory of Analytic Functions of One Complex Variable*. McGraw-Hill, third edition, 1979.

[20] Rouben Toumani. On the stability of lumped-distributed networks. *IEEE Transactions on Circuit Theory*, 20(5):606–608, 1973.

[21] N Öztürk and A Uraz. An analytic stability test for linear multivariable feedback systems with a time delay. *IFAC Proceedings Volumes*, 17(2):207–211, 1984.

[22] M De la Sen and R Barcena. Stability results for point time-delay systems obtained via Rouche's theorem. *Applicable Analysis*, 83(2):157–183, 2004.

[23] AK El-Sakkary. The symmetric Rouche's form for robustness. *IEEE Transactions on Automatic Control*, 37(6):810–812, 1992.

[24] A Huth and C Wissel. The simulation of the movement of fish schools. *Journal of Theoretical Biology*, 156(3):365–385, Jun 7 1992.

[25] Tamás Vicsek, András Czirók, Eshel Ben-Jacob, Inon Cohen, and Ofer Shochet. Novel type of phase transition in a system of self-driven particles. *Phys. Rev. Lett.*, 75:1226–1229, Aug 1995.

[26] A. Jadbabaie, Jie Lin, and A. S. Morse. Coordination of groups of mobile autonomous agents using nearest neighbor rules. *IEEE Transactions on Automatic Control*, 48(6):988–1001, June 2003.

[27] Wei Ren and R. W. Beard. Consensus seeking in multiagent systems under dynamically changing interaction topologies. *IEEE Transactions on Automatic Control*, 50(5):655–661, May 2005.

[28] R. Olfati-Saber. Flocking for multi-agent dynamic systems: algorithms and theory. *IEEE Transactions on Automatic Control*, 51(3):401–420, March 2006.

[29] August Mark, Yunjun Xu, and Benjamin T. Dickinson. Consensus-Based Decentralized Aerodynamic Moment Allocation Among Synthetic Jets and Control Surfaces. *IEEE Transactions on Control Systems Technology*, 27(6):2718–2726, NOV 2019.

[30] Michele Cucuzzella, Sebastian Trip, Claudio De Persis, Xiaodong Cheng, Antonella Ferrara, and Arjan van der Schaft. A Robust Consensus Algorithm for Current Sharing and Voltage Regulation in DC Microgrids. *IEEE Transactions on Control Systems Technology*, 27(4):1583–1595, JUL 2019.

[31] Johannes Schiffer, Thomas Seel, Joerg Raisch, and Tevfik Sezi. Voltage Stability and Reactive Power Sharing in Inverter-Based Microgrids With Consensus-Based Distributed Voltage Control. *IEEE Transactions on Control Systems Technology*, 24(1):96–109, JAN 2016.

[32] Naiming Qi, Qiufan Yuan, Yanfang Liu, Mingying Huo, and Shilei Cao. Consensus Vibration Control for Large Flexible Structures of Spacecraft With Modified Positive Position Feedback Control. *IEEE Transactions on Control Systems Technology*, 27(4):1712–1719, JUL 2019.

[33] C. C. Ioannou, V. Guttal, and I. D. Couzin. Predatory fish select for coordinated collective motion in virtual prey. *Science*, 337(6099):1212–1215, Sep 7 2012.

[34] Máté Nagy, Zsuzsa Akos, Dora Biro, and Tamás Vicsek. Hierarchical group dynamics in pigeon flocks. *Nature*, 464(7290):890, 2010.

[35] Fabio Fagnani and Paolo Frasca. *Introduction to averaging dynamics over networks*, volume 472. Springer, 2017.

[36] R. Olfati-Saber, J.A. Fax, and R.M. Murray. Consensus and cooperation in networked multi-agent systems. *Proceedings of the IEEE*, 95(1):215–233, Jan 2007.

[37] S. Devasia. Faster Response in Bounded-Update-Rate, Discrete-time Networks using Delayed Self-Reinforcement. *International Journal of Control*, Accepted, 2019, DOI: 10.1080/00207179.2019.1644537.

[38] Ruggero Carli, Fabio Fagnani, Alberto Speranzon, and Sandro Zampieri. Communication constraints in the average consensus problem. *Automatica*, 44(3):671–684, Mar 2008.

[39] Maria Pia Fanti, Agostino Marcello Mangini, Francesca Mazzia, and Walter Ukovich. A new class of consensus protocols for agent networks with discrete time dynamics. *Automatica*, 54:1–7, Apr 2015.

[40] Xiaoming Duan, Jianping He, Peng Cheng, and Jiming Chen. Exploiting a Mobile Node for Fast Discrete Time Average Consensus. *IEEE Transactions on Control Systems Technology*, 24(6):1993–2001, NOV 2016.

[41] Zhenhong Li and Zhengtao Ding. Robust Cooperative Guidance Law for Simultaneous Arrival. *IEEE Transactions on Control Systems Technology*, 27(3):1360–1367, MAY 2019.

[42] Eduardo Montijano, Sonia Martinez, and Carlos Sagues. Distributed Robust Consensus Using RANSAC and Dynamic Opinions. *IEEE Transactions on Control Systems Technology*, 23(1):150–163, JAN 2015.

[43] D. E. Rumelhart, G. E. Hinton, and R. J. Williams. *Learning Internal Representations by Error Propagation, pp. 318-362, in D. E. Rumelhart and J. L. McClelland (eds.) Parallel Distributed Processing, Vol. 1* . MIT Press, Cambridge, MA, 1986.

[44] Ning Qian. On the momentum term in gradient descent learning algorithms. *Neural Networks*, 12(1):145 – 151, 1999.

[45] Y. E. Nesterov. A Method of Solving a Convex Programming Problem with Convergence Rate of $O(1/k^2)$. *Soviet Mathematics Doklady*, 27(3):372–376, 1983.

[46] D. Jakovetić, J. M. F. Xavier, and J. M. F. Moura. Convergence rates of distributed nesterov-like gradient methods on random networks. *IEEE Transactions on Signal Processing*, 62(4):868–882, Feb 2014.

[47] B. Van Scoy, R. A. Freeman, and K. M. Lynch. The fastest known globally convergent first-order method for minimizing strongly convex functions. *IEEE Control Systems Letters*, 2(1):49–54, Jan 2018.

[48] S. Devasia. Rapid Information Transfer in Swarms under Update-Rate-Bounds using Delayed Self-Reinforcement. *ASME Journal of Dynamic Systems Measurement and Control*, 141(8):#081009 1–9, August Aug, 2019.

[49] Yongcan Cao and Wei Ren. Multi-Agent Consensus Using Both Current and Outdated States with Fixed and Undirected Interaction. *Journal of Intelligent & Robotic Systems*, 58(1):95–106, April 2010.

[50] Hossein Moradian and Solmaz Kia. Accelerated average consensus algorithm using outdated feedback. In *2019 European Control Conference ECC, June 25-28, Napoli, Italy*, 2019.

[51] J. Bu, M. Fazel, and M. Mesbahi. Accelerated consensus with linear rate of convergence. In *2018 Annual American Control Conference (ACC)*, pages 4931–4936, June 2018.

[52] S. Devasia. Accelerated Consensus for Multi-Agent Networks through Delayed Self Reinforcement. *IEEE International Conference on Industrial Cyber-Physical Systems, Taipei, Taiwan* , May 6-9, 2019.

[53] S. Devasia. Cohesive Networks using Delayed Self-Reinforcement. *Automatica*, 112:108699, 1–13, Feb 2020.

[54] R. Olfati-Saber and R. M. Murray. Consensus problems in networks of agents with switching topology and time-delays. *IEEE Transactions on Automatic Control*, 49(9):1520–1533, Sep. 2004.

[55] Hui Zhang and Junmin Wang. Robust two-mode-dependent controller design for networked control systems with random delays modelled by Markov chains. *International Journal of Control*, 88(12):2499–2509, DEC 2 2015.

[56] Ali Makhdoumi and Asuman Ozdaglar. Graph balancing for distributed subgradient methods over directed graphs. In *2015 54th IEEE Conference on Decision and Control (CDC)*, pages 1364–1371. IEEE, 2015.

[57] Ran Xin and Usman A Khan. Distributed heavy-ball: A generalization and acceleration of first-order methods with gradient tracking. *IEEE Transactions on Automatic Control*, 2019.

[58] M. Chen, Q. Hu, C. Mackin, J. F. Fisac, and C. J. Tomlin. Safe platooning of unmanned aerial vehicles via reachability. In *2015 54th IEEE Conference on Decision and Control (CDC)*, pages 4695–4701, 2015.

[59] S. Devasia and A. Lee. Scalable low-cost-unmanned-aerial-vehicle traffic network. *AIAA Journal of Air Transportation*, 24(3):74–83, July 2016.

[60] Santosh Devasia. Faster response in bounded-update-rate, discrete-time linear networks using delayed self-reinforcement. *International Journal of Control*, 94(5):1286–1296, 2021.

[61] Alessandro Attanasi, Andrea Cavagna, Lorenzo Del Castello, Irene Giardina, Tomas S Grigera, Asja Jelić, Stefania Melillo, Leonardo Parisi, Oliver Pohl, Edward Shen, et al. Information transfer and behavioural inertia in starling flocks. *Nature physics*, 10(9):691–696, 2014.

[62] Andrea Cavagna, Lorenzo Del Castello, Irene Giardina, Tomas Grigera, Asja Jelic, Stefania Melillo, Thierry Mora, Leonardo Parisi, Edmondo Silvestri, Massimiliano Viale, et al. Flocking and turning: a new model for self-organized collective motion. *Journal of Statistical Physics*, 158(3):601–627, 2015.

[63] Richard P Mann. Collective decision making by rational individuals. *Proceedings of the National Academy of Sciences*, 115(44):E10387–E10396, 2018.

[64] Amandine Ramos, Odile Petit, Patrice Longour, Cristian Pasquaretta, and Cédric Sueur. Collective decision making during group movements in european bison, bison bonasus. *Animal Behaviour*, 109:149–160, 2015.

[65] Larissa Conradt and Timothy J Roper. Consensus decision making in animals. *Trends in ecology & evolution*, 20(8):449–456, 2005.

[66] Matthew MG Sosna, Colin R Twomey, Joseph Bak-Coleman, Winnie Poel, Bryan C Daniels, Pawel Romanczuk, and Iain D Couzin. Individual and collective encoding of risk in animal groups. *Proceedings of the National Academy of Sciences*, 116(41):20556–20561, 2019.

[67] Kolbjørn Tunstrøm, Yael Katz, Christos C Ioannou, Cristián Huepe, Matthew J Lutz, and Iain D Couzin. Collective states, multistability and transitional behavior in schooling fish. *PLoS computational biology*, 9(2):e1002915, 2013.

[68] Andrew M Hein, Michael A Gil, Colin R Twomey, Iain D Couzin, and Simon A Levin. Conserved behavioral circuits govern high-speed decision-making in wild fish shoals. *Proceedings of the National Academy of Sciences*, 115(48):12224–12228, 2018.

[69] Roy Harpaz, Gašper Tkačik, and Elad Schneidman. Discrete modes of social information processing predict individual behavior of fish in a group. *Proceedings of the National Academy of Sciences*, 114(38):10149–10154, 2017.

[70] Michael A Gil and Andrew M Hein. Social interactions among grazing reef fish drive material flux in a coral reef ecosystem. *Proceedings of the National Academy of Sciences*, 114(18):4703–4708, 2017.

[71] Andrea Cavagna, Alessio Cimarelli, Irene Giardina, Giorgio Parisi, Raffaele Santagati, Fabio Stefanini, and Massimiliano Viale. Scale-free correlations in starling flocks. *Proceedings of the National Academy of Sciences*, 107(26):11865–11870, 2010.

[72] Tim Gernat, Vikyath D Rao, Martin Middendorf, Harry Dankowicz, Nigel Goldenfeld, and Gene E Robinson. Automated monitoring of behavior reveals bursty interaction patterns and rapid spreading dynamics in honeybee social networks. *Proceedings of the National Academy of Sciences*, 115(7):1433–1438, 2018.

[73] John E Treherne and William A Foster. Group transmission of predator avoidance behaviour in a marine insect: the trafalgar effect. *Animal Behaviour*, 29(3):911–917, 1981.

[74] Marco Dorigo, Guy Theraulaz, and Vito Trianni. Reflections on the future of swarm robotics. *Science Robotics*, 5(49):eabe4385, 2020.

[75] Özer Duman, Rolf E Isele-Holder, Jens Elgeti, and Gerhard Gompper. Collective dynamics of self-propelled semiflexible filaments. *Soft matter*, 14(22):4483–4494, 2018.

[76] Joshua P Hecker and Melanie E Moses. Beyond pheromones: evolving error-tolerant, flexible, and scalable ant-inspired robot swarms. *Swarm Intelligence*, 9(1):43–70, 2015.

[77] Michael Rubenstein, Alejandro Cornejo, and Radhika Nagpal. Programmable self-assembly in a thousand-robot swarm. *Science*, 345(6198):795–799, 2014.

[78] Melanie Schranz, Martina Umlauft, Micha Sende, and Wilfried Elmenreich. Swarm robotic behaviors and current applications. *Frontiers in Robotics and AI*, 7:36, 2020.

[79] Daniel Carrillo-Zapata, Emma Milner, Julian Hird, Georgios Tzoumas, Paul J. Vardanega, Mahesh Sooriyabandara, Manuel Giuliani, Alan F. T. Winfield, and Sabine Hauert. Mutual shaping in swarm robotics: User studies in fire and rescue, storage organization, and bridge inspection. *Frontiers in Robotics and AI*, 7, 2020.

[80] Sara Brin Rosenthal, Colin R Twomey, Andrew T Hartnett, Hai Shan Wu, and Iain D Couzin. Revealing the hidden networks of interaction in mobile animal groups allows prediction of complex behavioral contagion. *Proceedings of the National Academy of Sciences*, 112(15):4690–4695, 2015.

[81] Tamás Vicsek, András Czirók, Eshel Ben-Jacob, Inon Cohen, and Ofer Shochet. Novel type of phase transition in a system of self-driven particles. *Physical review letters*, 75(6):1226, 1995.

[82] Ankit Gupta and Mustafa Khammash. Universal structural requirements for maximal robust perfect adaptation in biomolecular networks. *Proceedings of the National Academy of Sciences*, 119(43):e2207802119, 2022.

[83] Alexandre Seuret, Dimos V Dimarogonas, and Karl H Johansson. Consensus under communication delays. In *2008 47th IEEE Conference on Decision and Control*, pages 4922–4927. IEEE, 2008.

[84] Alexandre Seuret, Dimos V Dimarogonas, and Karl H Johansson. Consensus of double integrator multi-agents under communication delay. *IFAC Proceedings Volumes*, 42(14):376–381, 2009.

[85] Reza Olfati-Saber and Richard M Murray. Consensus problems in networks of agents with switching topology and time-delays. *IEEE Transactions on Automatic Control*, 49(9):1520–1533, 2004.

[86] Dan Ma, Jianqi Chen, Renquan Lu, Jie Chen, and Tianyou Chai. Delay consensus margin of first-order multi-agent systems with undirected graphs and pd protocols. *IEEE Transactions on Automatic Control*, 2020.

[87] Nejat Olgac and Rifat Sipahi. An exact method for the stability analysis of time-delayed linear time-invariant (LTI) systems. *IEEE Transactions on Automatic Control*, 47(5):793–797, 2002.

[88] Rifat Sipahi and Nejat Olgac. A unique methodology for the stability robustness of multiple time delay systems. *Systems & control letters*, 55(10):819–825, 2006.

[89] Ali Fuat Ergenc, Nejat Olgac, and Hassan Fazelinia. Extended kronecker summation for cluster treatment of LTI systems with multiple delays. *SIAM Journal on Control and Optimization*, 46(1):143–155, 2007.

[90] Jie Chen, Guoxiang Gu, and Carl N Nett. A new method for computing delay margins for stability of linear delay systems. *Systems & Control Letters*, 26(2):107–117, 1995.

[91] John Chiasson. A method for computing the interval of delay values for which a differential-delay system is stable. *IEEE Transactions on Automatic Control*, 33(12):1176–1178, 1988.

[92] Naomi Ehrich Leonard and Edward Fiorelli. Virtual leaders, artificial potentials and coordinated control of groups. In *Proceedings of the 40th IEEE Conference on Decision and Control (Cat. No. 01CH37228)*, volume 3, pages 2968–2973. IEEE, 2001.

[93] J.M. Ortega. *Matrix Theory, A Second Course, The University Series in Mathematics, Classics in applied mathematics ; vol. 3)*. Plenum Press, New York, 1987.

[94] Lin Xiao and Stephen Boyd. Fast linear iterations for distributed averaging. *Systems & Control Letters*, 53(1):65–78, 2004.

[95] H. Zhang, F. L. Lewis, and Z. Qu. Lyapunov, adaptive, and optimal design techniques for cooperative systems on directed communication graphs. *IEEE Transactions on Industrial Electronics*, 59(7):3026–3041, July 2012.

[96] Euhanna Ghadimi, Hamid Reza Feyzmahdavian, and Mikael Johansson. Global convergence of the heavy-ball method for convex optimization. In *2015 European Control Conference (ECC)*, pages 310–315. IEEE, 2015.

[97] Yurii Nesterov. *Introductory Lectures on Convex Optimization: A Basic Course*. Springer Publishing Company, Incorporated, 1 edition, 2014.

[98] Laurent Lessard, Benjamin Recht, and Andrew Packard. Analysis and design of optimization algorithms via integral quadratic constraints. *SIAM Journal on Optimization*, 26(1):57–95, 2016.

[99] Ali Makhdoumi and Asuman Ozdaglar. Graph balancing for distributed subgradient methods over directed graphs. In *2015 54th IEEE Conference on Decision and Control (CDC)*, pages 1364–1371. IEEE, 2015.

[100] Ran Xin and Usman A Khan. Distributed heavy-ball: A generalization and acceleration of first-order methods with gradient tracking. *IEEE Transactions on Automatic Control*, 65(6):2627–2633, 2019.

[101] Tobias Louw, Scott Whitney, Anu Subramanian, and Hendrik Viljoen. Forced wave motion with internal and boundary damping. *Journal of applied physics*, 111(1):014702, 2012.

[102] Iasson Karafyllis, Maria Kontorinaki, and Miroslav Krstic. Boundary-to-displacement asymptotic gains for wave systems with kelvin–voigt damping. *International Journal of Control*, 94(10):2822–2833, 2021.

[103] A. E. Green and P. M. Naghdi. On undamped heat waves in an elastic solid. *Journal of Thermal Stresses*, 15(2):253–264, 1992.

[104] Charlotte K Hemelrijk and Hanno Hildenbrandt. Diffusion and topological neighbours in flocks of starlings: relating a model to empirical data. *PLoS One*, 10(5):e0126913, 2015.

[105] Jean-Jacques E Slotine, Weiping Li, et al. *Applied nonlinear control*, volume 199. Prentice hall Englewood Cliffs, NJ, 1991.

[106] Seth Chaiken and Daniel J Kleitman. Matrix tree theorems. *Journal of combinatorial theory, Series A*, 24(3):377–381, 1978.